

# **The morphology of trickle flow liquid holdup**

**Werner van der Merwe**

**Submitted in partial fulfillment of the requirements of the degree Masters in Engineering (Chemical Engineering) in the Faculty of Engineering, Built Environment and Information Technology, University of Pretoria, Pretoria.**

**3 December 2004**

**The morphology of trickle flow liquid holdup**

**by**

**Werner van der Merwe**

**Professor Willie Nicol**

**Department of Chemical Engineering**

**Masters in Engineering (Chemical Engineering)**

Gravity driven trickle flow of a liquid over a fixed bed in the presence of a gaseous phase is widely encountered throughout the process industry. It is one of the most common ways of contacting multi-phase fluids for reaction or mass transfer purposes. The presence of three phases greatly complicates the mathematical modelling of trickle-bed reactors and makes a description from first principles difficult.

Trickle flow performance is usually characterized in terms of hydrodynamic parameters. One such parameter is the liquid holdup. The value and morphology (shape or texture) of the holdup influences the catalyst contacting, wetting, mass transfer characteristics and ultimately the performance of the trickle flow unit.

This study is limited to the air-water-glass spheres system with no gas flow. It is partitioned into three sections. An investigation into the nature of the residual liquid holdup in beds of spherical particles revealed that the general assumption that all residual liquid is held in the form of pendular rings at particle contact points proves to be untrue. Instead, indication is that 48 % of the residual holdup is present in the form of agglomerated liquid globules in interstices of low local porosity. Theoretical residual liquid holdup models and residual liquid holdup-based mass transfer models should include this phenomenon.

In a subsequent section, the influence of the prewetting procedure on the operating holdup is investigated. Three distinct limiting cases are identified: Kan-

wetted, Levec-wetted and non-wetted. A volumetric utilization coefficient that describes the extent to which the bed is irrigated is developed. It indicates that large fractions of the bed remain non-irrigated in the Levec- and non-wetted modes. A momentum balance-based model is adopted to predict the Kan-wetted mode holdup. This model was successfully extended to predicting the holdup in the Levec- and non-wetted modes by simple incorporation of the volumetric utilization coefficient. The predictive capability of this model is highly satisfactory, especially in light of it using only the classical Ergun constants and no fitted parameters (AARE = 9.6 %). The differences in the hysteresis behaviour of holdup and pressure drop in the different modes are attributed to differences in the morphology of the operating holdup.

The existence of the three limiting prewetted modes is confirmed by residence time distribution (RTD) analysis of the stimulus-response behaviour of the system. This behaviour was quantified using a NaCl tracer and conductivity measurements at both the inlet and outlet of a bench scale bed. The analyses show that:

- There are large fractions of the holdup that is inaccessible to the tracer in the Levec-wetted and non-wetted modes.
- The mixedness in the three prewetted modes differ appreciably, with the Kan-wetted mode clearly less mixed than the Levec-wetted mode.

The RTD analyses also confirm the existence of the three prewetting modes in a porous system (spherical  $\alpha$ -alumina), with a large fraction of the holdup being inaccessible to the tracer in the Levec-wetted mode.

This study emphasizes the role of the morphology of the various types of liquid holdup on the hydrodynamic performance of a trickle flow unit. It is apparent that aspects of the morphology depend strongly on phenomena like globule formation, hysteresis and flow and prewetting history that have not been

adequately recognized to date. The visualization of the various modes of trickle flow is an intellectual platform from which future studies may be directed.

KEYWORDS: residual liquid holdup, hydrodynamics, trickle flow, pressure drop hysteresis

**Contents**

<b>Nomenclature</b>	<b>ix</b>
<b>Chapter 1. Introduction</b>	<b>1</b>
<b>Chapter 2. Residual liquid holdup: Literature</b>	<b>5</b>
2.1 Introduction	5
2.2 Influential parameters and correlations	7
2.3 The theoretical prediction of RLH	8
2.3.1 Hydrostatics of the meniscus (Saez & Carbonell, 1990, Mao et. al., 1993)	9
2.3.2 Stability criteria	10
2.3.3 Mapping to a randomly packed bed	11
2.4 Conclusions	12
<b>Chapter 3. Residual liquid holdup morphology</b>	<b>14</b>
3.1 Introduction	14
3.2 Experimental	14
3.2.1 Pendular ring geometry	15
3.2.2. RLH measurements	17
3.3 Results	18
3.3.1 Modeling of ring volume	18
3.3.2 Wetting angles	19
3.3.2 Contact angles	20
3.3.3 Elevation angle and its effect on wetting angle	20
3.3.4 Residual liquid holdup	21
3.4 Discussion	23
3.5 Conclusions	26
<b>Chapter 4. Operating holdup: Literature</b>	<b>27</b>
4.1 Introduction	27
4.2 Trickle flow types	29

4.3 Pressure drop hysteresis	31
4.3.1 Hysteresis in the Kan-wetted mode	33
4.3.2 Hysteresis in the Levec-wetted mode	36
4.3.3 Hysteresis in the non-pretetted mode	38
4.4 Wetting efficiency and liquid distribution	39
4.4.1 Wetting efficiency determination methods	39
4.4.2 Wetting efficiency correlations	40
4.5 Trickle flow visualization techniques	42
4.5.1 Reaction based colorimetrics (Lazzaroni <i>et. al.</i> , 1988,1989)	43
4.5.2 Longitudinal X-ray tomography (Lutran <i>et. al.</i> , 1991)	45
4.5.3 Dye-adsorption colorimetrics (Ravindra <i>et. al.</i> , 1997)	46
4.5.4 Cross-sectional magnetic resonance imaging (Sederman & Gladden, 2001)	48
4.6 Holdup models	50
4.6.1 Correlations	50
4.6.2 Momentum balances for fully wetted film flow (Boyer & Fanget, 2002)	52
4.6.3 Other holdup models for the Kan-wetted mode	54
4.7 Conclusions and rationalization	54
<b>Chapter 5. Operating holdup morphology</b>	<b>58</b>
5.1 Introduction	58
5.2 Experimental	58
5.2.1 Experimental setup	58
5.2.2 Experimental procedure	60
5.3 Results	65
5.3.1 Holdup in each pretetted mode	65
5.3.2 Volumetric utilization efficiency	66
5.4 Discussion	69
5.4.1 Holdup	69
5.4.2 Volumetric utilization and wetting efficiency	72
5.4.3 Utilization efficiency and holdup prediction	77
5.5 Conclusions	80

<b>Chapter 6. RTD analyses</b>	<b>83</b>
6.1 Introduction and background	83
6.2 Experimental	84
6.3 Results and discussion	86
6.3.1 Non-porous	86
6.3.2 Porous	92
6.4 Conclusions	94
<b>Chapter 7. Conclusions</b>	<b>95</b>
<b>References</b>	<b>97</b>
<b>Appendix A: RLH supporting information</b>	<b>109</b>
A.1 Influential parameters and trends	109
A.2 Residual liquid holdup correlations	114
A.3 Surface tension	116
A.4 Porosity of the packed bed	117
A.5 Contact angles	117
<b>Appendix B: Operating holdup: additional information</b>	<b>118</b>

**Nomenclature**

$a$	Coordinate of triple point	
$AARE$	Average absolute relative error	
$A$	Upper triple point (chapters 2,3)	
$A$	Liquid flux difference (chapters 3,4)	kg/m <sup>2</sup> s
$A_{GL,LS}$	Interfacial area (gas-liquid, liquid-solid)	m <sup>2</sup>
$B$	Lower triple point (chapters 2,3)	
$B$	Liquid flux difference (chapters 3,4)	kg/m <sup>2</sup> s
$Bo$	Bond number $\left(\frac{\rho g r^2}{\sigma}\right)$	
$C$	Conductivity (chapters 3,4,5,6)	μS/cm
$C$	Dimensionless datum pressure (chapter 2)	
$d$	Diameter (nominal length)	m
$dP/dz$	Pressure loss or gradient	Pa/m
$e$	Exponent	
$E$	Normalized response curve	
$\Delta E$	Internal energy change	J
$Eö$	Eötvös number $\left(\frac{\rho g d^2}{\sigma}\right)$	
$Eö^*$	Modified Eötvös number $\left(\frac{\rho g d^2 \varepsilon}{\sigma(1-\varepsilon)^2}\right)$	
$f$	Correction factor (chapters 2,3)	
$f$	Wetting efficiency (chapters 3,4)	
$f_s, f_w$	Slip factors	
$F$	Calibration function	
$g$	Gravity vector	m <sup>2</sup> /s
$G$	Gas mass flux	kg/m <sup>2</sup> s
$h$	Holdup	
$I$	Normalized stimulus curve	
$k$	Reaction rate constant	s <sup>-1</sup>



$L$	Liquid mass flux	kg/m <sup>2</sup> s
$N_{CP}$	Number of contact points per sphere	
$P$	Pressure	Pa
$q$	Coefficient	
$Q$	Volumetric flow	l/min
$r$	Reaction rate	mol/s
$R^2$	Average sum of square errors	
$R_h$	Hydraulic radius	
$RLH^*$	RLH of non-irrigated zone	
$RLH$	Residual liquid holdup	
$S$	Mass of salt (chapters 3,4)	
$S$	Curvature of sphere (chapters 2,3)	
$t$	Time	s
$t_E$	Apparent residence time	s
$v$	Volume of a single meniscus	m <sup>3</sup>
$v_L$	Superficial velocity	m/s
$\langle v_L \rangle$	Interstitial velocity	m/s
$V$	Bed volume	m <sup>3</sup>
$W$	Weight of washing water	g
$Y$	Normalized coordinate	
$z$	Vertical coordinate (chapters 2,3)	m
$z$	Axial coordinate (chapters 3,4)	m
$Z$	Normalized vertical coordinate	
<b><i>Greek letters</i></b>		
$\alpha$	Wetting angle	Degrees
$\chi$	Volumetric utilization coefficient	
$\wp$	Solid curvature locus	
$\varepsilon$	Porosity	
$\varepsilon_L$	Liquid holdup	

$\eta$	Effectiveness factor	
$\mu$	Viscosity	cP
$\mu_n$	n-th moment	
$\theta$	Contact angle	Degrees
$\sigma$	Surface tension	N/m
$\sigma_v$	Deviation of the response curve	
$\tau$	Shear stress	Pa/m
$\psi$	Elevation angle	Degrees

***Subscripts***

$G$	Gas
$GL$	Gas-liquid
$i$	Initial
$i,est$	Initial (estimated)
$L$	Liquid
$LS$	Liquid-solid
$n$	Indicates n-th moment
$RTD$	Obtained from RTD analysis
$sat$	Saturated

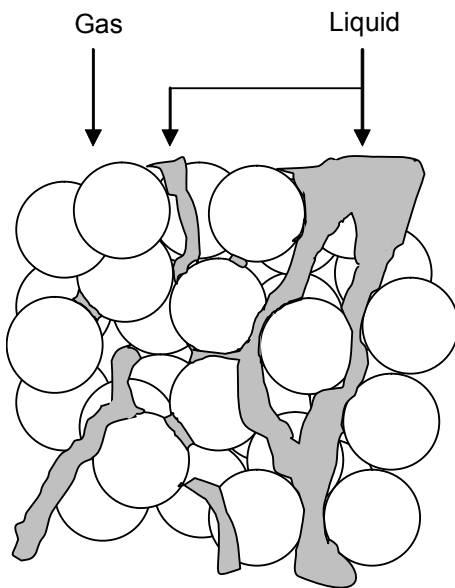
---

## Chapter 1. Introduction

---

Trickle flow is widely encountered in present day process industry, most notably in the petroleum, petrochemical, biological, chemical and electrochemical processes (Gianetto & Silveston, 1986: xv). It is one of the most common ways of contacting gas, liquid and solid phases and is present in trickle bed reactors, absorption columns, catalytic and packed distillation columns and trickling filters. A host of parameters are applicable to trickle flow hydrodynamics. These include various liquid holdups, wetting and contacting efficiencies, apparent particle effectiveness, two-phase pressure drop, liquid-solid, gas-liquid and gas-solid mass transport variables, residence times and others.

In this study, the trickle flow regime is defined to be gravity driven flow of a liquid over a stationary bed of packed particles (or structured packing) in the presence of a static or co-current flowing gaseous phase. A schematic representation is shown in figure 1-1.



**Figure 1-1.** A schematic of trickle flow

In trickle flow hydrodynamics the liquid holdup or saturation is of paramount importance, since it has a direct impact on all other influential parameters. A great number of studies regarding liquid holdup in packed beds have been done and different definitions of the various types of holdup exist. In this study, all holdups are expressed as volumetric fractions of the total bed volume (as opposed to saturations, which are volumetric fractions of the void space). The following definitions are necessary (Table 1-1):

**Table 1-1.** Definitions of the various types of holdup

<i>Total or operating liquid holdup</i>	The total amount of liquid inside the bed at steady state conditions during operation.
<i>Residual liquid holdup (RLH)</i>	The amount of liquid that ultimately remains in the packed section after the liquid feed was suddenly stopped and the bed was allowed to drain freely.
<i>Saturated residual liquid holdup</i>	The amount of liquid that ultimately remains in the packed section after the bed had been completely flooded with liquid and allowed to drain.
<i>Free-draining liquid holdup</i>	The part of the operating holdup that drains from the bed when the liquid flow is disrupted.
<i>Static or inactive liquid holdup</i>	The part of the operating holdup that is stagnant or semi-stagnant during operation.
<i>Dynamic liquid holdup</i>	The part of the operating holdup that is not stagnant during operation.

Both the free-draining and residual liquid holdup-pair, and the dynamic and static liquid holdup-pair, together comprise the operating holdup. Note that the dynamic and free-draining, and static and residual holdups are not necessarily equal, although this assumption is often made.

The morphology of the liquid holdup is an important aspect of reactor or unit performance. In the present context, the term “morphology” refers to the

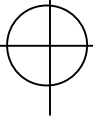
structure, geometry, shape or texture of the liquid within the packing, especially insofar as the agglomeration of liquid impacts the liquid-solid area.

Liquid holdup is split into two components (dynamic and static, or residual and free-draining) in order to represent two groups of parameters (Mao, Xiong & Chen, 1993). Residual liquid holdup is an indication of the bed structure, particle size and physical properties of the system. The dynamic and free-draining holdups are more directly associated with the operating variables. Regarding the similarity of static and residual liquid holdup, there is substantial indication in literature that the residual and static holdups are not equal (Bennet & Goodridge, 1970, Schubert, Lindner & Kelly, 1986, Kushalkar & Pangarkar, 1990). At least a part of the residual holdup is therefore influenced by the operating conditions. Furthermore, the existence, magnitude and possible significance of static zones in the operating holdup remain contentious issues (Stegeman *et. al.*, 1996, Kushalkar & Pangarkar, 1990, Sicardi, Baldi & Specchia, 1980a). It is therefore more advisable to consider the residual liquid holdup and the entire operating holdup as principal cases of liquid holdup.

Although the operating holdup is the only holdup that impacts the reactor or column efficiency, the RLH may be used (as intended) to represent bed structure, particle size and the physical properties of the system. The next two chapters are dedicated to the morphology and prediction of residual liquid holdup. In addition, this study proposes a novel use of residual liquid holdup to gain information on the morphology of the operating holdup in various limiting prewetting cases. The relevant literature is reviewed in chapter 4. The development and results are reported in chapter 5. Finally, residence time distribution analysis is used as an alternative technique to gain an additional perspective on the morphology of the operating holdup. The quiescent air-distilled water- 3 mm glass spheres system is used throughout this study, with a small section on the stimulus-response behaviour of a bed packed with porous alumina spheres. The air-water-glass system is chosen because its generality in

literature facilitates comparison with previous investigators. From a fundamental point of departure it is important to understand non-porous low-pressure systems first before the results can be extended to other operating conditions. The final section on porous spheres serves to confirm the applicability of the results to non-porous systems.

In general, this study aims to address some issues regarding the morphology of liquid holdup for packed beds of spheres under trickle flow irrigation. The purpose is to develop a fundamentally more sound understanding of the flow phenomena in trickle flow and the possible impact these phenomena may have on unit performance.



---

## Chapter 2. Residual liquid holdup: Literature

---

In subsequent sections, the RLH is used to gain insight into aspects of the flow morphology of the operating holdup. As such, the geometry of the RLH is important. In this chapter, the relevant RLH literature is reviewed.

### 2.1 Introduction

The residual liquid holdup is often used as a parameter that symbolizes the physical properties of the system under investigation (Mao *et. al.*, 1993). These include:

- packing properties (nominal diameter, sphericity and hydrophobicity)
- bed properties (voidage fraction and packing geometry)
- fluid properties (wettability, density, viscosity and surface tension)

The residual liquid holdup has featured in a number of models. Examples of trickle bed reactor models where RLH is seen as an additional mass transfer resistance are those presented by Patwardhan (1978), Llano *et. al.* (1997), Rajashekharam, Jaganathan & Chaudhari (1998), Nijhuis, Dautzenberg & Moulijn (2003) and Iliuta & Larachi (2001). It is also incorporated into pressure drop and holdup correlations such as those developed by Saez & Carbonell (1985), Škrbić & Cvejanov (1994), Stanek & Kolar (1973) and Matsuura, Akehata & Shirai (1979). The static liquid holdup, which is often assumed to be equal to the RLH, features in both the Piston-Exchange (cross-flow) and the Piston-Dispersion-Exchange residence time distribution models (Van Swaaij, Charpentier & Villermaux, 1969, Stegeman *et. al.*, 1996, Nigam, Iliuta & Larachi, 2002, Iliuta, Larachi & Grandjean, 1999). Finally, the RLH has an impact on wetting efficiency and the modeling thereof (Nigam *et. al.*, 2002, Pironti *et. al.*, 1999, Sicardi *et. al.*, 1980b, 1980c).

It is evident that the residual liquid holdup is considered to be an important and useful parameter. Numerous ways exist by which it can be determined. These include:

- direct empirical methods (like flooding, draining and weighing the column) (Saez & Carbonell, 1985)
- model based measurement (e.g. the fitting of predicted residence time distribution curves to stimulus-response data, assuming RLH is equal to static liquid holdup) (Stegeman *et. al.*, 1996)
- theoretical prediction, based on the principles of hydrostatics (only applicable to spherical packing) (Mao *et. al.*, 1993)

A host of empirical correlations has been suggested for the value of residual liquid holdup given certain system parameters. However, the experimental scatter of the data used in these correlations is immense (Saez & Carbonell, 1985, Ortiz-Arroyo, Larachi & Iliuta, 2003). In addition, these investigations do not offer any insight into the morphology of the residual holdup. In all of the mass transfer related applications mentioned above (e.g. PE and PDE models), the RLH morphology plays a pivotal role in determining its mass transfer resistance (see for example Reddy, Rao & Rao, 1990). On the other hand, theoretical predictions of the residual holdup are based on its geometry, and are therefore more useful. Unfortunately, most of the theoretical developments have not been validated except on their ability to predict an overall bed RLH.

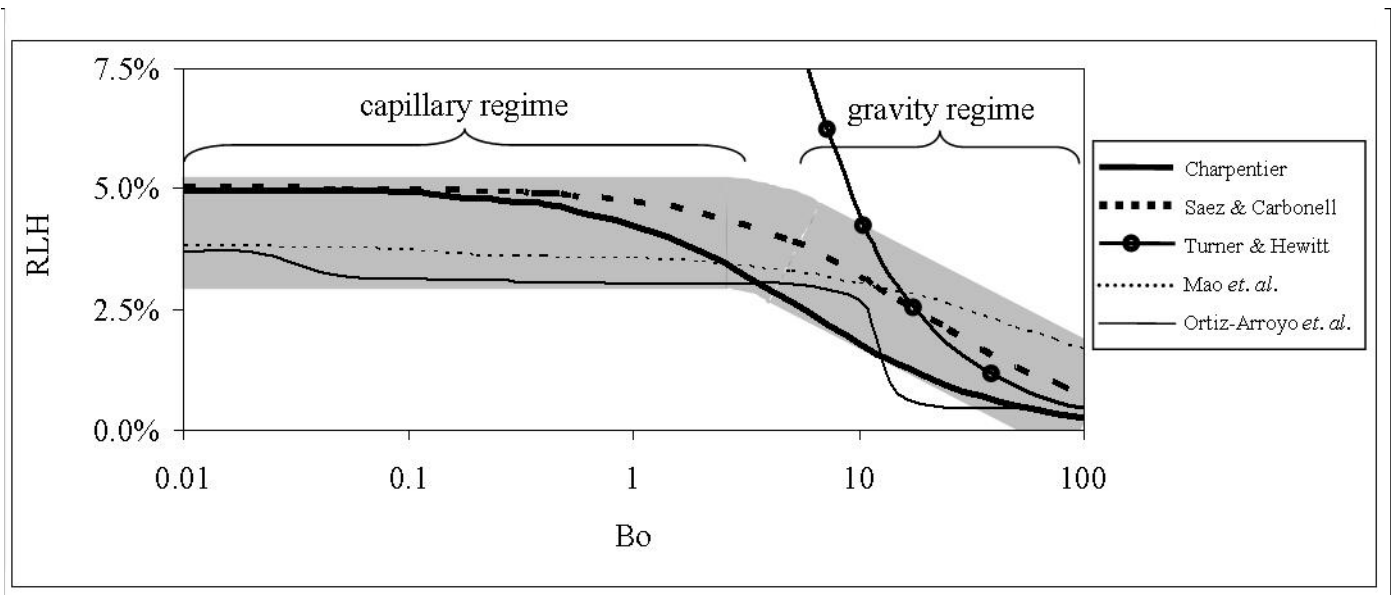
A great amount of research has been devoted to residual or static liquid holdup. A detailed discussion of all works is available from the author but will not be repeated here. Instead, only the essential information pertinent to the results of the present study is presented. In this context, an overview of the parameters that affect RLH is given, followed by a presentation of the most commonly used correlations and what they signify. This is followed by a summary of advances in theoretically predicting RLH.



## 2.2 Influential parameters and correlations

A complete summary of the parameters that influence the RLH is given in Appendix A. Also included in the Appendix is an overview of RLH correlations that have been used in literature.

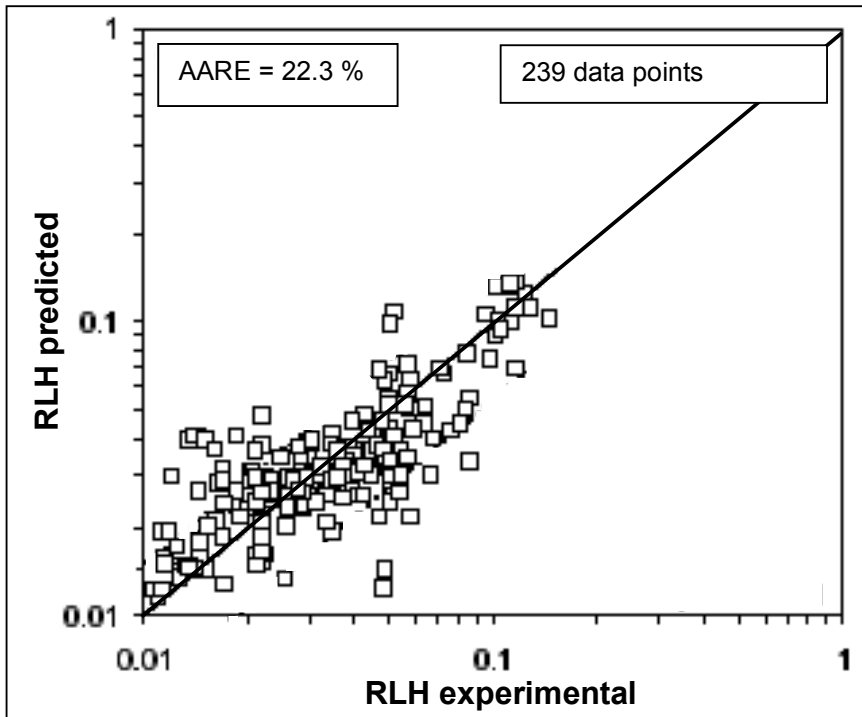
For the present discussion it is sufficient to note that the RLH is often correlated in terms of the Bond or Eötvös number, porosity and contact angle. It is informative to plot those correlations that are used preferentially (figure 2-1). The system is 3 mm glass spheres, water and air. Since the porosity varies little and the contact angle is fixed (see next chapter), the plot assumes the form of RLH versus Bond number.



**Figure 2-1.** Commonly used correlations for RLH as a function of Bond number

As indicated, there is a gravity dominant regime at high Bond numbers ( $Bo > 5$ ) and a capillary dominant regime at Bond numbers smaller than approximately 2. The latter covers most practical packing sizes (Charpentier *et al.*, 1968). In the capillary regime, residual liquid holdup values are usually approximately 5 %, although values exceeding 10 % have been reported (Saez *et al.*, 1991, Ortiz-Arroyo *et al.*, 2003). Ortiz-Arroyo *et al.* (2003) evaluated existing correlations

and their own artificial neural network based correlation and found that a large amount of scatter is evident in the data. Their own correlation performed the best with an average absolute relative error of 22.3 %. A parity plot of experimental versus calculated RLH data for this correlation is reproduced here in figure 2-2.



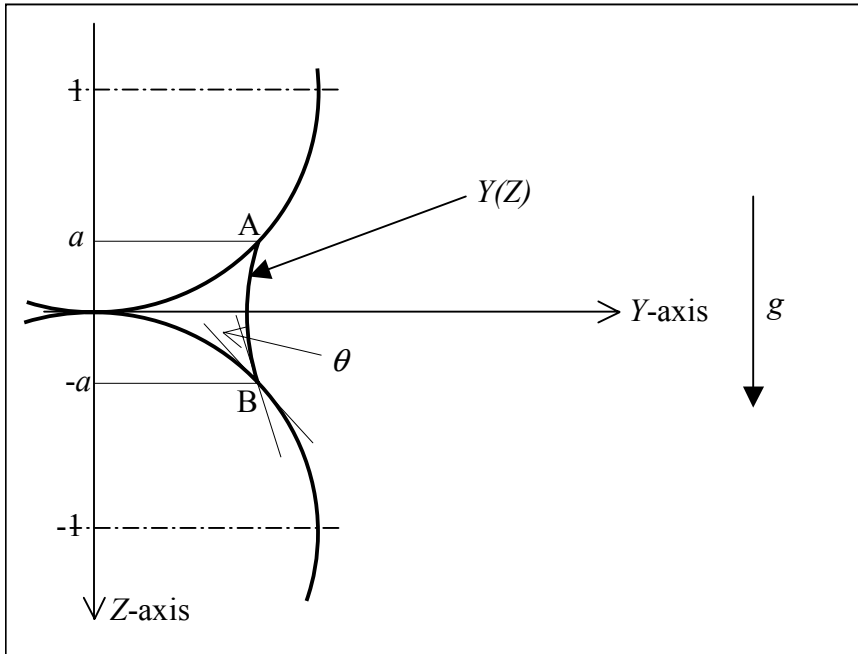
**Figure 2-2.** Parity plot of measured vs. calculated RLH data (from Ortiz-Arroyo *et. al.*, 2003)

Note that log-log scales are used in Figure 2-2 and that this plot is for the *best* known RLH correlation. It is evident that RLH prediction is not adequate and that the empirical approach has been exhausted and found wanting. It is concluded that the morphology of the RLH and the theoretical prediction thereof need investigation.

## 2.3 The theoretical prediction of RLH

In studies regarding the theoretical prediction of RLH, the focus has been almost exclusively on the RLH in packed beds of spheres. It is assumed that the liquid is

present in the form of pendular rings at the particle-particle contact points (figure 2-3, Saez & Carbonell, 1990, Mao *et. al.*, 1993, Kramer, 1998, Ortiz-Arroyo *et. al.*, 2003, Stein, 2000).



**Figure 2-3.** Pendular ring geometry and relevant variables

Here all variables have been normalized to the sphere radius. The objective is to find the solution of the function  $Y(Z)$ . There are two aspects to this solution:

- The shape of the liquid meniscus
- The location of the meniscus on the sphere surface (points A and B)

### **2.3.1 Hydrostatics of the meniscus (Saez & Carbonell, 1990, Mao *et. al.*, 1993)**

Consider the liquid held in a pendular ring at the contact point between two *vertically aligned touching* spheres (figure 2-3). Under the assumptions of negligible surface tension gradients and negligible gas density, the momentum balance across the gas-liquid interface reduces to the Young-LaPlace equation.

The meniscus shape is known to be symmetrical around the  $Z$ -axis. In the cylindrical coordinate system the equation is:

$$Y'' = \frac{1+Y'^2}{Y} - (1+Y'^2)^{3/2} (Bo.Z - C) \quad (2-1)$$

Here primes denote differentiation with respect to  $Z$ . Pertinent boundary conditions are:

$$Y|_{Z=a} = Y|_{Z=-a} = \sqrt{1-(1-a)^2} \quad (2-2)$$

$$\theta = \left| \tan^{-1} Y' - \tan^{-1} S' \right| \quad \text{at } Z = -a, a \quad (2-3)$$

$$S(Z) = \begin{cases} \sqrt{1-(1+Z)^2} & -2 \leq Z \leq 0 \\ \sqrt{1-(1-Z)^2} & 0 \leq Z \leq 2 \end{cases} \quad (2-4)$$

Here  $a$  is the positive  $Z$ -value of the triple point and may also be expressed as a wetting angle ( $\alpha$ ), where  $\alpha = 2\cos^{-1}(1-a)$ .  $S$  describes the surface of the spheres. Given values of  $Bo$ ,  $\theta$  and  $a$ , the solution for  $Y$  can be obtained numerically.

### **2.3.2 Stability criteria**

The Bond number and contact angle are fully determined by the system properties. Two arguments have been raised in order to fix the location of the triple point on the sphere surface ( $a$ ). The first is the thermodynamic stability criterion of Mao *et. al.* (1993). It is claimed that the value of  $a$  that yields the minimum internal energy change for the liquid is assumed. This involves minimization of the equation:

$$\Delta E = \sigma(A_{GL} - A_{LS} \cos \theta) \quad (2-5)$$

$$A_{GL} = 2\pi \int_{-a}^a Y dZ \quad \text{and} \quad A_{LS} = 4a\pi$$

Kramer (1998) presents an argument for fixing the limits of  $\alpha$  based on the assumption that the pendular rings are at critical percolation (i.e. drainage stops as soon as a percolating path downwards ceases to exist). The lower limit is set by envisioning three touching spheres in an equilateral arrangement (12 contact points per sphere). For wetting angles smaller than  $60^\circ$ , the rings are separated and liquid ceases to drain. Since closer contact arrangements do not exist, this is taken as the lower limit for  $\alpha$ . The upper limit is set by a body-centered cubic array (6 contact points per sphere), where the rings will touch one another (and liquid will drain away) for wetting angles above  $70^\circ$ . This is taken as the upper limit. The author suggests using  $\alpha \approx 65^\circ \pm 2^\circ$ . The wetting angles of Mao *et. al.* and Kramer differ appreciably and neither reports extensive experimental verification.

### **2.3.3 Mapping to a randomly packed bed**

The volume of a single meniscus between vertically aligned spheres can now be calculated from (Mao *et. al.*, 1994):

$$v = d^3 \int_{-a}^a \frac{\pi}{8} (Y^2 - S^2) dZ \quad (2-6)$$

In the Mao *et. al.* (1993) correlation, the mean volume of a set of *randomly inclined* pendular rings is determined by an averaging procedure based on the findings of Turner & Hewitt (1959). They studied the mass of water held between two glass spheres at different elevation angles and found the average ring to have a mass of approximately 30 % of the maximum ring (which was found at vertical alignment). Unfortunately, the result only holds for large diameter spheres where gravity plays a significant role in distorting the meniscus shape ( $Bo \gg 5$ ). Turner & Hewitt warn that their result cannot be extrapolated to small

diameter spheres. Nevertheless, Mao *et. al.* (1993) multiplies the volume by a correction factor ( $f$ ) to account for smaller rings at other than vertical alignments.

Kramer (1998) uses a smaller wetting angle of  $65^\circ$ , a contact angle of zero and no correction factor.

The number of contact points per particle can be readily expressed in terms of the overall bed porosity using available correlations (Kramer, 1998, German, 1989). Since the number of particles per unit bed volume can be estimated at  $6(1-\varepsilon)/\pi d^3$ , the residual liquid holdup is given by:

$$RLH = \frac{6(1-\varepsilon) \frac{N_{CP}}{2}}{\pi d^3} f.v \quad (2-7)$$

Stein's (2000) empirical correlation for the number of contact points per sphere as a function of porosity is:

$$N_{CP} = 22(1-\varepsilon)^2 \quad (2-8)$$

In equation 2-7, the number of contact points is divided by two since each sphere "owns" half a pendular ring per contact point (Mao *et. al.*, 1994). The value of the residual holdup is critically influenced by the wetting angle and the correction factor, whereas the contact angle is less influential.

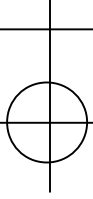
## 2.4 Conclusions

In summary, there are a few assumptions that are yet to be verified experimentally. These assumptions are:

- RLH is made up of pendular ring structures at particle-particle contact points

- The rings are at thermodynamic equilibrium and this condition determines the value of the wetting angle for vertically aligned spheres (Mao *et. al.*, 1993)
- The extension to non-vertical alignment in the capillary regime can be made from the Turner & Hewitt (1959) correction factor for large spheres in the gravity regime (Mao *et. al.*, 1993)
- The rings are at critical percolation (Kramer, 1998)

In this study, specific emphasis is placed on validating the core assumptions of the existing theoretical predictions insofar as these assumptions impact the proposed morphology of the RLH. This is done by direct microscopic photography of residual liquid holdup structures in a packed bed of spheres.



---

## Chapter 3. Residual liquid holdup morphology

---

### 3.1 Introduction

In this chapter the residual liquid holdup morphology is investigated by means of direct microscopic photography. The investigation is limited to the quiescent air-distilled water-spherical glass beads system. The aim is to investigate the validity of the assumptions listed in section 2.4.

### 3.2 Experimental

The focus here is on the morphology of residual liquid holdup inside a randomly packed bed of 3 mm glass spheres. Water is exclusively used as the wetting phase, with ambient air as gaseous phase. The air-water-glass system at ambient conditions is chosen because of its generality in literature. The Bond number for this system is equal to 0.3, indicating that capillary forces dominate over the gravitational force (figure 2-1). Gravity can be neglected for  $Bo < 0.5$  (Saez & Carbonell, 1990). The relevant physical properties of the chosen system are given in Table 3-1.

The surface tension was determined in a series of capillary rise experiments (Appendix A.3). The porosity was determined from the weight of glass beads that filled the column and the known bed volume. It was found to be constant upon every repacking (Appendix A.4). Consequently, the packing procedure is deemed to be reproducible.

Two sub-sections that each describes a specific experiment follow.



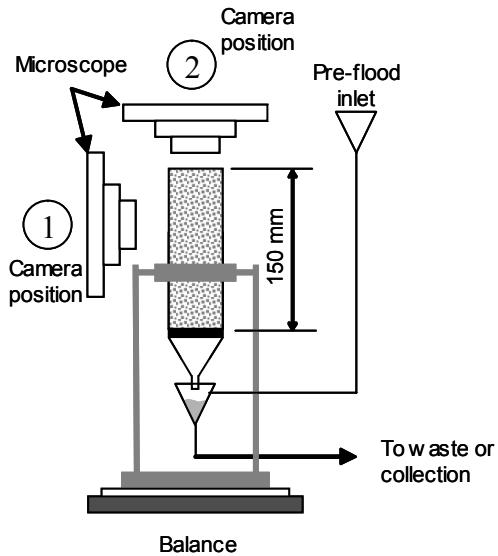
**Table 3-1.** Physical properties of the liquid, gas and solid

Property	Value
Water density	998 kg/m <sup>3</sup>
Surface tension	0.067 N/m
Porosity	0.365
Air density	1.03 kg/m <sup>3</sup> (assumed negligible)

### **3.2.1 Pendular ring geometry**

The aim is to measure the wetting angle, angle of elevation and contact angle of pendular rings throughout the bed. A 58 mm diameter (15 cm height) bed is thoroughly pre-wetted by flooding the entire column with water. The water is allowed to drain for at least 10 minutes, after which the weight stayed constant. The packed bed is then digitally photographed through a standard bench microscope. This is done by tilting the microscope as shown (figure 3-1) and photographing the image through the eye piece. Enlargement of 50 times was achieved. Two sets of microscopic photographs were undertaken. In the first, the column was photographed through the opening at the top of the column (camera position 2). In the second, the column interior was photographed from the side through the glass wall (camera position 1). Pendular rings a few particle diameters into the bed could be seen, although those inside the bulk bed away from the wall escaped notice. The influence of the curvature of the glass wall was deemed to be negligible after evaluation of the shape of the spheres on the photos (which would deviate from circular if the distortion was significant). The porosity close to the wall (camera position 1) is expected to be lower than the average porosity, and the results may well be influenced by this. Camera position 2 does not suffer from this effect. A schematic of the setup follows (figure 3-1).

Both sets of photographs yielded images upon which the pendular rings and their wetting angles could be clearly discerned.

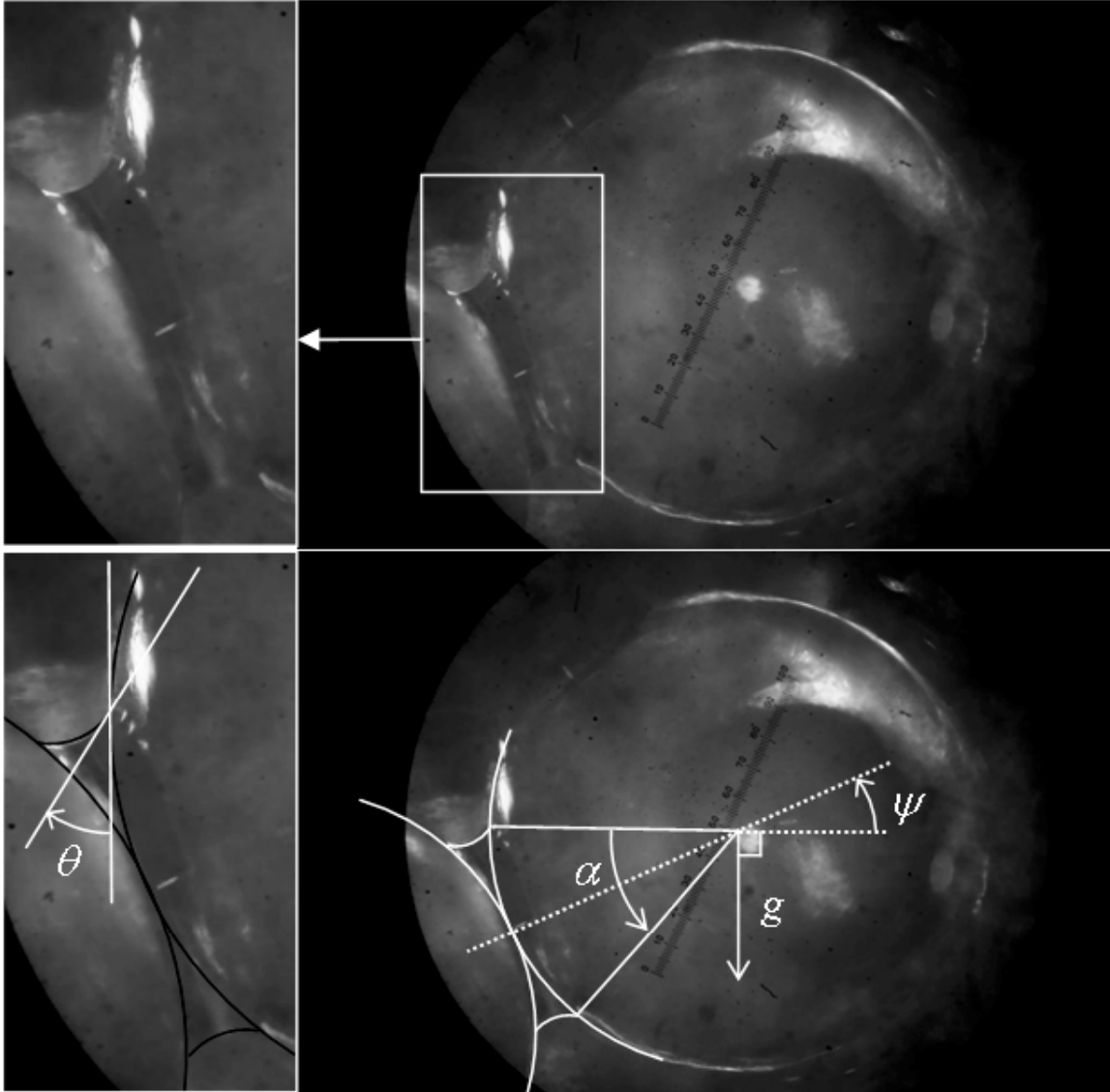


**Figure 3-1.** Schematic of the experimental setup

Contact angles were more difficult to ascertain because the slope of the meniscus at the triple point was not distinguishable on all the photographs. Angles of elevation (relative to the horizontal) were measured from the side-on images. All angles were measured by construction in the MS-Visio environment. An example of a typical analysis is shown in figure 3-2. The number of angles measured is reported in Table 3-2.

**Table 3-2.** Number of measurements in each set of experiments

	$\alpha$ (wetting angle)	$\theta$ (contact angle)	$\psi$ (elevation angle)
<b>Top View</b>	33	16	N/A
<b>Side View</b>	31	19	31



**Figure 3-2.** Typical analysis of a pendular ring

### **3.2.2. RLH measurements**

The residual liquid holdup was measured by the difference in weight between a dry bed (9252 g, which includes the weight of the support structure) and a pre-wetted and drained bed (9334 g on average). The balance employed has a resolution of 0.1 gram. The column was 58 mm in diameter and bed height was increased to 900 mm (to minimize end effects). The supporting grid was a steel wire mesh. An end effect was evident in that a 7 mm portion of the bed above the grid remained saturated in liquid indefinitely. This corresponds to approximately 7

grams of liquid. The measured weights were duly adjusted. Ten measurements were made. The setup is equivalent to figure 3-1, except for the bed height.

It has often been speculated that the rate of drainage should influence the RLH (Saez & Carbonell, 1985, Ortiz-Arroyo *et. al.*, 2003). Therefore, in a separate evaluation, the rate of drainage was controlled through a valve at the column exit. The total time that it took the liquid level to drop to the sieve was taken as an indication of the inverse of the draining rate. These times are shown along with their associated RLH values in Figure 3-6.

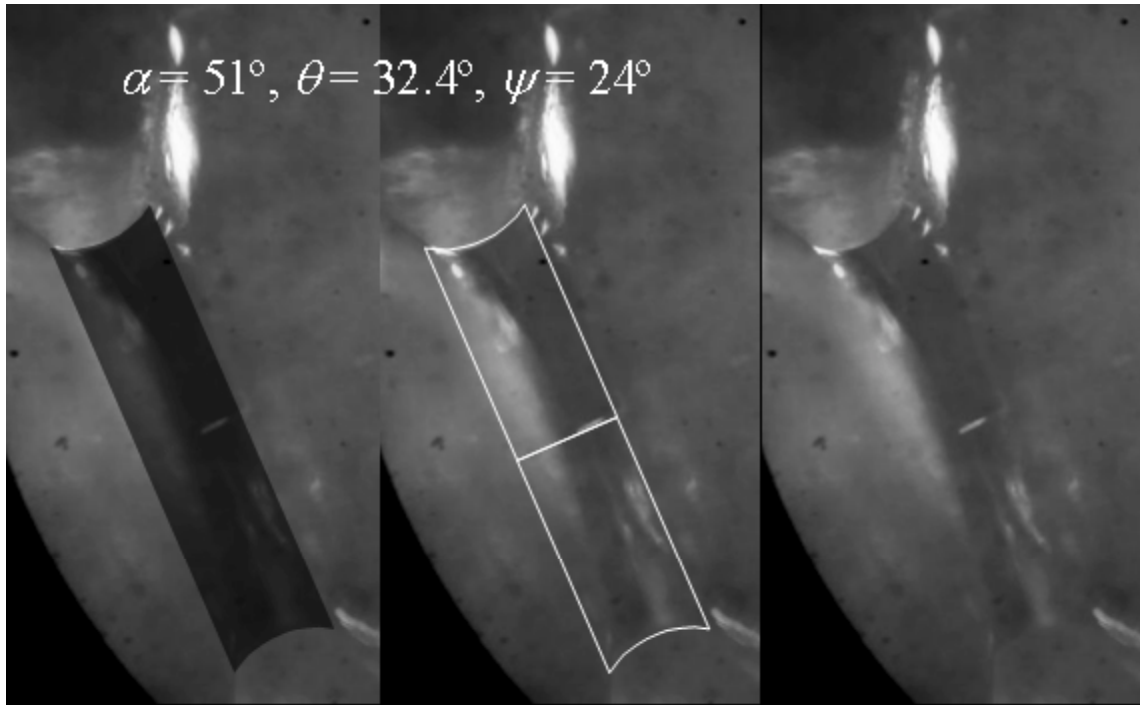
## 3.3 Results

### 3.3.1 Modeling of ring volume

Given measured values of the wetting, contact and elevation angles, solution of the Young-Laplace equation proceeds as follows (Mao *et. al.*, 1993):

- An initial arbitrary guess is made for the dimensionless datum pressure ( $C$ )
- Equations 2-1 to 2-4 are solved numerically over the interval  $[-a, a]$
- The intersection angle ( $\theta$ ) at  $Z = a$  is computed and compared to the boundary condition (equation 2-3)
- The value of  $C$  is adjusted and the procedure repeated until equation 2-3 is satisfied

The volume of the pendular ring is then calculated through equation 2-6. The ability of this procedure to accurately represent a pendular ring is demonstrated in figure 3-3. The image on the right is the original and those on the left have the solution superimposed for the values of wetting, elevation and contact angles as shown. The meniscus closely resembles a circular arc.

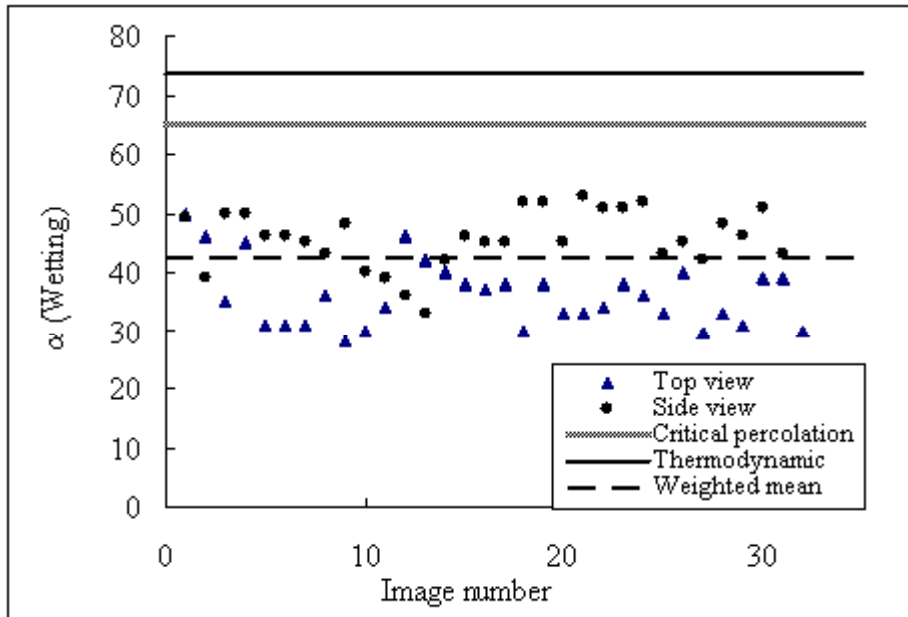


**Figure 3-3.** Comparison between modeled and experimental pendular ring shape

### **3.3.2 Wetting angles**

Wetting angle measurements are shown in figure 3-4 for both side-on and top view experiments. Since the ring volume is a non-linear function of wetting angle, the volume of each ring is computed and the mean of these is taken as the average ring volume. This wetting angle that yields this average ring volume is the mean wetting angle. Its value is  $42.4^\circ$ , as indicated in figure 3-4.

Also indicated in figure 3-4 is the wetting angle obtained by applying the thermodynamic stability criterion. Minimization of the internal energy (equation 2-5) yields a wetting angle of  $73.7^\circ$  for the present conditions ( $Bo = 0.3$ ,  $\theta = 32.4^\circ$ ). Kramer's (1998) suggested wetting angle of  $65^\circ$ , based on the critical percolation assumption, is also indicated.



**Figure 3-4.** Measured wetting angles

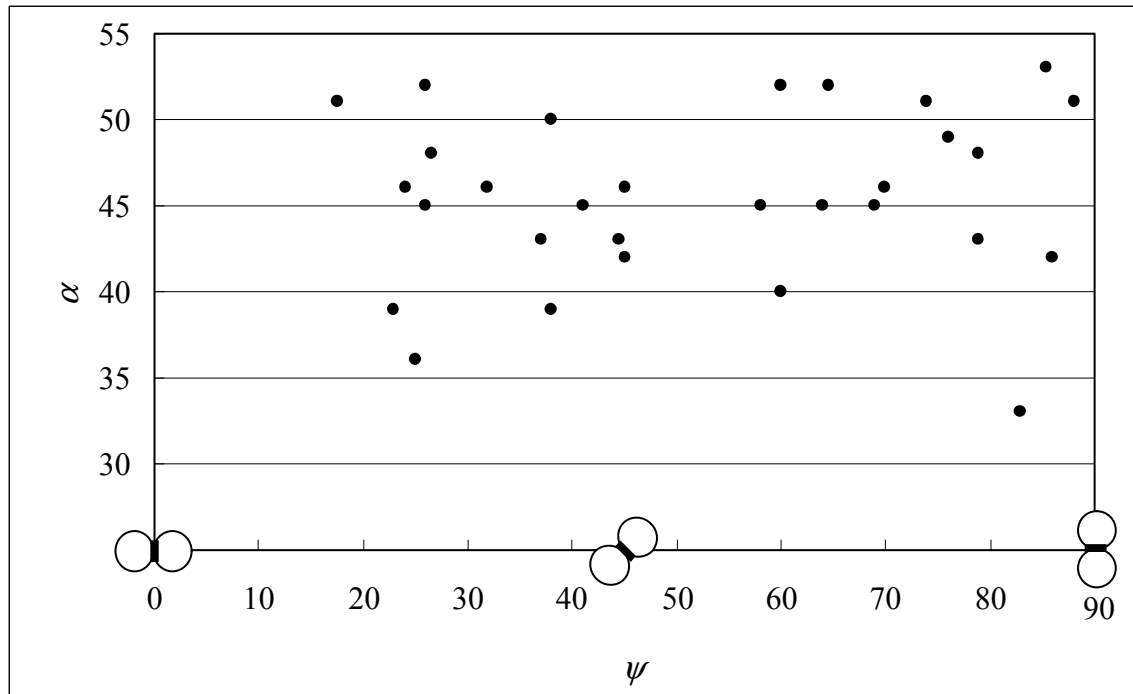
From figure 3-4 it is seen that the top view wetting angles were generally smaller than the side view angles. The weighted mean, however, was based on all the data. Importantly, the rings are neither at thermodynamic stability nor at critical percolation.

### **3.3.2 Contact angles**

The measured contact angles were found to be approximately constant with a mean of  $32.4^\circ$ , with values ranging between  $29^\circ$  and  $35^\circ$  (RSD = 6 %). Considering the difficulty in measuring these angles, the results compare well with the value of  $31.7^\circ$  widely reported in literature.

### **3.3.3 Elevation angle and its effect on wetting angle**

From the side-on images the angle of elevation and the wetting angle could both be measured. The result is shown in figure 3-5.



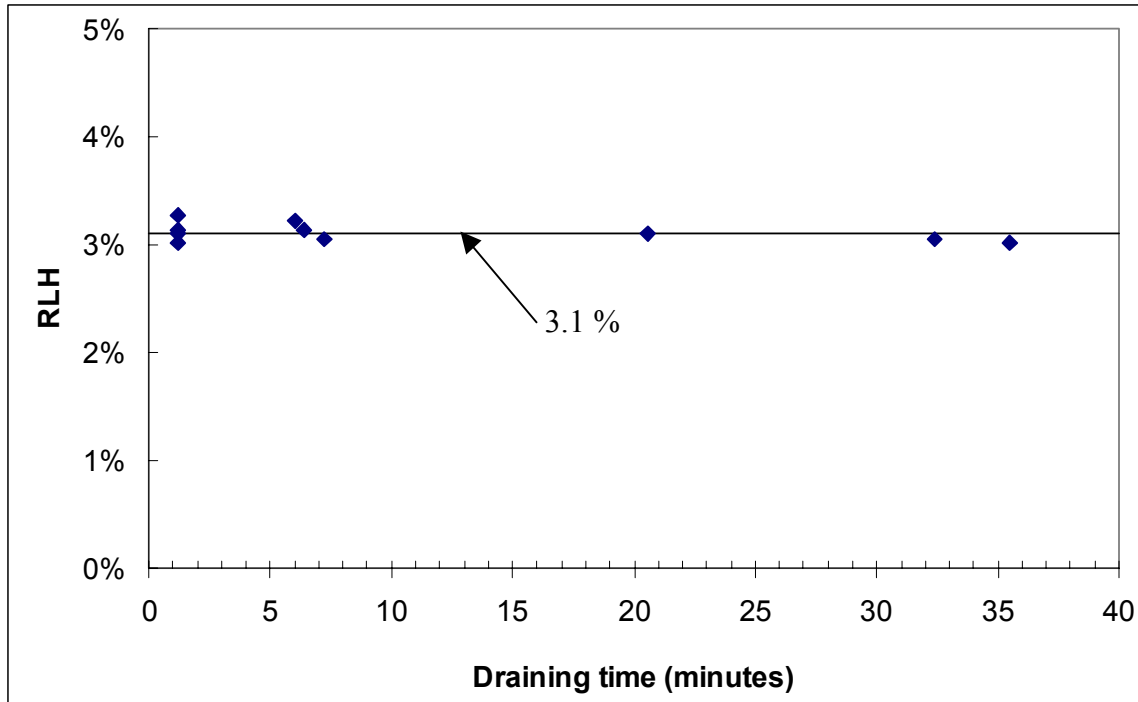
**Figure 3-5.** Wetting angle versus elevation angle

This is clear evidence that:

- In the capillary regime the wetting angle is not uniquely determined by the elevation angle, as is the case for the gravity regime (Turner & Hewitt, 1959)
- The correction factor of 30 % cannot be extrapolated to the capillary regime

### **3.3.4 Residual liquid holdup**

Using the drain-and-weigh technique, the residual liquid holdup measured reproducibly at 3.1 %. (RSD = 2.4 %). This is exactly equal to the value obtained from the most recent empirical correlation (Ortiz-Arroyo *et. al.*, 2003) for the given system. The draining rate was found to have a negligible effect on the RLH (figure 3-6).

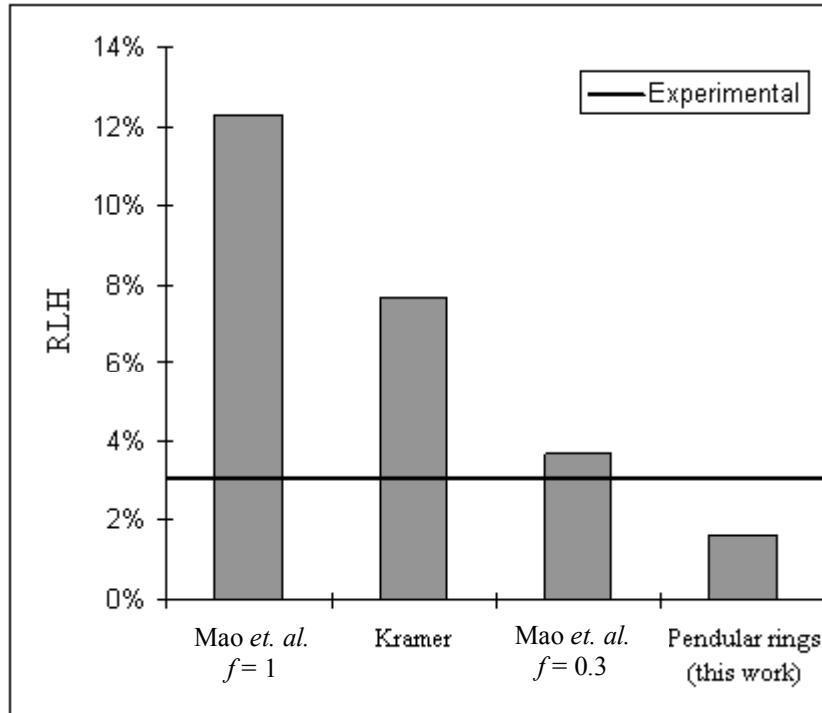


**Figure 3-6.** RLH showing no variance with draining rate

The critical percolation (Kramer, 1998) boundary condition yielded a RLH value of 7.7 %. The internal energy minimization (Mao *et. al.*, 1993) procedure predicted a RLH of 12.3 % (3.7 % with correction factor of 30 %).

In terms of the procedure followed herein, the mean ring volume (from section 3.3.1) is entered into equation 2-7 (with equation 2-8 substituted) to yield an estimate of the residual liquid held in pendular rings throughout the bed. The value obtained is 1.6 %. In summary, the relevant values are compared in figure 3-7 below.



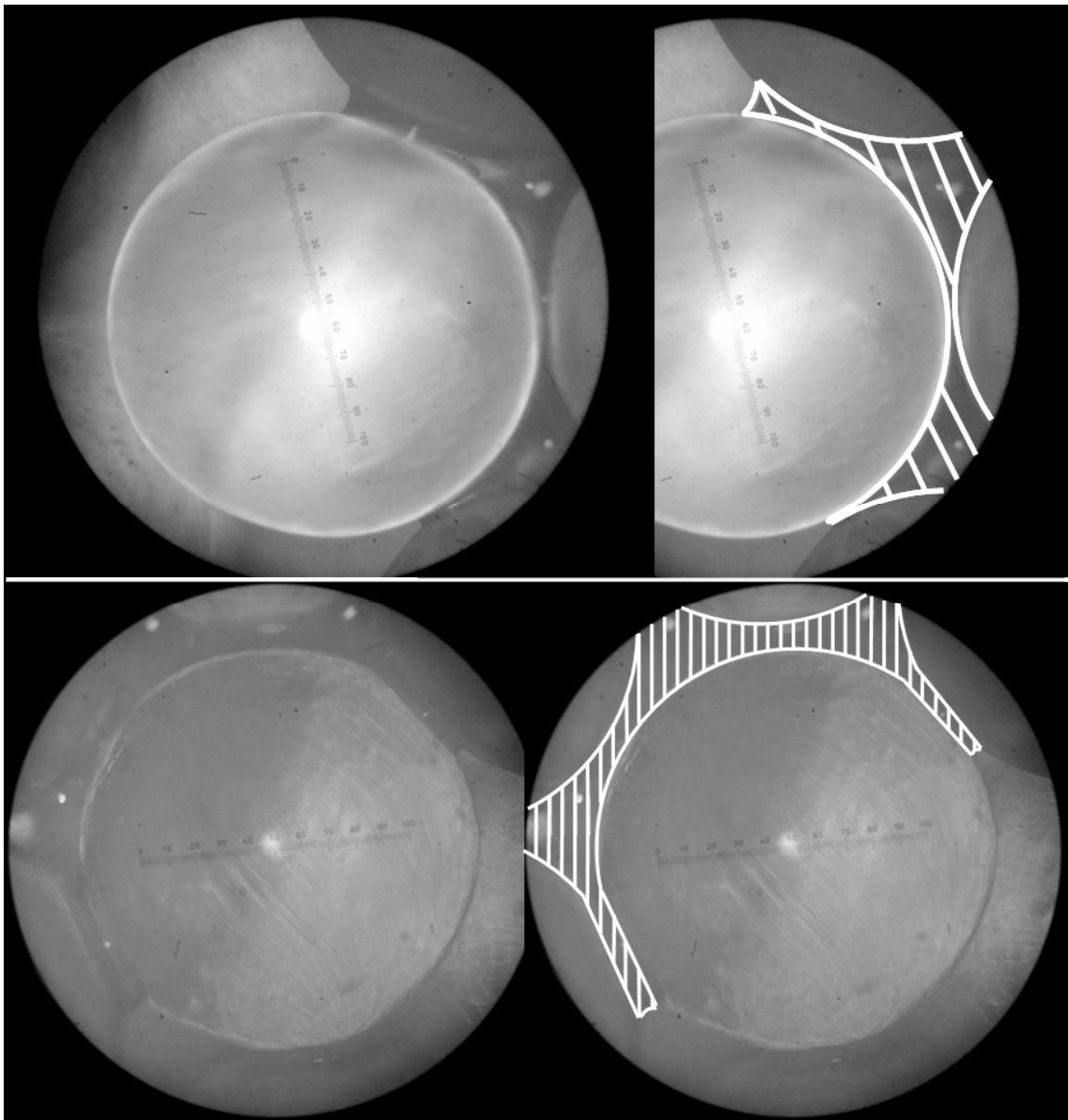


**Figure 3-7.** Comparison of residual holdup predictions and experimental value

### 3.4 Discussion

From the values of the measured wetting angles (figure 3-4 and 3-5) it is evident that the wetting angle is not uniquely determined by the choice of system parameters. It likely depends on additional factors that may include localized draining kinetics, porosity variations and the mechanism of liquid deposition (as was found by Turner & Hewitt, 1959). All wetting angles are between  $28^\circ$  and  $53^\circ$ . This is significantly smaller than the wetting angles used by both Mao *et. al.* (1993) and Kramer (1998). In the case of Mao *et. al.* the thermodynamic criterion is seen to overpredict the size of the rings, even for vertically aligned spheres. Since the correction factor does not apply when small diameter spheres are used, the procedure grossly overestimates the RLH. Kramer's assumption of the rings being at critical percolation cannot be validated – the liquid probably continues to drain through film flow even after the rings have become separated.

The procedure of using the weighted average wetting angle to predict the RLH, clearly underpredicts the experimental result (figure 3-7). It is therefore concluded that the residual liquid holdup is present in forms other than pendar rings. Photographic evidence of such phenomena is given below in figure 3-8, where liquid filled areas have been explicitly indicated on the right hand side images.



**Figure 3-8.** Proof of the existence of liquid globules

The liquid is trapped in globules at locations where more than two particles are in close contact. It is evident that the amount of liquid held in such a globule is more than the sum of the respective pendular rings. The liquid in globules does not drain even though a percolating path downwards exists. Since we have already established that rings continue to drain after separation, both arguments for fixing the wetting angle based on critical percolation seem to fail.

This analysis indicates that 52 % of the RLH is present as pendular rings, whereas the remainder is made up of globules of liquid that cannot be directly associated with particle-particle contact points. The existence of these structures can be rationalized through equation 2-5. Compared to pendular rings, globules have large liquid-solid areas and small gas-liquid areas. Since glass is hydrophilic, the globules represent a thermodynamically more stable liquid configuration. It is probable that this minimum internal energy configuration is only possible in areas of low porosity and that pendular rings represent the minimum configuration in areas of high porosity. In this way, the fraction of RLH made up of globules is an indication of the hydraulic diameter distribution of the packing.

Pendular rings are not at thermodynamic equilibrium as calculated because the act of drainage reduces the amount of liquid below that required for equilibrium. The mechanism of liquid deposition and the local packing porosity are therefore the main contributors to the volume of liquid retained.

Residual liquid holdup is often seen as a dead zone for mass transfer and as a consequence pendular ring geometry has been used to estimate the gas-liquid and liquid-solid interfacial areas (Reddy *et. al.*, 1990). Since a large fraction of the liquid is present in globular form, the pendular ring geometry-based calculations do not apply. Moreover, the globules represent relatively large volumes of liquid that have comparatively small interfacial areas. The globules will therefore influence the mass transfer characteristics of the dead zone.

Consequently, the existence of such structures should be incorporated into gas-liquid-solid transfer models that use residual liquid holdup-gas and residual liquid holdup-solid areas.

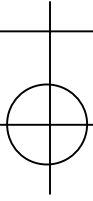
## 3.5 Conclusions

It is concluded that:

- RLH is made up of pendular ring structures at particle-particle contact points and liquid globules at locations where more than two particles are in close proximity
- The rings are not at thermodynamic equilibrium as formulated by Mao *et al.* (1993)
- Neither the thermodynamic stability criterion nor the critical percolation criterion determines the value of the wetting angle for vertically aligned spheres
- The extension to non-vertically alignment in the capillary regime cannot be made from the Turner & Hewitt (1959) correction factor for large spheres in the gravity regime and no equivalent correlation that can be made in the capillary regime seems evident

In the present treatment, the predicted residual holdup is only about half of the measured value, indicating that a large number of globules exist throughout the bed. This has an important impact in terms of the gas-solid and liquid-solid mass transfer in the bed since these regions are expected to represent significant dead zones.

Importantly, the theoretical prediction of RLH is not possible through modeling of pendular ring geometry alone.



---

## Chapter 4. Operating holdup: Literature

---

### 4.1 Introduction

The morphology of the operating holdup is of paramount importance in the design and optimization of trickle flow units. The shape and value of the liquid holdup influences the following factors that may impact unit performance (Iliuta, Larachi & Al-Dahhan, 2000):

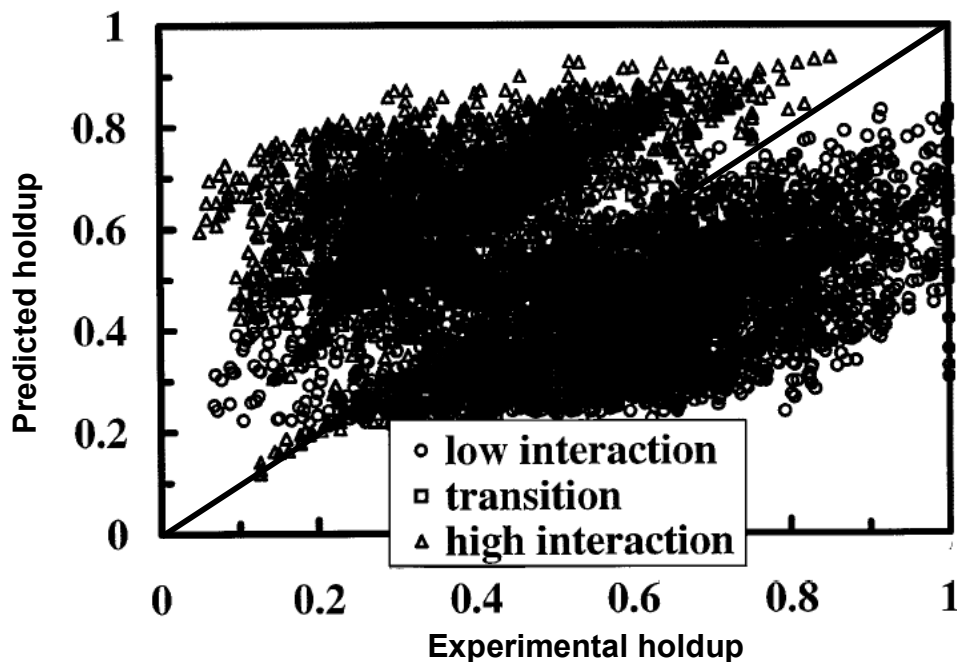
- Catalyst utilization
- Wetting efficiency (including the physical liquid-solid area, the renewal of wetted areas and the liquid velocity distribution)
- Liquid distribution
- Gas-liquid mass transfer (including gas-liquid interfacial area and gas velocity)
- Residence time distribution and axial dispersion
- Pressure drop
- Heat transfer characteristics (including particularly effective radial thermal conductivity and the convective wall heat transfer coefficient)

Sederman & Gladden (2001) state that a great deal of research has concentrated on bed-scale averaged properties (like the value of the liquid holdup), where the reactor is treated as a pseudo-homogeneous system (as reviewed by Satterfield, 1975 and Gianetto *et. al.*, 1978). However, this approach ignores the complexities and local properties of the flow within the inter-particle space despite the fact that these complexities may well be the most important factors in terms of unit performance (or indeed in understanding the bed-scale behaviour).

In this chapter a comprehensive overview of various aspects of the operating holdup is presented as background to chapter 5. The focus is on the existence of multiple flow morphologies within the trickle flow regime that results from

differences in the prewetting procedure. Previous results are reported, but no attempt at explaining them are made until the very last section where a coherent picture of trickle flow is presented.

The operating holdup as a bed-averaged parameter has been the subject of a multitude of studies and a great many empirical and phenomenological models for its prediction have been suggested. For the sake of brevity, the development of all of these models is not discussed. Instead, an indication of the level of understanding of the fundamental phenomena governing liquid holdup is given in figure 3-1 (from Dudukovic, Larachi & Mills, 1999). It is a parity plot of 8000 external liquid holdup data against the predicted holdup using the Ellman *et. al.* (1988) empirical correlation (which is considered to be one of the better holdup correlations). Specifically in the low interaction and transition regimes (trickle flow), it is clear that present predictive capabilities are inadequate.



**Figure 4-1.** Prediction of external liquid holdup (from Dudukovic *et. al.*, 1999)

More accurate empirical correlations have been suggested, but they are very elaborate and the great number of fitted parameters has little physical

significance. Dudukovic *et. al.* (1999) suggest an increased reliance on fundamental approaches in order to enhance holdup predictions. From this perspective, the factors that determine the geometrical form or shape (and by implication the macroscopic value) of the operating holdup should be identified and their effects isolated and quantified if possible.

A brief overview of the relevant literature follows. This chapter is structured as follows:

- The first section describes types or textures of trickle flow that have been identified (and the terminology used through subsequent sections).
- The existence of multiple steady states was discovered through inconsistencies in pressure drop hysteresis studies. The relevant findings are reviewed.
- Since wetting efficiency and flow distribution are pertinent to the results of this study, a summary of wetting efficiency determination is presented.
- This is followed by a review of trickle flow visualization methods and their results.
- Finally, all reported findings are rationalized in terms of a proposed flow morphology.

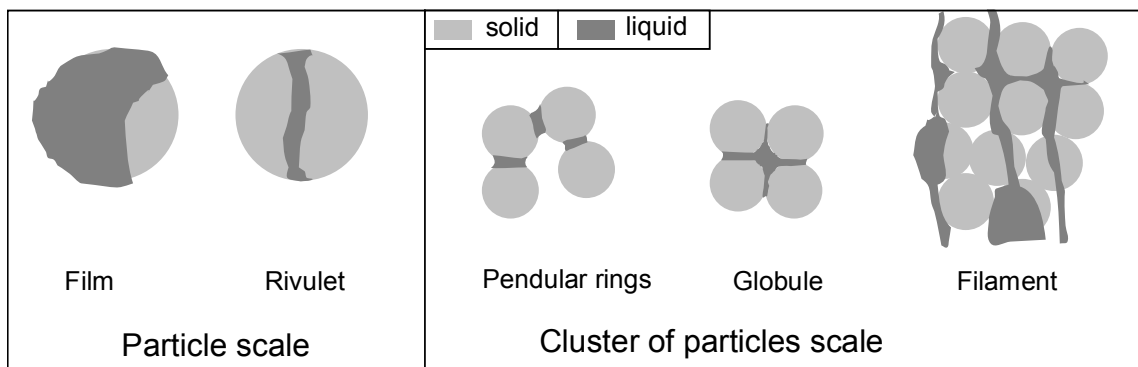
## 4.2 Trickle flow types

It has been suggested that the operating holdup is made up of the following types of flow or flow textures (Zimmerman & Ng, 1986, Ravindra, Rao & Rao, 1997, Lutran, Ng, & Delikat, 1991, Sederman & Gladden, 2001):

- *Films* – Thin laminar liquid streams that cover a particle (or partially cover a particle; characterized by large liquid-solid areas for the given volume liquid)
- *Surface-liquid rivulets* – A continuous stream of liquid over the surface of a particle

- *Pore-liquid rivulets* – Liquid streams that flow down the column in the channels between the particles
- *Pendular rings* – As in chapter 2 except that it may be irrigated
- *Globules* – Liquid pockets that exist in the interstices between particles that are in close contact (when irrigated, these globules may differ in size from those discussed in chapter 2)
- *Filaments* – Liquid pockets connected by film or rivulet flow.

Schematics are shown in figure 4-2.



**Figure 4-2.** Schematics of flow textures

There is an important distinction between particle scale (micro), clusters of particle scale (mesa), and bed-average (macro) flow phenomena (Jiang, Al-Dahhan & Dudukovic, 2001). Films and surface-rivulets are associated with individual particles, whereas pendular structures, globules and filaments are associated with clusters of particles. There is some indication that the liquid globules and pendular rings are irrigated by thin liquid films (Sederman & Gladden, 2001), as opposed to the static residual holdup discussed in chapter 2. It is recognized that many macro-scale reactor parameters including wetting efficiency, holdup and pressure drop are closely coupled to these micro- and mesa-scale flow complexities.

In this study, flow phenomena are described in terms of the texture of the operating holdup. In this regard, a filament is considered to be made up of liquid



pockets (globules or pendular rings) connected by rivulet or film flow (Sederman & Gladden, 2001).

## 4.3 Pressure drop hysteresis

Presently, the focus is on the properties of the various steady states that are obtained as a result of different prewetting procedures. Although the importance of the prewetting procedure had been recognized earlier (Sedriks & Kenney, 1973), the existence of the three distinct states discussed here was discovered through inconsistencies between the pressure drop hysteresis experiments of Kan & Greenfield (1979) and Levec, Grosser & Carbonell (1988).

Before reviewing their pressure drop hysteresis findings, it is prudent to define the various prewetting procedures that have been used in literature. They are:

- **Non-prewetted** (“Non-wetted”)
- **Levec-type prewetting** (“Levec-wetted”) (Levec *et. al.*, 1988)
- **Kan-type prewetting** (“Kan-wetted”) (Kan & Greenfield, 1979)

A non-prewetted bed is a bed packed with completely dry particles. Irrigation starts at the desired flow rate. A Levec-type prewetted bed is a bed that was fully prewetted by flooding the packed column or, alternatively by operating in the pulsing flow regime for a prolonged period (it is known that all the particles are wetted in pulsing flow, Sederman & Gladden, 2001). Once the bed had been prewetted, it is drained under gravity until only the residual liquid holdup remained, or for a specified time (for example 20 minutes, Levec *et. al.*, 1988). Only then is the liquid fed into the column at the desired flow rate. Kan-type prewetting (Kan & Greenfield, 1979) involves the wetting of the bed by flooding or by pulsing flow, followed by draining of the bed *under irrigation*. For a flooded bed, this would imply the liquid being introduced at the desired flow rate at the top as draining commences. For a bed wetted by pulsing flow, the liquid flow rate is reduced from the pulsing rate to the desired level. The first is a limiting case of

the second. Table 4-1 lists references of studies that have used the different prewetting procedures. These studies were conducted with bench scale apparatus with uniform distributors at low pressure. The effect of high pressure on the hysteresis behaviour has not been explored in literature.

**Table 4-1.** Studies grouped by prewetting procedure(s) used

<b>Non-wetted</b>	<b>Levec-wetted</b>	<b>Kan-wetted</b>
Sicardi <i>et. al.</i> (1980a)	Levec <i>et. al.</i> (1988)	Kan & Greenfield (1978)
Kushalkar & Pangarkar (1990)	Levec, Saez & Carbonell (1986)	Kan & Greenfield (1979)
Lazzaroni, Keselman & Figoli (1988)	Christensen, McGovern & Sundaresan (1986)	Lazzaroni, Keselman & Figoli (1988)
Lazzaroni, Keselman & Figoli (1989)	Lutran <i>et. al.</i> (1991)	Lazzaroni, Keselman & Figoli (1989)
Kantzas (1994)	Stegeman <i>et. al.</i> (1996)	Lutran <i>et. al.</i> (1991)
	Sederman & Gladden (2001)	Ravindra <i>et. al.</i> (1997)
	De Klerk (2003)	Sederman & Gladden (2001)

It is important to note that within each flow state (non-wetted, Levec- or Kan-wetted) there exists pressured drop hysteresis. For the non-prewetted and Levec-wetted cases, the hysteresis is associated with the maximum liquid flow rate to which the bed had been subjected (Lazzaroni *et. al.*, 1989, Levec *et. al.*, 1986). For the Kan-wetted bed, the maximum gas flow rate that the bed was subjected to is the determining factor (Kan & Greenfield, 1978). Levec *et. al.* (1986) attributed their hysteresis findings to parts of the bed switching between prewetted modes. In the Kan-wetted case the hysteresis was not associated with changes in the prewetted state.

The focus here is on the existence of the three different hydrodynamic states as *a consequence* of the prewetting procedure and also on the differences in the

texture of liquid holdup in each of these states. It is in this latter sense that the findings of pressure drop hysteresis in each prewetted state are important.

### **4.3.1 Hysteresis in the Kan-wetted mode**

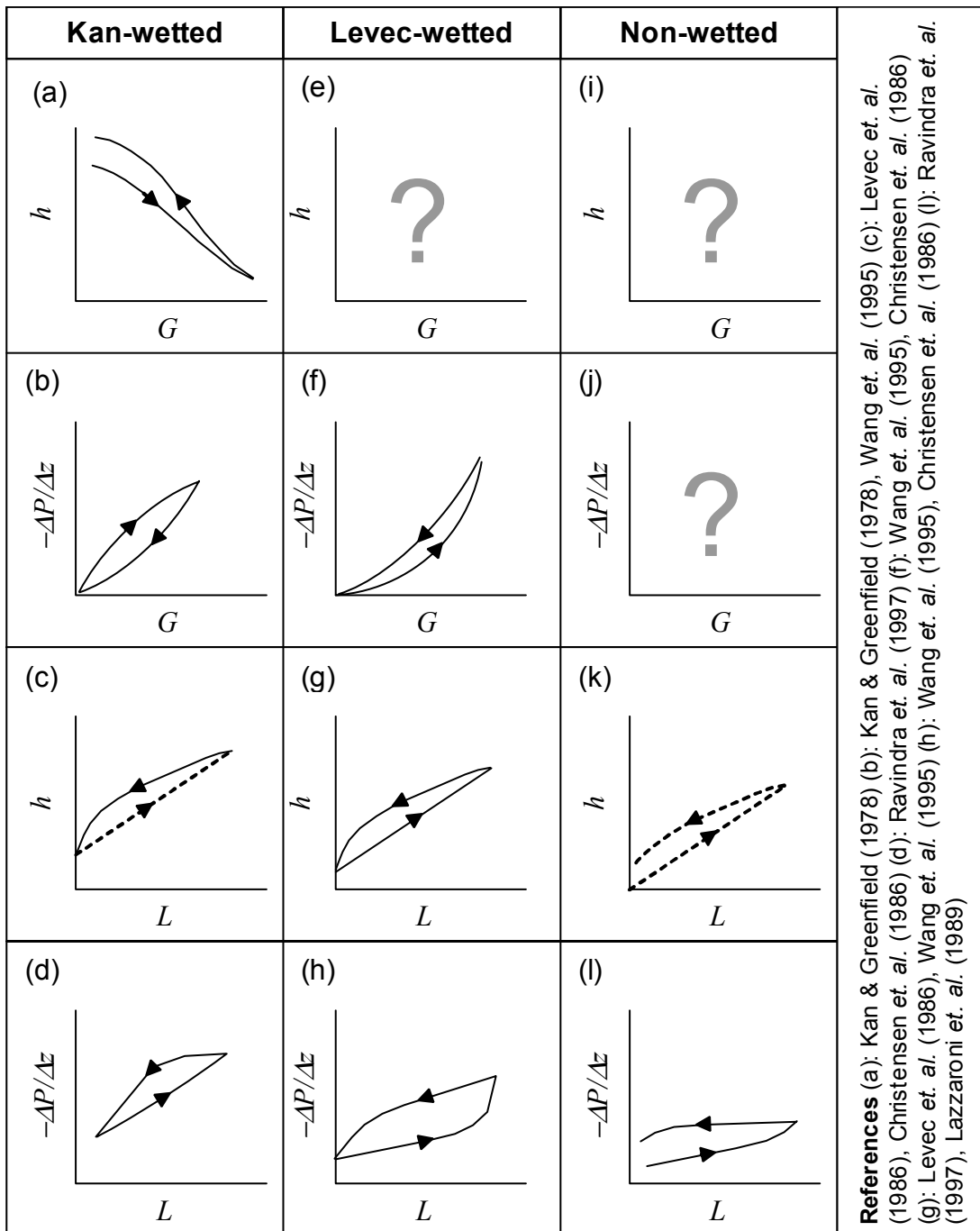
The Kan-wetted mode hysteresis was reported by Kan & Greenfield (1978). Figure 4-3 (a) and (b) show qualitative trends ((a) on log-log scales) of pressure drop and holdup as functions of the gas mass flux history (between 0.01 and 1 kg/m<sup>2</sup>s) in the Kan-wetted mode.

Kan & Greenfield (1978) found that the maximum gas flow rate to which the bed was subjected was the determining factor. They explained the results as follows:

- In the initially wetted bed, liquid bridges are orientated randomly
- An increased gas flux breaks liquid bridges that are orientated transversely to the gas flow, thereby reducing the tortuosity of the gas flow paths
- Upon reduction of the gas flux, the high surface tension effect serves to stabilize the flow pattern
- By virtue of the reduced gas path tortuosity, the pressure drop is now lower than before
- The same liquid volumetric flow is now flowing in smaller channels, resulting in effectively higher velocities and an increased drag force – hence the increased holdup

No hysteresis was observed when the liquid flow rate was changed (from 1 to 3 kg/m<sup>2</sup>s), indicating that this increase was insufficient to re-create the liquid bridges. The holdup hysteresis also disappeared for larger particles ( $\geq 1.8$  mm) although it was still evident in terms of pressure drop.

Note that in this explanation, the flow is visualized as being channeled. It also seems as though the hysteresis is explained by saying that the increased gas flow creates liquid maldistribution.



**Figure 4-3.** Pressure drop and holdup hysteresis trends

This is probably because large gas velocities were used ( $G > 0.05$  m/s) for which an increased gas flow has been linked with increased maldistribution (Marcandelli *et al.*, 2000). It is further supported by the findings of Lazzaroni *et al.*

*al.* (1988) who found that gas flow increases radial maldistribution and that the liquid flow has little effect. Tsochatzidis *et. al.* (2002) and Ravindra *et. al.* (1997) also report the trend that maldistribution results in lower pressure drop. Wang, Mao & Chen (1995) confirm that maldistribution results in higher holdup, but they also associate it with higher pressure drop. Sederman & Gladden (2001) found holdup to be independent of gas flow rate fluctuations (in contrast to figure 3-3 (a)), but they only varied the flux between approximately 0.08 and 0.4 kg/m<sup>2</sup>s for a liquid flux of 3 (instead of 1 kg/m<sup>2</sup>s).

The dashed line in figure 4-3 (c) was not directly observed, but are included by implication of figure 4-3 (d). This may be done because Kan & Greenfield (1978) report that the relation between holdup and pressure drop can be represented satisfactorily by the Specchia & Baldi (1977) correlation. This relationship associates a high pressure drop with a high holdup and vice versa.

The visualizations of Lutran *et. al.* (1991), Ravindra *et. al.* (1997) and Maiti *et. al.* (2004) (of a Kan-rewetted bed's flow being in the form of liquid filaments - connected film flow - over all particles at zero gas velocity) seem to agree with the explanation given above. An increased gas flow rate serves to rupture the thinner films (which are acting as liquid bridges), thereby moving parts of the bed into the Levec-rewetted regime (recall that gas flow may be seen as a desaturation driving force). This has to be supported by pressure drop and holdup trends and values in the Levec-wetted mode. Christensen *et. al.* (1986) supports this idea by assuming that the Kan-wetted mode comprises of film flow only.

Finally, the hysteresis behavior depicted in figures 4-3 (c) and (d) is attributed to different flow uniformities within the Kan-wetted mode. Ravindra *et. al.* (1997) measured liquid distribution in the Kan-mode for increasing and decreasing liquid flow rates, and found the liquid to be more uniformly distributed for decreasing rates (hence the higher pressure drop). That is, the liquid distribution in the Kan-

wetted mode is a function of the flow history and in turn influences the pressure drop and holdup.

### **4.3.2 Hysteresis in the Levec-wetted mode**

Levec *et. al.* (1986) investigated the effect of the liquid flow rate history on pressure drop and holdup. Some of their results are shown in figure 4-3 (g) and (h). Most importantly, they drained the bed for 20 minutes after prewetting, i.e. their results are applicable to the Levec-wetted mode. As a result, they found hysteresis behavior even in the absence of gas flow, and concluded that the maximum liquid flow rate to which the bed had been subjected is the controlling parameter.

In figure 4-3 (g), the higher liquid holdup on the decreasing leg may be explained as follows:

- Liquid films rupture upon initial drainage
- As the liquid flow is increased the bed is operating with channeled liquid flow (although the residual holdup facilitates liquid spreading to a degree)
- The greater liquid velocity spreads the liquid more uniformly (because some channels are filling up). The holdup increases because the liquid-solid interaction is higher (larger liquid-solid area).
- As the liquid flow is decreased, parts of the bed that had received enough liquid to form pore-rivulets are drained *under irrigation*. These parts are now in the Kan-wetted mode.
- For these parts, the increased liquid-solid shear stress associated with film flow results in higher holdups. The macroscopic holdup will therefore be the summation of a small part Kan-wetted holdup and a large part Levec-wetted holdup.

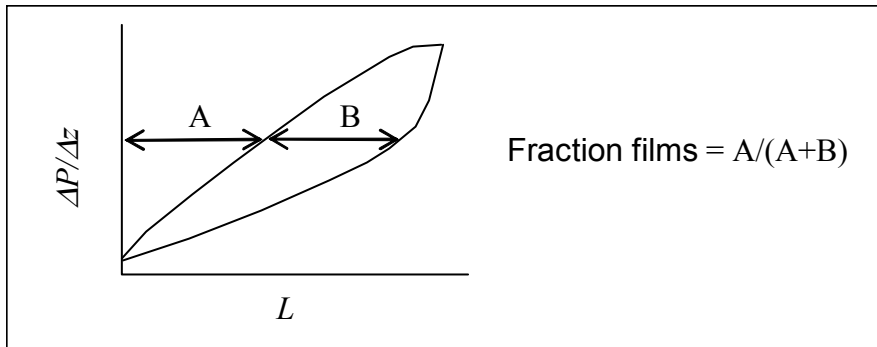
Interestingly, Levec *et. al.* (1986) continued to increase the liquid flow until the column flooded and only then decreased it. Their decreasing leg is therefore in

the Kan-wetted regime (which has higher holdups than the Levec-mode). The same procedure was adopted by Christensen *et. al.* (1986). Note that the hysteresis exist even when the pulsing velocity was not reached. The authors attribute the hysteresis behavior to partial wetting of the packing in the Levec-mode, but make no attempt to quantify the extent of partial bed utilization.

The pressure drop hysteresis results of Wang *et. al.* (1995) in the Levec-wetted mode is informative, especially when compared to that of the Kan-wetted mode (compare figures 4-3 (b) and (f)). They attribute the seemingly contradictory trends to different flow morphologies in the two modes, with the Levec-wetted mode comprised mainly of rivulets and the Kan-wetted mode of films.

Christensen *et. al.* (1986) found the reverse of the trend shown in figure 4-3 (g). Admittedly, their experimental procedure were hampered by the lack of accuracy in the technique used to determine the holdup (the experimental error induced by the microwave probes were larger than the difference in holdup between the increasing and decreasing legs). Their explanation that a higher average liquid velocity in the decreasing leg (which fell in the Kan-wetted mode) would result in lower holdups appear to be erroneous, especially in light of all other investigations that indicated increased holdup at higher velocities. They continue to make a rough estimate of the fraction of liquid flow that is in the form of films. It is the liquid flow rate yielding the same pressure drop as would be the case for pure film flow (upper leg) divided by the actual flow rate. The calculation is shown in figure 4-4.

This shows that the fraction of film flow increases with flow rate. At low gas velocities the fraction of films is roughly constant at approximately 20 % and increases rapidly to 100 % as the pulsing velocity is approached. With higher gas flows this fraction is larger, indicating better liquid spreading.



**Figure 4-4.** Calculation of fraction of film flow in Levec-wetted mode

### **4.3.3 Hysteresis in the non-pretweted mode**

Lazzaroni *et. al.* (1989) studied the hysteresis behavior of a non-pretweted bed of glass spheres. The observed trends are shown in figures 3-3 (k-l). Figure 3-3 (k) is shown with dashed lines because it was inferred from (l) and the fact that the holdup is an increasing function of pressure drop (as stated by the authors). The trends are explained by the fact that increased liquid flow rate results in liquid spreading (because the channels become filled). A reduction in flow rate causes these regions to drain under irrigation, placing them in the Kan-wetted mode. The result is higher liquid holdup and higher pressure drop (by virtue of the decreased cross-section available for gas flow). Note that the holdup in this mode is less than the holdup of the Levec-wetted mode minus the residual holdup. This is mainly because in the non-pretweted mode the lateral spreading effect of the residual holdup is absent.

#### **Note**

The hysteresis trends reviewed here (along with the information of subsequent discussions) are rationalized at the conclusion of this chapter (section 4.7) in terms of a proposed liquid morphology.



## 4.4 Wetting efficiency and liquid distribution

Wetting efficiency is defined as the fraction of the total external solid area that is covered by liquid. However, in its determination researchers often digress toward measuring a solid-liquid contacting effectiveness (Gianetto & Specchia, 1992). This may be particularly important if the solid is wetted in a time-averaged sense as suggested by Mills & Dudukovic (1981). This means that liquid rivulets may meander over the catalytic surface thereby installing a temporal nature to the wetting at a given location.

The operating holdup morphology impacts the wetting efficiency by virtue of the differing liquid distributions associated with the prewetting procedure, as well as by the differences in the nature of the flow textures. This section reviews wetting efficiency determination methods, correlations and trends.

### 4.4.1 Wetting efficiency determination methods

Wetting efficiency has been determined by the following methods:

- Reaction based methods (Morita & Smith, 1978, Llano *et. al.*, 1997). Effective rate constants, for completely externally dry  $(\eta k)_G$  and completely externally wetted  $(\eta k)_L$ , are obtained. With these, the reaction rate is expressed as the sum of reaction rates on dry and wetted surfaces, where the wetting efficiency is used to indicate the relative amounts:

$$r = f(\eta k)_L r_L + (1 - f)(\eta k)_G r_G \quad (4-1)$$

Llano *et. al.* (1997) has shown that there is a discrepancy between wetting efficiencies obtained in this manner and those obtained from tracer data. They attribute the discrepancy to a fraction (16 %) of the catalyst surface

that is not available for reaction because it is covered by non-renewable static liquid.

- The square root of the ratio of the intraparticle effective diffusivities for trickle and liquid-filled operation obtained, as estimated from tracer data (Dudukovic, 1977, Al-Dahhan & Dudukovic, 1995)
- The product of the liquid-solid shear stress and the specific liquid-solid area for two-phase flow as a fraction of the same product for liquid-filled flow (Pironti *et. al.*, 1999). This requires knowledge of the liquid holdup and of the pressure drops for liquid-filled, gas-filled and two-phase flows. These may be obtained by Ergun-type equations or empirically.
- The ratio of apparent adsorption equilibrium constants for two-phase flow and liquid-filled flow, measured by using a two-tracer method (Schwartz, Wegwe & Dudukovic, 1976)
- The ratio of apparent volumetric liquid-solid mass transfer coefficients for two-phase and liquid-filled flow at the same intrinsic velocity (i.e. superficial velocity divided by the holdup). The coefficients were measured with the dissolution of soluble packing (Lakota & Levec, 1990, Gonzalez-Mendizabal, Aguilera & Pironti, 1998)
- The ratio of the intraparticle effective diffusivities for trickle and liquid-filled operations (Colombo, Baldi & Sicardi, 1976)
- Tomographic and colorimetric methods (see discussion below)

#### **4.4.2 Wetting efficiency correlations**

Wetting efficiency is usually correlated in terms of the physical properties of the system and the liquid and gas flow rates. Figure 4-5 shows some of the more commonly used wetting correlations applied to the system: spherical 3 mm glass beads wetted by water, with quiescent air at atmospheric conditions.

It is informative to plot the wetting efficiency as functions of the liquid flow rate on log-log scales (figures 4-6).

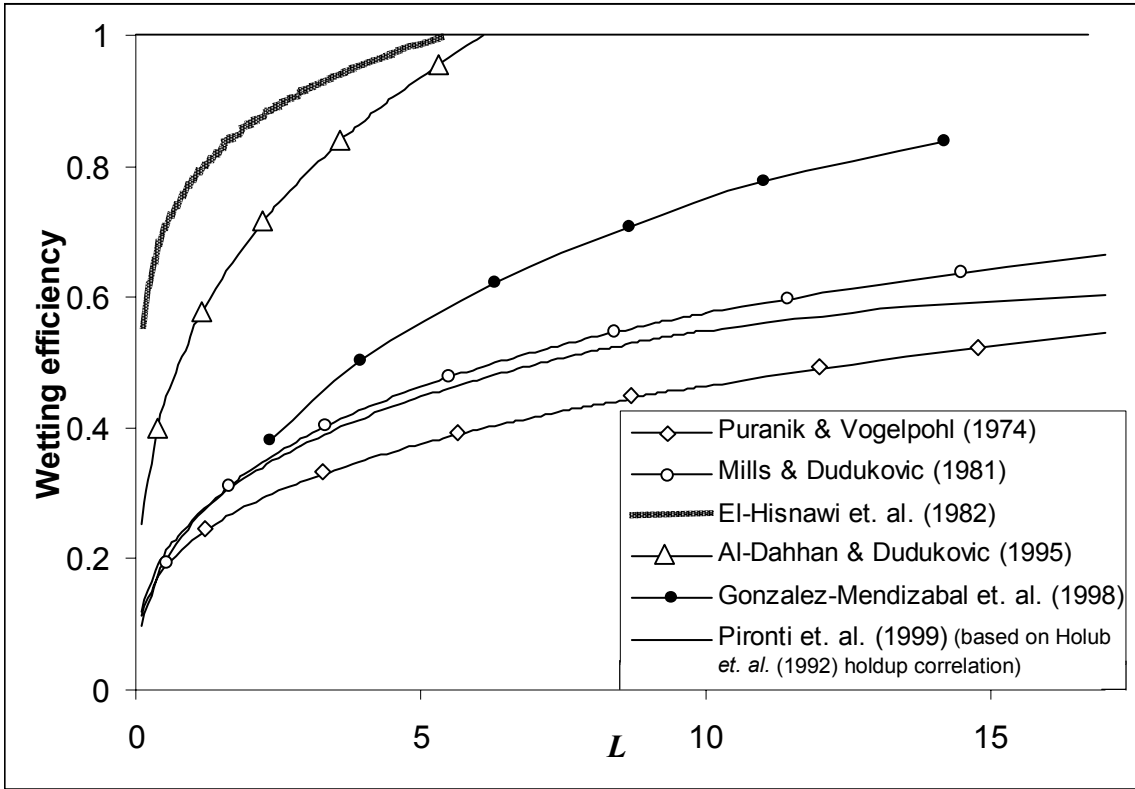


Figure 4-5. Wetting efficiency correlations (air-water-glass system)

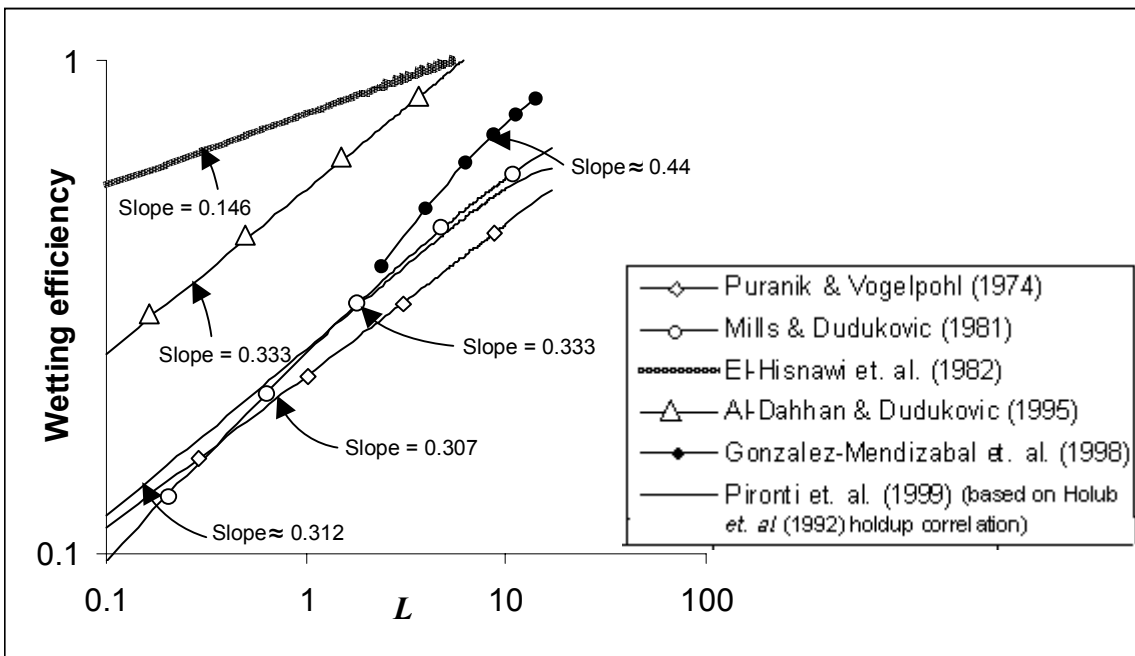


Figure 4-6. Wetting efficiency functional dependency

In figure 4-6, the slopes indicate the power of the liquid flux to which the wetting efficiency is proportional. Of these correlations, only the Al-Dahhan & Dudukovic (1995) correlation is applicable to high pressure.

Importantly, all wetting efficiency trends predict that an increased gas flow rate will result in better wetting (Al-Dahhan & Dudukovic, 1995, Al-Dahhan *et. al.*, 1997). An increased gas flow results in increased gas-liquid shear stress. This corresponds to decreased liquid holdup and decreased film thicknesses. The pressure drop increases despite the fact that the tortuosity of the gas path decreases. This is because the increased velocity is accompanied by an increased drag force which overcomes the tortuosity effect. The increased shear stress results in improved liquid spreading, which results in a higher wetting efficiency.

## 4.5 Trickle flow visualization techniques

Two ways of directly studying the morphology of trickle flow directly are computed tomography and colorimetric testing. Table 4-2 lists various visualization techniques that have been used to study two-phase flow through packed beds.

Some of these studies were on systems vastly different from spherical glass beads under water and air flow and are therefore ignored. In other cases, the investigators specifically researched the pulsing flow regime. Many of these authors did not explicitly state the prewetting procedure employed. For example, Yin *et. al.* (2002) appeared to have worked with a non-prewetted bed. Their holdup distribution results seem to indicate that channeled flow did indeed occur within the bed. Another example is Marcandelli *et. al.* (2000), who report that increased gas and liquid flow rates decrease maldistribution except at high flow rates where increased gas flow rate increases maldistribution. They do not however, state their prewetting procedure.

**Table 4-2.** Two-phase flow visualization techniques and references

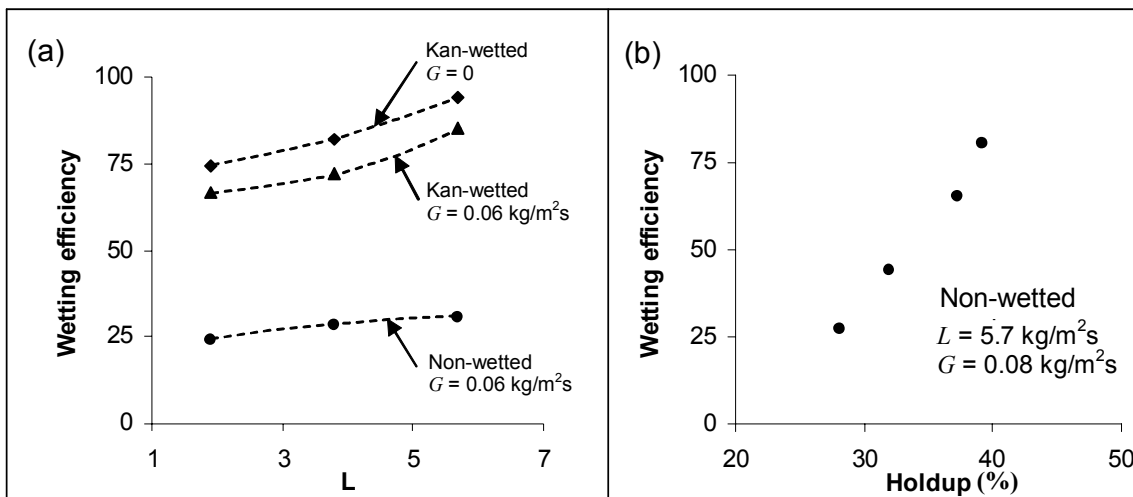
	<b>Technique</b>	<b>Reference(s)</b>
<b>Computed tomography</b>	X-ray tomography	Lutran <i>et. al.</i> (1991) Kantzas (1994) Toye <i>et. al.</i> (1998)
	Gamma-ray tomography	Boyer & Fanget (2002) Kumar <i>et. al.</i> (1995) Yin <i>et. al.</i> (2002)
	Magnetic resonance imaging (MRI)	Sederman & Gladden (2001) Gladden <i>et. al.</i> (2003)
	Capacitance tomography	Marcandelli <i>et. al.</i> (2000) Reinecke & Mewes (1997)
<b>Colori-metric</b>	Dye adsorption	Ravindra <i>et. al.</i> (1997)
	Coloring reactant	Lazzaroni <i>et. al.</i> (1988) Lazzaroni <i>et. al.</i> (1989)

The comprehensive studies of Lazzaroni *et. al.* (1988,1989), Lutran *et. al.* (1991), Ravindra *et. al.* (1997) and Sederman & Gladden (2001) warrant a more detailed discussion. The focus here is on non-porous particles and on the morphologies of the liquid holdup in the different prewetting modes.

#### **4.5.1 Reaction based colorimetrics (Lazzaroni *et. al.*, 1988,1989)**

Chrome-Azurol-S is reacted on alumina for non-prewetted and Kan-wetted beds. It is an irreversible reaction that leaves the particles discolored where they were wetted. Measurement of the intensity of the color from a mixed sample of particles makes it possible to determine how much area had been wetted.

In the Kan-wetted mode, it was found that increased gas flow caused distortions in the radial wetting efficiency profiles, whereas liquid flow rate did not affect the radial wetting distribution. Importantly, the wetting efficiency differed drastically for the Kan-wetted and non-prewetted modes. Figure 4-7 (a) repeats some of the results. For the non-prewetted mode, the wetting efficiency as a function of holdup is shown in figure 4-7 (b) for the flow rates shown.



**Figure 4-7.** Wetting efficiency results for Kan- and non-prewetted modes (Lazzaroni *et. al.*, 1988,1989 data)

This is clear indication that parts of the bed remained non-irrigated for the time that the reactant was passed through the reactor (20 minutes). Furthermore, it shows that the maldistribution of liquid in the non-prewetted mode is far more severe than in the Kan-wetted mode. An increased gas flow decreases the wetting efficiency in the Kan-wetted mode because liquid films are ruptured (as seen from the pressure drop hysteresis trends reported earlier). Unfortunately, the effect of gas flow rate was not investigated for the non-prewetted mode.

#### **4.5.2 Longitudinal X-ray tomography (Lutran et. al., 1991)**

The authors scanned a square column packed with glass spheres with a medical CT scanner, yielding pictures of longitudinal slices of the bed. All three prewetted modes were investigated in this manner, although in the results the only distinction reported between Kan- and Levec-wetted beds is that the holdup appears to be higher in the former mode and that this indicates a possible hysteresis effect. In this technique the wetting is not explicitly measured, but inferred visually.

For the non-prewetted bed, pore-rivulet flow could be clearly discerned. Only about 6 rivulets were evident in the bed although the inlet distributor had 25 point inlets. The rivulets meandered back and forth and also merged and split with seemingly random frequency. An increased liquid flow resulted in the lateral expansion of existing rivulets (leading to branching in a few cases) and sometimes in the creation of new rivulets. However, when large particles were used (6 mm), there was predominantly film flow with a few incomplete pore-rivulets at low liquid flows. The creation of rivulets took place at higher liquid flow rates.

In the Kan-wetted regime, film flow was evident. Liquid filled pockets formed at locations of several particles in close contact and these were connected by the films (filament flow). Increased liquid flow resulted in increased film thickness and eventually to increased rivulet flow as pore channels became filled and connected.

Again, prewetting is seen to decrease maldistribution.

### **4.5.3 Dye-adsorption colorimetrics (Ravindra et. al., 1997)**

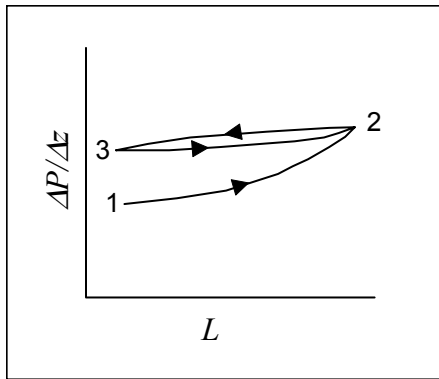
In this method, a bed is packed with glass bead and irrigated by water until steady state is reached. A methylene-blue solution is then introduced into the column for 4-5 minutes. The methylene-blue adsorbs onto the glass, allowing analysis of the liquid distribution and the wetting phenomena. The feed is then stopped and the column is drained. The bed is photographed from the top. A specified height of packing is then removed and the bed is photographed, yielding a cross-sectional image. This procedure is repeated for various packing heights. Both a non-pretreated and a Kan-wetted bed were investigated. In this procedure, no wandering surface-rivulets were observed, and it was assumed that colored surfaces were always wetted with liquid.

For the non-pretreated mode, channel flow was observed. The pore-rivulets meandered, merged and split randomly with bed depth. At all depths, about 50 % of the bed was wetted by liquid ( $d = 1.6 \text{ mm}$ ,  $L = 1 \text{ kg/m}^2\text{s}$ ,  $G = 0.05 \text{ kg/m}^2\text{s}$ ). For large particles, the channels were in filament flow. Medium sized particles exhibited pore-rivulets with surrounding film flow. For very small particles, the lateral capillary force is large and the liquid spreads, perhaps forcing the gas into channeled flow. Interestingly, no particles were found to be partially wetted, contradicting the statement of Dudukovic (1977).

The hysteresis of the non-pretreated bed is shown qualitatively for more than one liquid rate variation cycle in figure 4-8.

In the first cycle (1→2), increased liquid rate help liquid spreading, wetting parts of the bed that had been dry. When the rate is decreased (2→3), those parts of the bed are in the Kan-wetted mode.





**Figure 4-8.** Hysteresis in the non-pretweted mode (qualitatively)

When the liquid rate is increased again it re-wets these pretweted zones - as in the Kan-mode (3→2). Here, the pressure drop does not change dramatically because only a small part of the bed is in the Kan-mode, and the gas flows through the large part of the bed that remains dry. The liquid therefore does not change the tortuosity of the gas path much.

This effect is more pronounced for bigger particles (i.e. the smaller holdup associated with bigger particles influences the gas flow even less). This is why the second increasing leg (3→2) practically falls on the decreasing leg (2→3) when larger particles are used (as found by Ravindra *et. al.*, 1997).

In the Kan-pretweted bed all particles acquired color, indicating that film flow prevailed (and that the wetting efficiency is close to one). The procedure does not allow the division of liquid-filled pockets and film flow covered regions (since both will discolor) and filaments can therefore not be identified. In this pretweted bed, the liquid distribution (as measured by annular collectors) was shown to be more uniform for decreasing liquid rates (explaining the hysteresis). This is attributed to the phenomenon that thick and thin films exist in the increasing mode, but that the film thicknesses are more uniform in the decreasing mode.

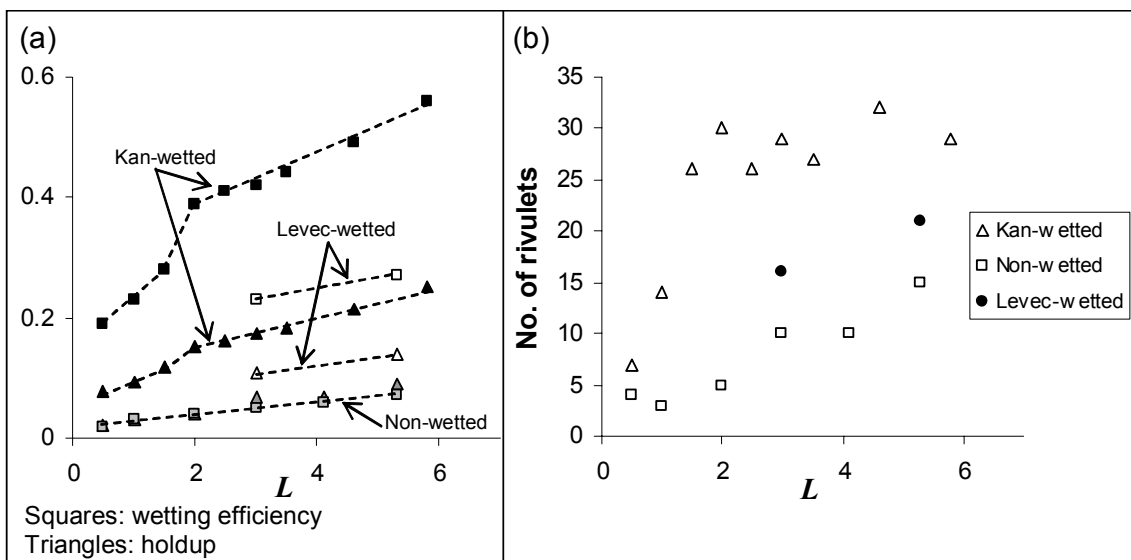
Interestingly, the authors state that a pretweted and drained bed (Levec-wetted) is expected to behave as a non-pretweted bed. This is expected to be true for

large particles because the RLH left upon draining is small and far apart and does not aid lateral liquid distribution.

#### **4.5.4 Cross-sectional magnetic resonance imaging** **(Sederman & Gladden, 2001)**

A MRI scanner is used to obtain cross-sectional images of trickle flow through a bed packed with 5 mm glass ballotini. The image is discretized into voxels spanning  $313 \mu\text{m} \times 313 \mu\text{m}$ . The fraction of these voxels that contain liquid is a measure of the holdup. Wetting efficiency may be determined by the fraction of surface-touching voxels that contain liquid. All three prewetting modes are investigated.

The authors further define a pore as a portion of the void space bounded by solid surfaces and by “necks” where the hydraulic radius of the void space exhibits local minima. This allows the identification of pore-rivulets inside these pores. The number of pore-rivulets can then be determined unambiguously. The results for the three modes are shown in figure 4-9.



**Figure 4-9.** Results of MRI investigation, (a): Holdup and wetting efficiency, (b): Number of rivulets (Gas velocity = 66 mm/s)

The results clearly indicate the differences in holdup, wetting efficiency and rivulet count for each flow regime. Importantly, in contrast to the expectations of Ravindra *et. al.* (1997) there is a marked difference between the Levec-wetted and non-pretwetted modes, even for the large particles used here (5 mm).

The wetting efficiency is far below that of other investigators (see section 4.4), even for the Kan-wetted mode. This is contradictory to the colorimetric results reported above that indicated that all particles were wetted in this mode. This may be because the MRI method does not detect thin liquid films, and can therefore not distinguish filament flow. In addition, the particle size may well play a role. For such large particles, the gas flow strips the thinner films and the Kan-wetted mode tends toward local Levec-wetted areas. This is even further supported by the fact that gas flow rate changes had no effect on either the holdup or the wetting efficiency (because the thinner films were already broken). Nevertheless, this is qualitative indication that severely low wetting efficiency is encountered in the non-pretwetted mode, and that the wetting efficiency is lower in the Levec-wetted mode than in the Kan-wetted mode. The same trend is evident in the holdup data. This is indication that the extent of liquid distribution in the three modes differs appreciably, with distribution being better in the Kan-wetted mode, followed by the Levec-wetted mode and then the non-pretwetted mode.

The authors state that in the Kan-wetted mode and at low liquid rates, most of the liquid is present as films. An increase in liquid rate up to  $L = 2 \text{ kg/m}^2\text{s}$  results in the formation of rivulets. After this, the existing rivulets expand and no new rivulets are created (figure 4-9 (b)). Above and below this threshold, the wetting efficiency exhibits a functional dependency on the liquid velocity. The wetting efficiency is proportional to the 0.33 power of the liquid velocity. This compares well with Puranik & Vogelpohl's (1974) suggested power of 0.32 and with the power of 0.333 of the Al-Dahhan & Dudukovic (1995) correlation. Above and below the threshold velocity, the wetting efficiency is proportional to the

saturation to the power of 0.27. This compares reasonably well with the 0.224 reported by Al-Dahhan & Dudukovic (1995).

The rivulets observed in the Levec-wetted mode were larger and more distinct than those in the Kan-wetted mode, indicating that the former was dominated by rivulet flow and the latter by film flow.

In the Kan-wetted mode, a liquid velocity of 3 mm/s was accompanied by two distinct pore filling fractions, namely 20 % full and 90 % full. The former clearly corresponds to film flow and the latter to pore-rivulet flow. When the velocity was decreased to 1 mm/s, not only were there fewer rivulets, but the pore channels were not full (i.e. the 90 % peak disappeared). At lower velocities, there is predominantly film flow, with rivulets being created at higher velocities.

Finally, there is indication that particles with more contact points have greater surface wetting fractions. In this case, the authors report that nearly all particles were partially wetted (as opposed to the results of Ravindra *et. al.*, 1997).

## 4.6 Holdup models

Since the bed-averaged value of the holdup appears to be dependent on the prewetting mode, a review of holdup correlation is necessary.

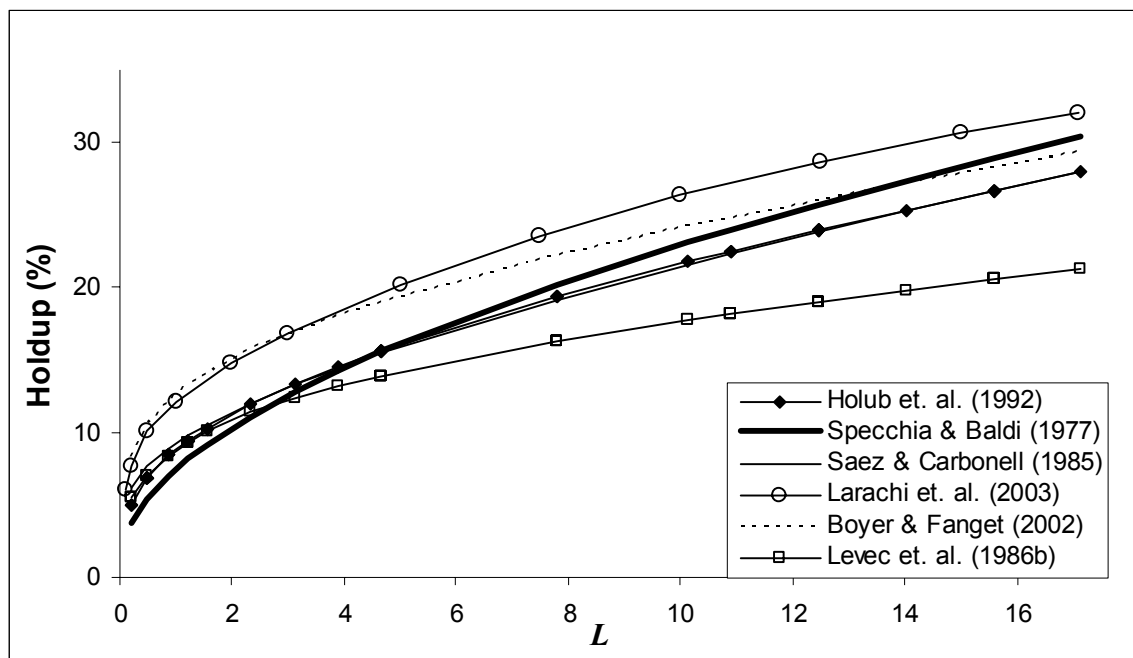
### 4.6.1 Correlations

Numerous holdup correlations have been suggested. Many of these are empirical and lack generalization (Iliuta, Larachi & Al-Dahhan, 2000). The models can be roughly grouped into (Carbonell, 2000):

- Empirical and semi-empirical models (e.g. Specchia & Baldi, 1977 and the artificial neural networks of the Laval University group, e.g. Larachi *et. al.*, 2003)

- Phenomenological models (e.g. the slit model of Holub, Dudukovic & Ramachandran, 1992 and its many extensions)
- Relative permeability models (Saez & Carbonell, 1985)
- Fluid-fluid interfacial force model (e.g. Boyer & Fanget, 2002)

A plot of holdup as a function of the liquid mass flux for commonly preferred models are shown in figure 4-10 for the 3 mm glass spheres-quiescent air-water system. Note that some models correlate the free-draining holdup. In figure 4-10, the residual holdup as obtained through the most recent correlation (Ortiz-Arroyo *et. al.*, 2003) was added to the free-draining holdup in order to determine the operating holdup.



**Figure 4-10.** Commonly used liquid holdup correlations for no gas flow

Larachi *et. al.* (2003) recommend the slit model of Holub *et. al.* (1992) or their own ANN correlation for trickle flow without gas flow. However, for the choice of system parameters shown, there is a marked difference between these correlations. The proposed correlation of Boyer & Fanget (2002) also does not

consider gas flow, whereas the correlations of Specchia & Baldi (1977) and Saez & Carbonell (1985) are valid for zero gas velocity and seen to be practically equivalent.

Interestingly, the double slit model (Iliuta *et. al.*, 2000) predicts a linear relationship between holdup and liquid velocity for the case of no gas flow. Specifically for no gas flow, the correlation proposed by Wammes, Mechielsen & Westerterp (1991) is, for all practical purposes, equivalent to the Specchia and Baldi (1977) correlation for  $Re > 5$  and to the Holub *et. al.* (1992) correlation for  $Re < 4$ . Recently, it was found that the Specchia & Baldi (1977) and Saez & Carbonell (1985) correlations are more suitable for the low liquid flux region (De Klerk, 2003). Also, the Holup *et. al.* (1992) and Saez & Carbonell (1985) correlations coincide for this system.

#### **4.6.2 Momentum balances for fully wetted film flow**

##### **(Boyer & Fanget, 2002)**

The fluid-fluid interfacial force models are based on momentum balances of the liquid and gas phases. For fully wetted film flow, they are given below for the liquid and gas phases respectively:

$$-\frac{\varepsilon_L}{\varepsilon} \frac{dP}{dz} = \frac{\tau_{LS}\phi_{LS}}{S} - \frac{\tau_{LG}\phi_{LG}}{S} - \frac{\varepsilon_L \rho_L g}{\varepsilon} \quad (4-2)$$

$$-\left(1 - \frac{\varepsilon_L}{\varepsilon}\right) \frac{dP}{dz} = \frac{\tau_{LG}\phi_{LG}}{S} - \left(1 - \frac{\varepsilon_L}{\varepsilon}\right) \rho_G g \quad (4-3)$$

Elimination of the pressure drop yields:

$$\frac{\tau_{LS}\phi_{LS}}{S} - \frac{1}{1 - \left(\frac{\varepsilon_L}{\varepsilon}\right)} \frac{\tau_{LG}\phi_{LG}}{S} - \frac{\varepsilon_L (\rho_L - \rho_G) g}{\varepsilon} = 0 \quad (4-4)$$

It is assumed that the gas density is negligible compared to the liquid density (which is the case for the ambient air-water system). Given this, a zero gas velocity (quiescent air) results in a zero gas-liquid stress force and the second term of equation 4-4 may be omitted.

Classically (Ergun, 1952), the liquid-solid stress term is expressed as the sum of a laminar term and a turbulent term (Kozeny-Carman formalism). For the laminar term, the velocity profile in the liquid is assumed to be parabolic, making it possible to use a space-averaged velocity and the hydraulic radius to express the term as:

$$\left. \frac{\tau_{LS} \wp_{LS}}{S} \right)_{\text{laminar}} = f_s \frac{2}{R_h^2} \mu_L \langle v_L \rangle \quad (4-5)$$

$$R_h = \frac{\varepsilon_L d}{1 - \varepsilon} \quad \text{and} \quad \langle v_L \rangle = \frac{v_L}{\varepsilon_L} \quad (4-6)$$

The factor  $f_s$  is taken as 25/12 to take into account the bed tortuosity (Bird, Stewart & Lightfoot, 1966, cited by Boyer & Fanget, 2002). It is the ratio of the actual path length to the vertical distance traveled.

Also, the turbulent term is expressed as:

$$\left. \frac{\tau_{LS} \wp_{LS}}{S} \right)_{\text{turbulent}} = f_w \frac{1}{2} \rho_L \langle v_L \rangle^2 \frac{\wp_{LS}}{S} \quad (4-7)$$

The shear stress coefficient  $f_w$  is taken as 7/12 (Bird *et. al.*, 1966, cited by Boyer & Fanget, 2002). The ratio  $\frac{\wp_{LS}}{S}$  is the specific surface area ( $6(1-\varepsilon)/d$  for spheres).

The right hand side of the turbulent term can be expressed in terms of the particle diameter, the bed porosity, the holdup and the superficial velocity.

Summation of the laminar and turbulent terms and substitution into equation 4-4, yields:

$$150\mu_L \frac{(1-\varepsilon)^2}{\varepsilon_L^3} \frac{v_L}{d^2} + 1.75\rho_L \frac{(1-\varepsilon)v_L^2}{\varepsilon\varepsilon_L^2 d} - \frac{\rho_L\varepsilon_L g}{\varepsilon} = 0 \quad (4-8)$$

This is the Boyer & Fanget (2002) holdup correlation presented in figure 4-7. Note that it is applicable to *film flow over the entire available solid surface area*.

### **4.6.3 Other holdup models for the Kan-wetted mode**

Two holdup models were specifically correlated for two cases of the Kan-wetted mode. Kan & Greenfield (1979) extended the Turpin & Huntington (1967) holdup correlation by incorporating a parameter that accounts for the maximum gas flow rate to which the bed had been subjected. It is not applicable to stagnant gas conditions and is therefore not discussed further.

Levec *et. al.* (1986b) obtained a correlation for the decreasing liquid flow rate leg of the Kan-wetted mode. Its results are shown in figure 4-10. It is seen to differ appreciably from the other generally accepted correlations.

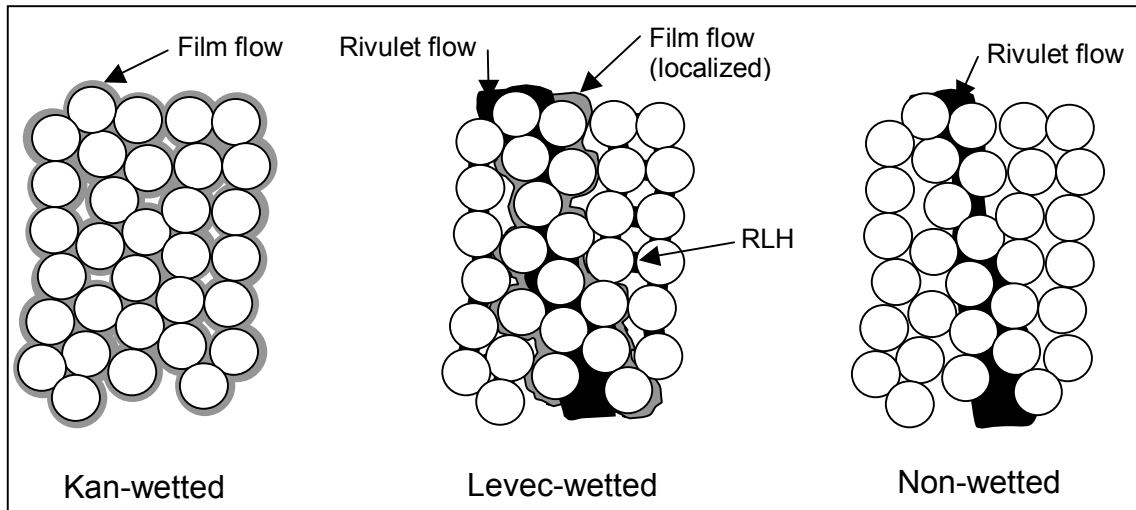
## **4.7 Conclusions and rationalization**

From the review of the literature the following conclusions can be drawn:

- There are multiple stable liquid morphologies in trickle flow, and if left alone, a bed will not revert to any other configuration than the one it is currently in.
- There appear to be three limiting cases to prewetting: Kan-wetted, where film and filament flow dominate, Levec-wetted, where dispersed rivulet (channeled) flow dominate, and non-wetted, where channeled flow dominates (fewer channels than Levec-wetted).
- The wetting efficiency in each prewetted mode differs appreciably.



When all the information is considered, a coherent picture of the flow morphologies in each prewetted mode emerges. It is depicted schematically in figure 4-11.



**Figure 4-11.** A 2-D depiction of the proposed liquid holdup morphologies in each prewetted mode

This trickle flow visualization allows the rationalization of the trends observed in literature to date and reported in preceding sections. First, the poor prediction of holdup (illustrated by figure 4-1) may be partially explained by Table 4-1, where it is evident that researchers have used vastly different prewetting procedures and in many cases did not report the prewetting procedure. Importantly, depending on the exact prewetting conditions and the flow history, the bed may be operating anywhere between the non-prewetted and Kan-wetted modes. This may well explain some of the seemingly insoluble differences in experimental holdup and wetting efficiency data sets.

The discussion around the pressure drop and holdup hystereses trends (figure 4-3) can be summarized in terms of the liquid morphology in each prewetted mode as follows. In the Kan-wetted mode, increased gas flow increases the gas-liquid shear and results in the breakage of the thinner films. Upon decreasing the gas

flow these films are not reestablished and these parts of the bed operate in the Levec-wetted mode (which has lower holdup per volume because a part of the volume is not utilized for flow). The gas flows predominantly through these regions where the gas-liquid interaction is less (i.e. lower pressure drop). This explains figure 4-3 (b). Note that increased gas velocity naturally decreases the holdup because of the increased gas-liquid drag. This effect cannot adequately explain the hysteresis however.

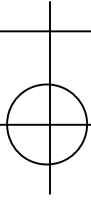
Figure 4-3 (a) warrants further discussion. The instant the films are broken, there is a decrease in the liquid-solid area that reduces the liquid-solid shear stress-area product (see equation 4-2). Simultaneously, there is a momentary increased liquid velocity in the remaining films, resulting in an increased liquid-solid drag and a thickening of the films. This thickening corresponds to a decreased velocity and a new equilibrium is established (to satisfy the momentum balance). In fact, the effect is fully enclosed in equation 4-5 if the effect of the gas is contained to a breaking of films. A decrease in the specific liquid-solid area  $\left(\frac{\phi_{LS}}{S}\right)$  is balanced by a decrease in the interstitial velocity (i.e. an increased holdup, by equation 4-6).

Figures 4-3 (c) and (d) are now easily understood when it is recognized that increased liquid flow reestablishes film flow. Upon decreasing the liquid flow the film flow are preserved and both pressure drop and holdup is higher. This also explains figures (g), (h), (k) and (l) since the increased liquid flow establishes film flow where it did not previously exist and this film flow is preserved when the flow rate is reduced.

Figure 4-3 (f) is interesting in that it predicts a pressure drop versus gas flow trend for the Levec-wetted mode that is opposite to that of the Kan-wetted mode. Increased gas flow spreads the films surrounding the pore-rivulets more thinly, invariably causing some to break but also establishing thin film flow on previously

dry surfaces (by virtue of an increased gas-liquid shear stress). Another possible explanation that follows from the fact that the pore channels are only 90 % filled (Sederman & Gladden, 2001), is that the gas flow competes with the liquid inside the pore channel and increased gas flow therefore forces some of the liquid out into the surrounding volume. Gas flow increases liquid spreading in this mode. When the gas flow is reduced, the newly established film flow is retained and the gas now has a smaller cross-sectional area to flow through – resulting in a higher pressure drop. The pressure drop hysteresis is less pronounced in the Levec-mode possibly because the increased liquid spreading is partially negated by breakage of the thinner films surrounding the rivulet. Since enhanced liquid spreading means that more of the solid surface is covered by liquid, the wetting efficiency will increase with gas flow.

In a bed operated somewhere in between the Kan- and Levec-wetted modes the effect of increased gas flow can also be rationalized as follows. If not all of the solid surface is covered by liquid (partial wetting) at given fluid flow rates, an increase in gas flow rate may spread the liquid more thinly over more area. This will increase the liquid-solid interaction area (wetting efficiency), thereby increasing holdup, but simultaneously lower the effective interstitial velocity of the liquid, thereby lower the drag force and the holdup. Which of these effects will dominate will depend on the solid geometry and the mechanism of spreading. However, it seems as though it may well be the latter as trends of increased wetting but decreased holdup with increased gas flow are generally accepted (Al-Dahhan & Dudukovic, 1995).



---

## Chapter 5. Operating holdup morphology

---

### 5.1 Introduction

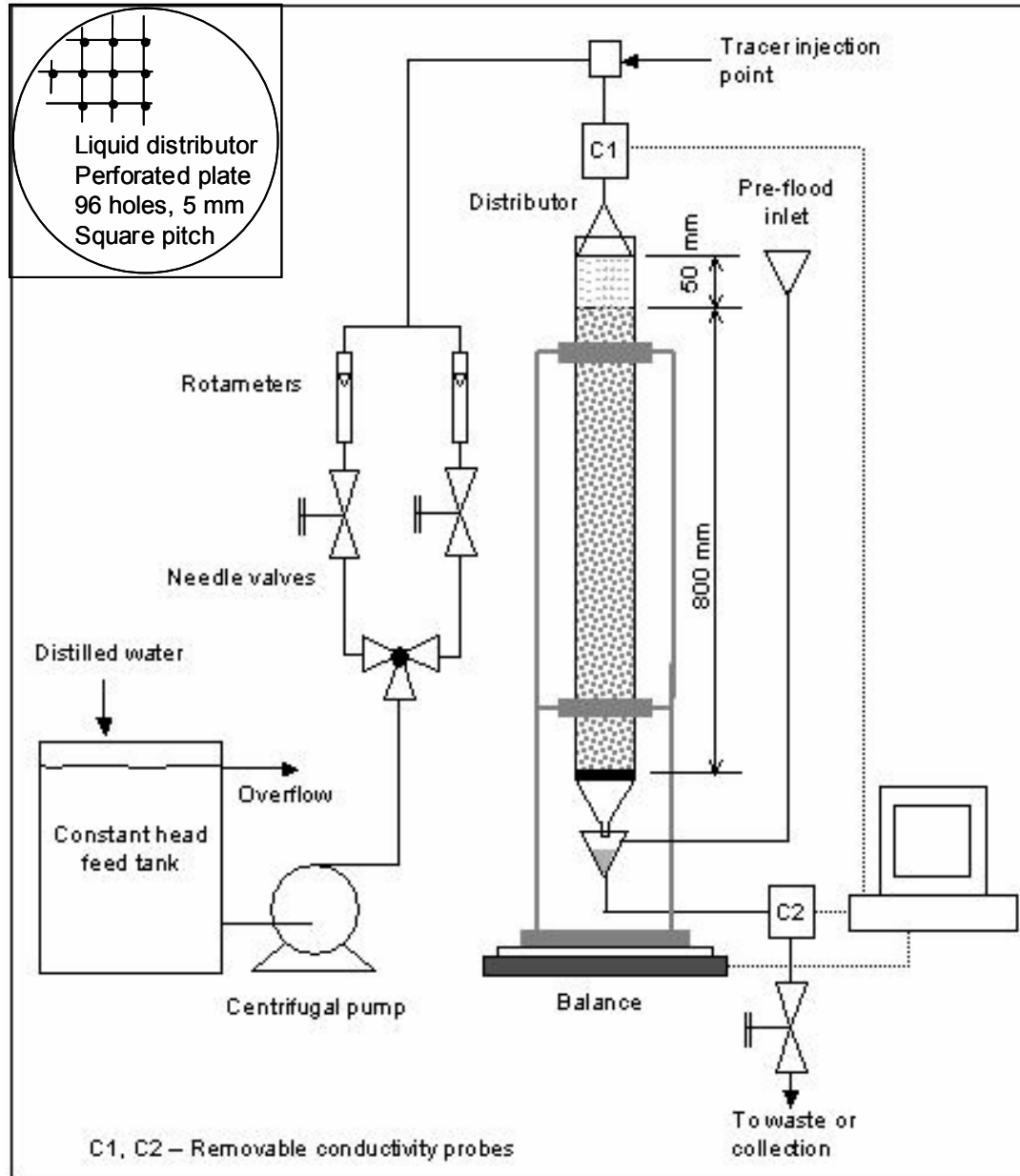
Three limiting cases of prewetting have been identified from literature. From the proposed liquid holdup morphologies in each mode, it is apparent that different fractions of the bed may be actively wetted by liquid flow in each prewetted mode. In this chapter the extent of bed utilization is investigated by using residual liquid holdup measurements in a novel way. The focus is on the circumstances that lead to the existence of multiple operating holdup states and their associated holdup morphologies. An effort is made to confirm the proposed flow morphologies, to reconcile existing holdup data with prewetting procedures and to gauge the effect of such procedures on the wetting efficiency, catalyst utilization and liquid distribution.

### 5.2 Experimental

#### 5.2.1 Experimental setup

A schematic of the experimental setup is shown in figure 5-1. In order to measure holdup by gravimetric means, the setup allows online weighting of the column. In addition, it has residence time distribution recording capabilities (using a dissolved salt as tracer).

The setup consists of a glass column (outer diameter 70 mm or 40 mm) mounted on an Ohaus Explorer Pro 22001 balance (accuracy 0.5 %, resolution 0.1 gram). The measured weight is recorded every second during a run by software developed in the Matlab environment. Distilled water is introduced through a liquid distributor at the top of the column (schematic included in figure 5-1). The distributor fits into the column.



**Figure 5-1.** Experimental setup

Rotameters are used to measure the liquid flow rate, one for low liquid flow rates (0.04 – 0.25 l/min) and one for high liquid flow rates (0.24 – 1.84 l/min). The rotameters are equipped with needle valves with which the flow rate may be set manually. With a combination of the correct column and the appropriate rotameter, the liquid flux can be adjusted in the range 0.2 – 28 kg/m<sup>2</sup>s. It will be

shown that this is well above the flooding velocity when no gas flow is used. No gas flow is used in these experiments.

An important factor in the study of trickle flow hydrodynamics is the liquid distributor design. Burghardt *et. al.* (1995) report that their results were independent of the number of feed points in the distributor given that this value exceeded 5000 points per square meter. In this study, the two distributors were of the “shower head” type, and had 96 and 16 holes for the 70 mm and 40 mm columns respectively. The holes were approximately 0.5 mm in diameter in square pitch arrangements (hole density exceeds 15000 points per square meter). The same distributors were used to investigate all three prewetted modes. From the results, it is concluded that the uniformity of the inlet distribution was adequate.

Conductivity probes are installed in the line before the distributor and after the column exit. These are connected to a Eutech PC 5500 conductivity instrument, which is in turn connected to the computer. A Matlab program was developed in order to record the conductivities with a frequency of one reading every 1 or 2 seconds. With the probes used, the conductivity can be measured to an accuracy of 0.5 % in the range 1  $\mu\text{S}/\text{cm}$  to 500  $\text{mS}/\text{cm}$ . For the sake of comparison, the conductivity of distilled water is usually between 2 and 8  $\mu\text{S}/\text{cm}$  and that of a saturated NaCl solution is approximately 200  $\text{mS}/\text{cm}$ . More detail on the conductivity cells are given in chapter 4. No gas bubbles were entrained in the liquid conductivity cells.

### **5.2.2 Experimental procedure**

The column is packed with 3 mm glass beads up to a height of 800 mm. This system is chosen for the sake of comparison with previous studies. The mass of beads needed to achieve this height is noted and from it the porosity is calculated. The porosity was found to be approximately constant at 0.385. From then on, the procedure for each prewetted mode differs.

### Non-pretwelled mode

In the non-pretwelled mode, an initially dry bed was used. Irrigation of the liquid starts at the minimum liquid flow rate to be investigated (0.2 kg/m<sup>2</sup>s). Once steady state was achieved (as judged by a stable column weight which was reached after only a few minutes), the holdup was noted, the liquid flow was stopped and the column was allowed to drain until only the residual holdup (RLH) remained. This procedure took 20-30 minutes. The RLH thus attained is associated with that flow rate. The column is then flooded and drained, and the RLH thus attained is noted as the saturated RLH ( $RLH_{sat}$ ).

The column is repacked with dry beads and the procedure is repeated for various liquid flow rates.

### Levec-wetted mode

The column is prepared as in the non-pretwelled mode. However, once packed, it is flooded with a NaCl solution. This is done by connecting the pre-flooding inlet to the column exit and flooding the column through this tube (figure 3-9). This allows the column to be flooded from the bottom in order to avoid the entrapment of bubbles. It also means that only distilled water is present in the feed line (i.e. no salt can enter with the feed) which facilitates accurate conductivity measurement in this line. The column is then drained under gravity. The concentration of the NaCl solution is kept low enough not to drastically alter the physical properties (as evidenced by almost no difference in the RLH when this solution was used instead of water), but high enough to allow accurate measurements. The conductivity of this solution was usually around 30 mS/cm. More dilute solutions were also used and it was found that the results were independent of this conductivity as needs be. After drainage, the RLH retained in the column contained a calculable amount of salt:

$$S_i = V_{bed} \times RLH \times F(C) \quad (5-1)$$

Here,  $V_{bed}$  is in liters,  $C$  is the conductivity of the salt solution in  $\mu\text{S}/\text{cm}$  and the function  $F$  is the calibration curve of concentration versus conductivity of the appropriate probe (gram salt per liter, given by equation B-1).

Irrigation with distilled water then starts at the desired flow rate and continues for 2 hours (see discussion below). A quantity of salt is washed out of the column. This quantity was measured either as the time integral of the exit concentration profile (equation 3-10) or by collecting the washed liquid and measuring the conductivity and volume thereof. Alternatively, once the allotted time had passed, the column was flooded and drained repeatedly (at least 6 times) and this water was collected and the conductivity and volume thereof measured. The conductivity is related to the concentration by the calibration curve. The amount of salt left in the column after 2 hours could therefore be determined by any of the three methods. Table 5-1 shows typical results.

$$S_{washed\ out} = \int_0^{\infty} F[C(t)] Q(t) dt \quad (5-2)$$

**Table 3-3.** Determination of the amount of salt left in the column

Method	Mass of salt left ( $S_{left}$ , grams)
1. Time integral of exist concentration profile	0.3220
2. Exit water volume and conductivity	0.2241
3. Washing water volume and conductivity	0.2271

It is seen that the last two methods proved adequate. The time integral method was hampered by difficulty in integrating the product of the outlet concentration profile with the outlet flow rate since the latter was not measured (it was inferred from the column weight). Recall that the column is not at steady state when initial irrigation occurs. In any case, since two other methods are available, use of method 1 was not pursued. Method 3 was preferred because it was easier to accomplish. In method 3:



$$S_{left} = \frac{W}{\rho_L} F(C) \quad (5-3)$$

Here,  $W$  is the mass of liquid used to wash the column and  $F(C)$  yields the concentration of the solution.

### **Kan-wetted mode**

The procedure in this mode is exactly the same as for the Levec-wetted mode with a few exceptions. Once draining of the salt solution starts, the distilled water irrigation at the top of the packing commences. The mass of salt left in the column after operation is determined as in the Levec-mode (method 3). Note that in this case it is not possible to determine the initial salt mass in the column. Instead, the RLH (saturated) of the bed is measured after the experimental run.  $S_i$  is determined from this value and the conductivity of the original salt solution used to pre-flood the column.

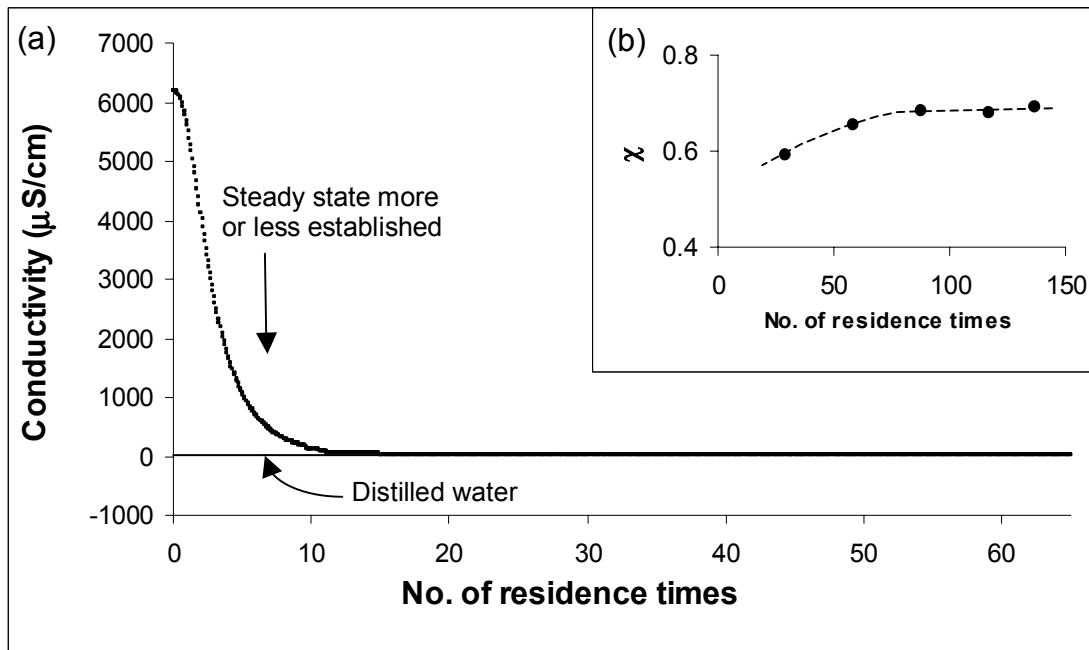
### **Time of irrigation**

Note that in all of the cases above, the column was irrigated for 2 hours at steady state (as adjudged by the weight of the column). Two hours was deemed adequate for all transfer processes to come to completion on the following basis:

- Sederman & Gladden (2001) report that trickle flow is stable for periods between a few seconds and 24 hours and that the rivulets do not change their paths during that time.
- Ravindra *et. al.* (1997) irrigated their beds for 2 hours to ensure that all dynamic distribution effects could be neglected, and irrigated with dye solution for only 5-6 minutes before stopping the flow.
- In this study, when this time was shortened to 30, 60 and 90 minutes, it was found that the results were dependent on the time at steady state if that time was less than 90 minutes. The results of 90, 120 and 140 minute runs compared well. It is concluded that any time greater than 90

minutes is adequate (figure 5-2 (b), refer to results section for an explanation of  $\chi$ ). Here, the residence time is taken as the volume of liquid in the column divided by the volumetric flow rate, i.e. space time).

- The outlet conductivity profile drops in a fashion analogous to that of a step decrease in tracer concentration. A typical profile for the Levecwetted mode is shown in figure 5-2 (a). In this case (and others not shown) the concentration of the exit water dropped rapidly to a value close to that of distilled water. In fact, after only 11.3 residence times (approximately 38 minutes for the lowest liquid flow rate), the difference in conductivity between the effluent and that of distilled water had dropped to less than 1 % of the difference between the conductivities of the original salt solution and distilled water. After 65 residence times (about 220 minutes), this had dropped to  $\ll 0.1$  %. This value stands at 0.1 % at 120 minutes for the lowest liquid flow rate. The integral of the curve beyond this time is deemed negligible.

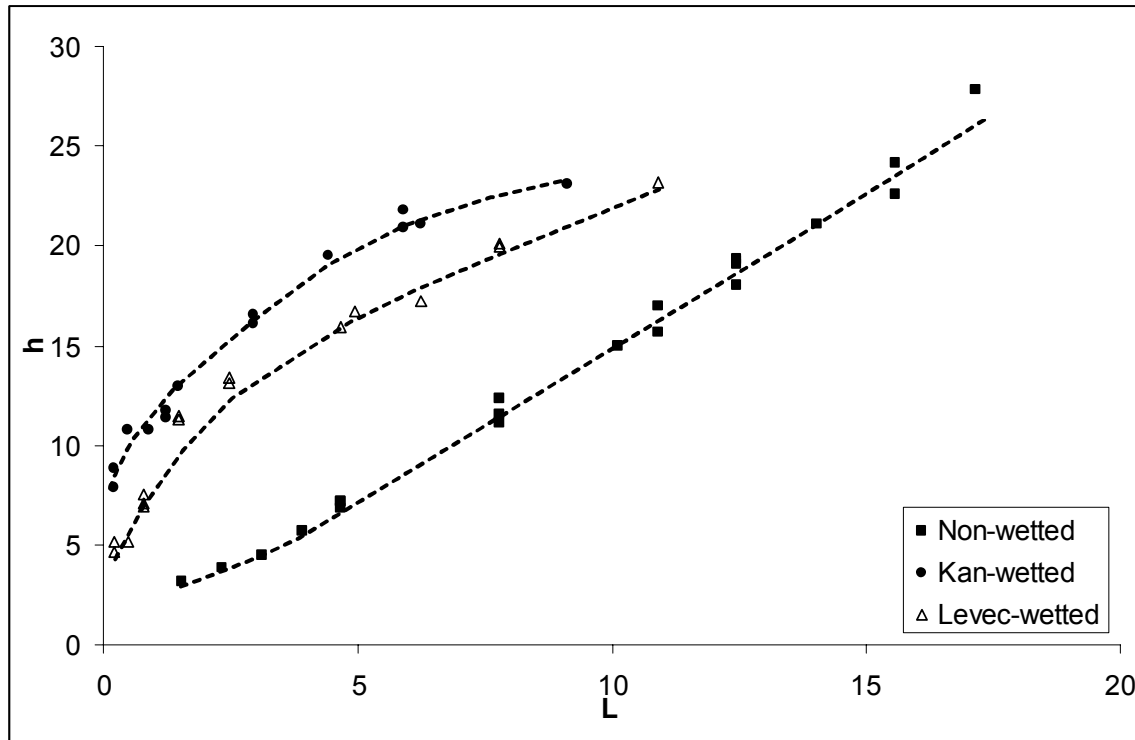


**Figure 5-2.** Effect of washing time on results

## 5.3 Results

### 5.3.1 Holdup in each prewetted mode

The total operating holdup, as determined by the steady state weight of the column, in each prewetted mode is shown as a function of liquid mass flux in figure 5-3. The dashed lines have been added to aid interpretation.



**Figure 5-3.** Total operating holdup in the three prewetted modes

The holdup differed by as much as 400 % between the non-prewetted and the Kan-wetted modes. Also, a significant difference was apparent between the Levec- and Kan-wetted modes.

Figure 5-4 is a repeat of figure 5-3 for the Kan- and Levec-wetted modes, with an envelope showing the region that are encompassed by the correlations generally used for this system (as in figure 4-10, with the Levec *et. al.* (1986b) correlation omitted).

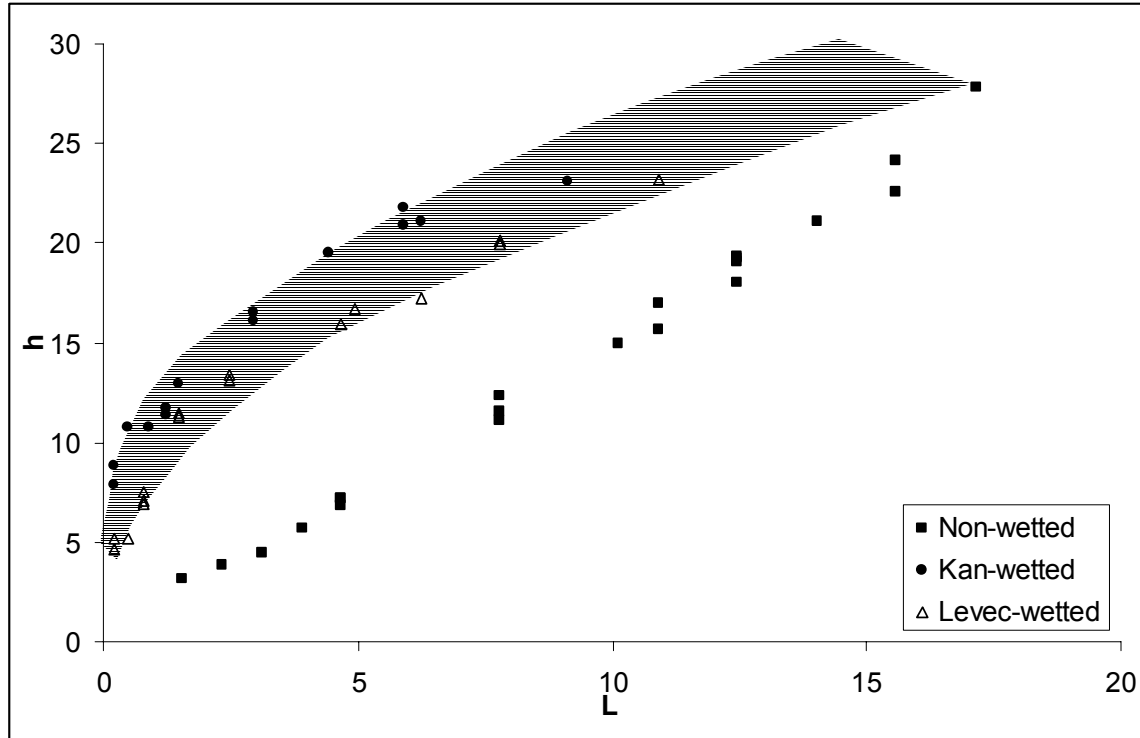


Figure 5-4. Holdup in comparison with the envelope of existing correlations

### **5.3.2 Volumetric utilization efficiency**

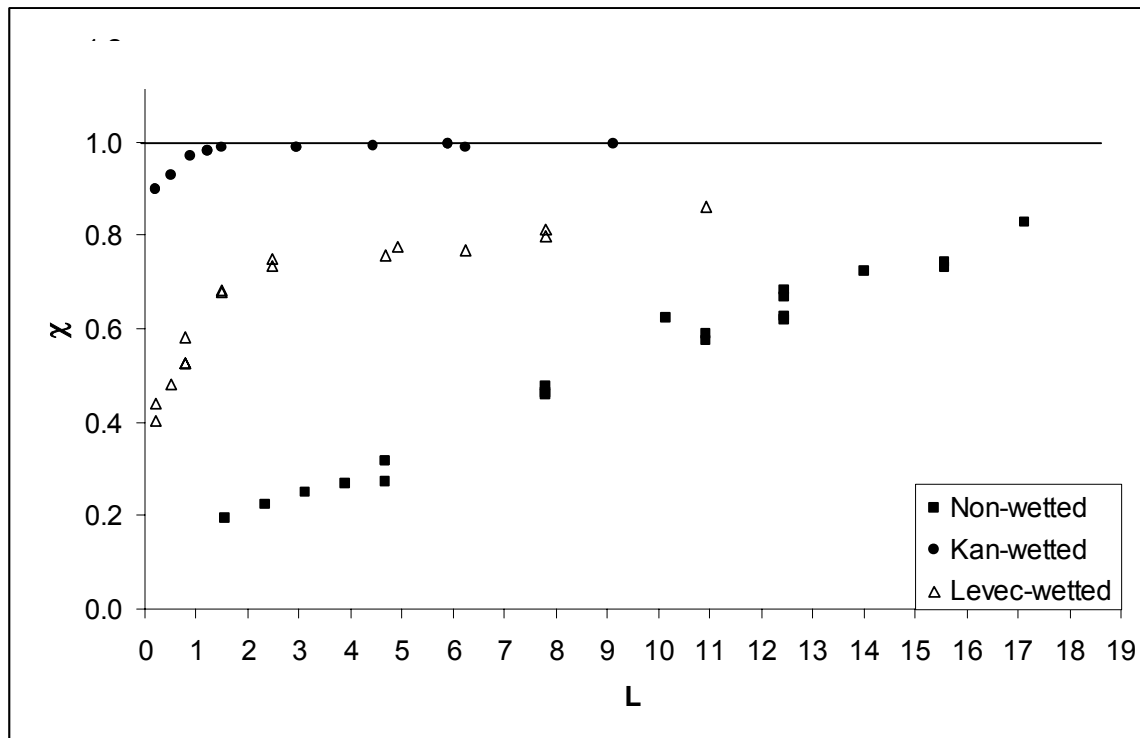
The experimental procedure described above allows the estimation of a bed “volumetric utilization coefficient”, here designated with the symbol  $\chi$ . It is defined as the fraction of the bed volume that receives liquid renewal, i.e:

$$\text{Non-wetted:} \quad \chi = \frac{RLH}{RLH_{sat}} \quad (5-4a)$$

$$\text{Levec-wetted:} \quad \chi = 1 - \frac{S_{left}}{S_i} \quad (5-4b)$$

$$\text{Kan-wetted:} \quad \chi = 1 - \frac{S_{left}}{S_{i,est}} \quad (5-4c)$$

Note that the initial amount of salt retained in the Kan-wetted column is a very large amount (since the entire column is flooded with salt water). If this was used as  $S_i$ , the value of  $\chi$  would always be approximately equal to 1. Instead, an estimated initial amount of salt is used ( $S_{i,est}$ ). It is equal to the amount of salt that would have been retained in the column's RLH had it been allowed to drain. The dependency of the volumetric utilization coefficient on the liquid flow rate in each prewetted mode is shown in figure 5-5.



**Figure 5-5.** Volumetric utilization coefficient in each prewetted mode as a function of liquid flux

Figure 5-5 is to be interpreted as follows. The fraction  $\chi$  indicates the fraction of the bed that had received irrigation during operation. Since operation continued for 2 hours after steady state was reached, all transfer processes may be assumed to be complete. This is important in the light of many residence time distribution (RTD) models (e.g. the cross flow models and the piston-dispersion-exchange model, see Gianetto *et. al.* (1978) for a review of RTD models) that

assume that a part of the liquid is stagnant and exchanges mass with the dynamic part. Here, the assumption is that a negligible amount of salt remained in the static holdup after 2 hours. Wandering rivulets that irrigate different parts of the bed will wash out a greater amount of salt than non-wandering rivulets. In this sense, the fraction  $\chi$  indicates the upper limit of the volumetric fraction of the bed that encountered liquid flow.

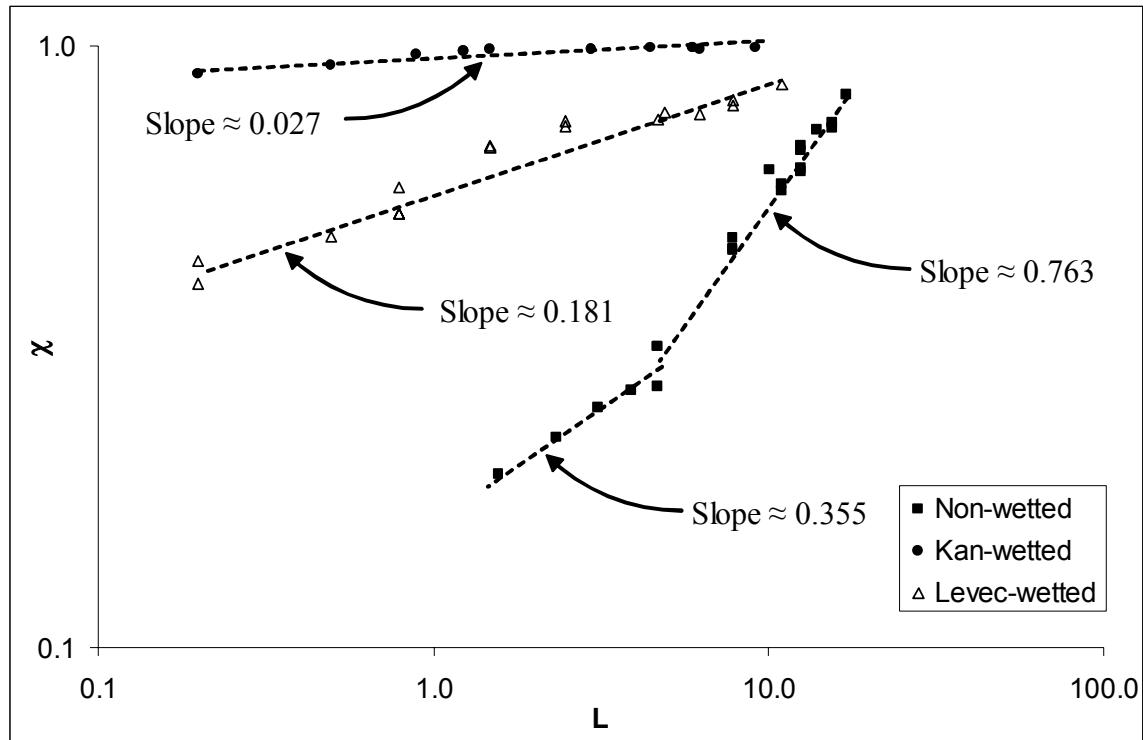
The volumetric utilization coefficient may also be interpreted as an upper estimate of the wetting efficiency, since it is impossible for the wetting efficiency to be higher than this parameter. However, the wetting efficiency in each mode may well be below the utilization coefficient because of two reasons:

- The existence of temporal wandering rivulets, where this term refers to a liquid stream that changes position with time after steady state had been established. In the extreme case, a wandering rivulet of small size that traverses the entire bed over 2 hours will yield a utilization coefficient of 1. However, if no wandering rivulets exist, the utilization coefficient is equal to the wetting efficiency because the volume and surface area are related by the specific surface area:

$$f = \frac{\text{Wetted area}}{\text{Total area}} = \frac{\text{Wetted area}}{\left(\frac{6(1-\varepsilon)}{d}\right)V_{bed}} = \frac{\text{Wetted volume} \times \left(\frac{6(1-\varepsilon)}{d}\right)}{\left(\frac{6(1-\varepsilon)}{d}\right)V_{bed}} = \chi \quad (5-5)$$

- If the contacting efficiency is used as the wetting efficiency, it is possible that the effective contacting efficiency in parts of the bed that are wetted is less than one. While these parts will have a utilization coefficient of 1, their contacting efficiencies will be below 1.

The functional dependency of the volumetric utilization coefficient on the liquid flow rate is shown in figure 5-6. The slopes indicate the power of the liquid flux to which the coefficient is proportional.



**Figure 5-6.** Functional dependency of utilization coefficient on liquid flux

These slopes mostly disagree with the generally accepted slope of around 0.333 (see figure 4-6). Despite the apparently adequate fits shown above, it has to be noted that the power law equations fitted to the data did not describe the data very well. In fact, the correlation coefficients ( $R^2$ ) were low (Kan-wetted: 84 %, Levec-wetted: 94 % and Non-wetted: 98 % for lower values and 97 % for higher values). The present data do not adhere to a power law dependency.

## 5.4 Discussion

### 5.4.1 Holdup

Referring to figure 5-4, it is quite clear that the holdups in the Levec- and Kan-wetted modes are well within the envelope of commonly used correlations. Interestingly, the Levec-wetted holdups fall almost exactly on the lower edge of this envelope, while the Kan-wetted holdups fall almost exactly on the upper edge of the envelope.

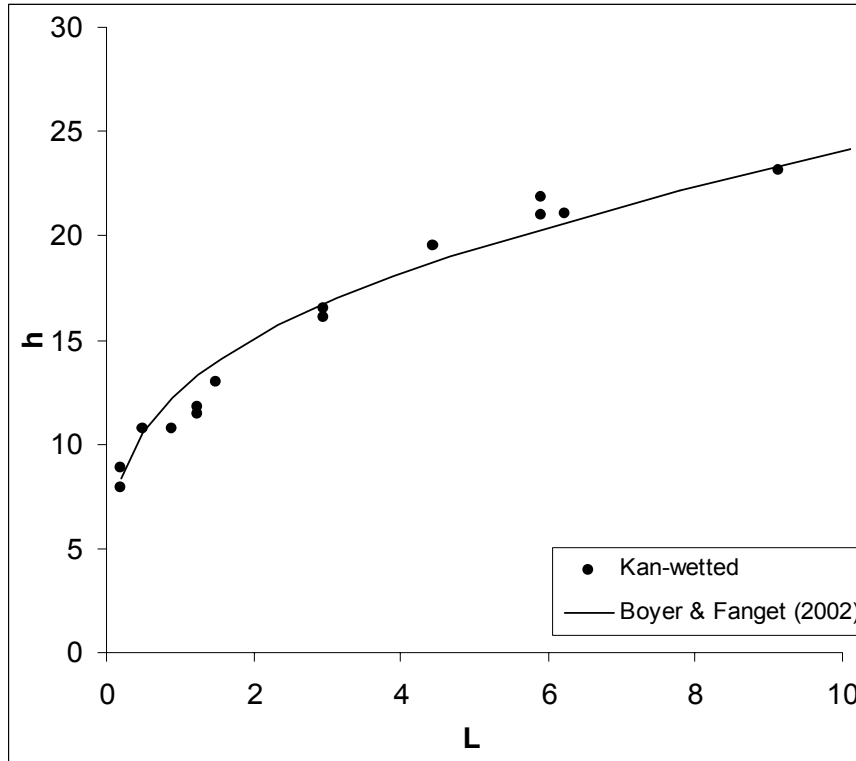
Comparing figure 4-10, it is concluded that the Levec-wetted mode holdup is described by the Holup *et. al.* (1992) and Saez & Carbonell (1985) correlations at higher velocities and the Specchia & Baldi (1977) correlation at lower velocities. This latter result was also found by De Klerk (2003). It is interesting to note that the Holup *et. al.* correlation incorporates the idea of “channeled” flow in the correlation. The “channels” are inclined slits with annular liquid flow. The Saez & Carbonell correlation is based on relative permeabilities and incorporates a hydraulic radius as the characteristic length.

The Kan-wetted holdup is well described by the Boyer & Fanget (2002) correlation (figure 5-7). This result is particularly important, since this model was developed for film flow over fully wetted particles. The average absolute relative error (AARE) is equal to 7.2 %. For the sake of comparison, Larachi *et. al.* (2003) report an AARE for the Holup *et. al.* (1992) correlation of 21.3 % and an AARE for their own ANN correlation of 14 %. Considering that the Boyer and Fanget (2002) model required no fitting of parameters and used only the classical Ergun constants, its superior performance is remarkable. Admittedly, only 14 data points are used in this evaluation.

It is informative to note that this model assumes full wetting of the solid. The volumetric utilization coefficient (which is an indication of the wetting efficiency) data also support this notion. This coefficient was close to 1 at all liquid velocities in the Kan-wetted mode. The results here support the notion that the liquid is present in the form of films and that these films cover the particles entirely (except at very low liquid velocities).

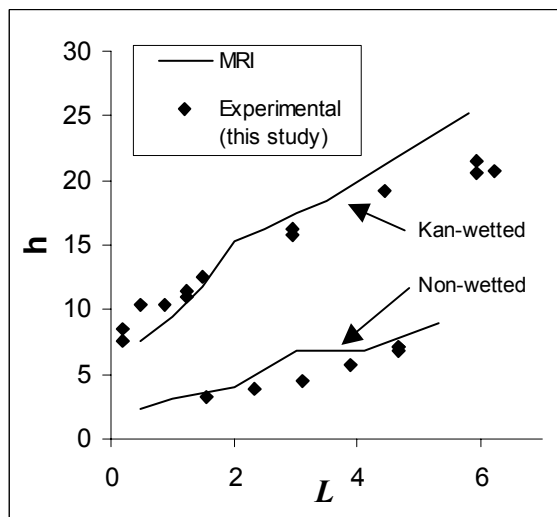
The non-wetted mode’s holdup is far below that of the other two modes. The reason is evident from figure 5-5 which indicates that large parts of the bed remained completely dry.





**Figure 5-7.** Boyer & Fanget (2002) fit to the Kan-wetted mode holdup

The results of Sederman & Gladden (2001) at low liquid velocities were similar to those seen here (figure 5-8). This validates the present experimental data.



**Figure 5-8.** Comparison of experimental holdups with MRI (from Sederman & Gladden, 2002) holdups

No model is available for the non-wetted mode, but we will refrain from proposing any correlations based on only the few data points obtained herein. Instead, see section 5.4.2.

### The extent of flow turbulence

When the liquid holdup is correlated as a power law function of the liquid flow rate, the exponent of the Reynolds number is an indication of the extent of turbulence in the flow. Typically, an exponent in the region 0.3-0.4 (or the generally accepted average of 0.33) is indicative of laminar flow, while higher exponents indicate turbulent flow (Wammes *et. al.*, 1991). The present holdup data was correlated in the Excel environment with an equation of the form:

$$h = qL^e \quad (5-6)$$

Exponents and correlation coefficients for each prewetted mode is given in Table 5-2. The increased turbulence in the Levec- and non-wetted modes is due to the increased liquid channeling and the increased interstitial velocity.

**Table 5-2.** Liquid flux exponents in holdup correlation and correlation coefficients

Mode	Exponent	Correlation coefficient
Kan-wetted	0.29	95.8 %
Levec-wetted	0.41	96.7 %
Non-wetted	0.95	98.8 %

### **5.4.2 Volumetric utilization and wetting efficiency**

From figure 5-5 it is evident that the volumetric utilization in each prewetted mode is vastly different. For the Levec-wetted and non-wetted modes large parts of the bed are not irrigated. Even for the Kan-wetted mode, as much as 10 % of the bed is not irrigated at very low liquid velocities. Note that the same liquid distributors were used in every prewetted mode. The differences in utilization coefficient can

therefore not be attributed to initial distribution. This is another reason why the initial distribution was deemed adequate.

As reported in the literature review, increased liquid fluxes lead to better spreading of the liquid. Moreover, the results are coherent with the visualization of film and filament type flow in the Kan-wetted mode and channeled flow in the Levec-wetted mode.

The fact that the Levec-wetted mode results did not change much after an initial wash-out period (figure 5-2), leads to the conclusion that wandering rivulets either did not exist (as reported by Ravindra *et. al.*, 1997, and Reddy *et. al.*, 1990) or meandered only locally around a pore channel. In this case, the utilization coefficient should be comparable to the bed-scale wetting efficiency. Figure 5-9 repeats figures 4-5 and 5-5 and allows this comparison to be made.

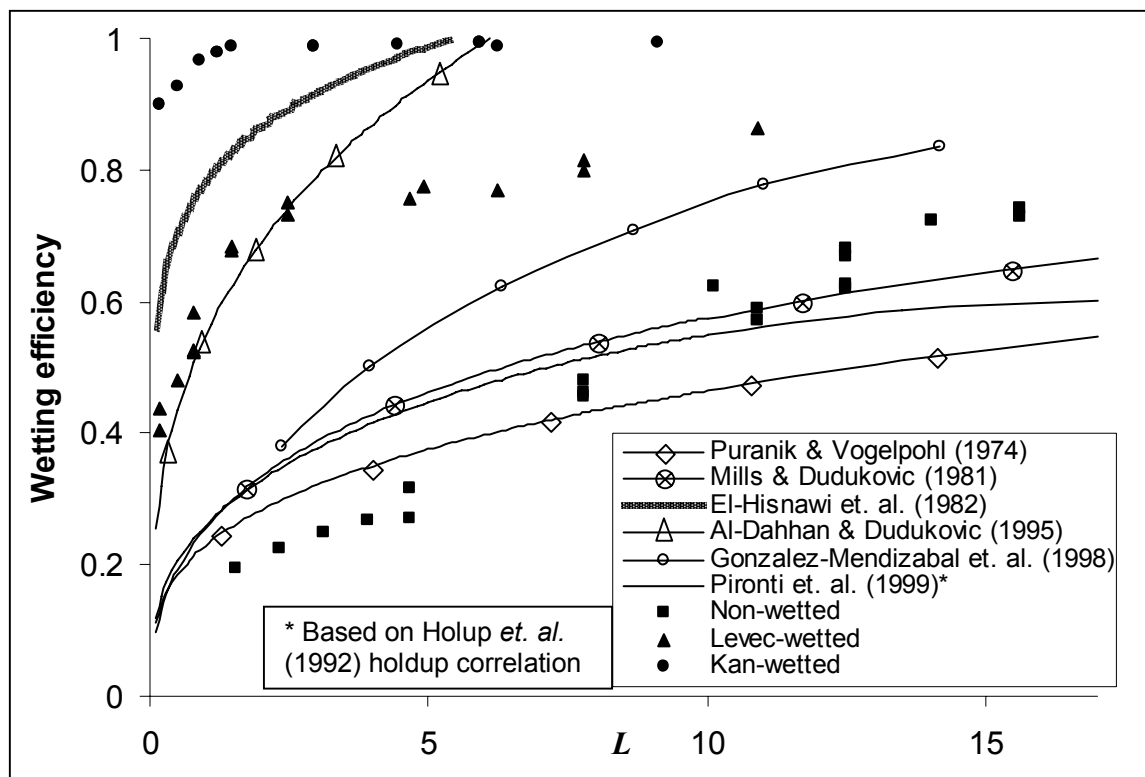


Figure 5-9. Utilization coefficient compared to wetting correlations

It is evident that the experimental utilization coefficients in the Kan-wetted mode are well above the wetting efficiencies predicted by any of the commonly used correlations. Interestingly, the trend of complete wetting predicted here corresponds to the results of Lutran *et. al.* (1991) who also found total wetting in the Kan-wetted mode. Sederman & Gladden's (2001) results (figure 4-9) are well below those reported here (they are practically on the Gonzalez-Mendizabal *et. al.* (1998) correlation). This may be due to the fact that the MRI visualizations could not detect thin films on the particles. Lazzaroni *et. al.* (1989) wetting efficiencies are also below those found here (they are comparable the El-Hisnawi *et. al.* (1982) correlation, see figure 4-7). As found by Sederman & Gladden (2001), the critical value of  $2 \text{ kg/m}^2\text{s}$  is also seen here, with partial bed-scale wetting being found below this value and complete wetting above it. The partial wetting is explained in terms of the morphology by recognizing that films are broken because the liquid velocity is insufficient to maintain them. The liquid coalesces into rivulets and leaves areas of the bed non-irrigated.

The Levec-wetted mode exhibits interesting behavior and may be explained as follows. The liquid flux value of  $2 \text{ kg/m}^2\text{s}$  is again seen to be critical. Below this value as liquid flux increases, new rivulets form in previously non-irrigated parts. The slope of the curve is therefore high. Above this value, no new rivulets are created and the existing rivulets expand laterally in small increments. The RLH rings and pockets around the rivulets that are washed out in this manner are far less than those washed out by new rivulets; hence the smaller slope of this section. The wetting efficiency below the critical value is well described by the Al-Dahhan & Dudukovic (1995) correlation. The fact that the experimental points are slightly above the predicted values may be due to the existence of wandering rivulets. If the pore-rivulets oscillated a little around a channel centre, the rivulet edges will wash out more RLH than is actually contained in the wetted volume. In this case the utilization coefficient will be larger than the wetting efficiency. The effect appears to be small, although this is a tentative explanation that needs confirmation. Above the critical liquid velocity, the present results are below that

predicted by the Al-Dahhan & Dudukovic (1995) correlation. One possible reason is the fact that the correlation is applicable to porous media. The porous nature enhances the liquid spreading to such a degree that a larger part of the bed becomes active. This is mostly due to the change in contact angle and is a mechanism that has been thoroughly recognized (Maiti *et. al.*, 2004). It seems that the Al-Dahhan & Dudukovic (1995) correlation may be applicable to the Levec-wetted mode and that the use of a porous packing will aid in spreading the liquid around a rivulet but will not contribute to the creation of new rivulets.

Of course, the utilization coefficient is based on RLH. This means that surfaces far from the contact points that may be dry in the Kan-wetted mode will not be recognized by the utilization coefficient as such. Since these areas are exactly those that may be expected to be non-wetted, the comparison of utilization coefficient and wetting efficiency is suspect. However, it is still useful to evaluate trends such as the critical liquid flux of  $2 \text{ kg/m}^2\text{s}$  and the differences between the prewetting modes.

The non-prewetted mode utilization coefficients are in the region of the lower three wetting correlations. In this case it is difficult to conclude whether an increased liquid flux serves to create new rivulets or expand existing rivulets. However, the latter seems more likely, especially when judging from the fact that the utilization coefficient remains low even at high liquid velocities. It is worth mentioning that the wetting efficiencies found by Lazzaroni *et. al.* (1989) for this mode compares very well with those found here (figure 4-7).

The dependency of the wetting efficiency on the liquid holdup is summarized in Table 5-3. Agreement is seen in the non-prewetted mode only.

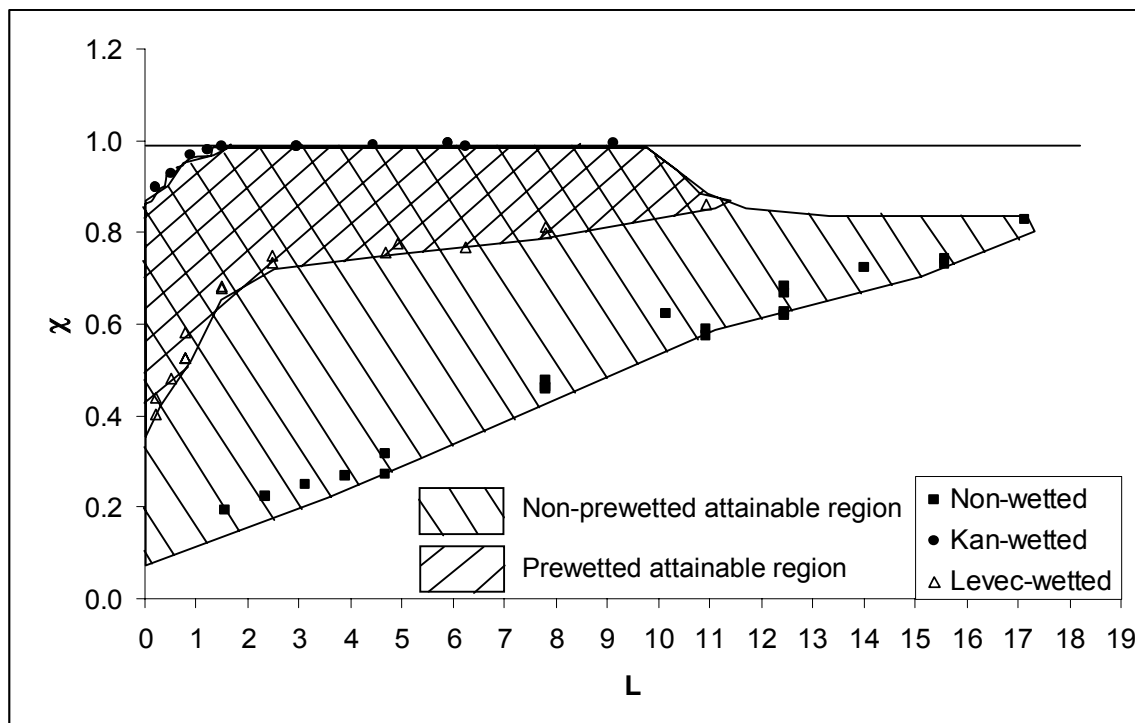
Importantly, these results have shown that bed-scale partial wetting exist regardless of the prewetting procedure, but is more pronounced for non-wetted and wetted-and-drained (Levec-wetted) beds.

**Table 5-3.** The power of the holdup to which the wetting efficiency is proportional

Author	Mode	Power
El-Hisnawi <i>et. al.</i> (1982)	Not specified	0.224
Lazzaroni <i>et. al.</i> (1989)	Non-pretweted	≈ 1
Present study	Kan-wetted	0.083
Present study	Levec-wetted	0.44
Present study	Non-pretweted	≈ 1

### Obtainable region

The volumetric utilization coefficients shown here are those for the limiting cases as described for each mode. Specifically, it is the increasing liquid velocity leg. Non-pretweted beds in general may operate anywhere between the lower leg shown here and the Kan-wetted leg depending on the exact flow history. Similarly, the Levec-wetted mode may be anywhere above the Levec-leg shown, but can never be below it (for a given gas flux). Figure 5-10 shows the attainable regions – actual beds will be in these regions depending on the flow history.

**Figure 5-10.** Attainable region for each pretweted mode

### **5.4.3 Utilization efficiency and holdup prediction**

Refer to the proposed morphology in each prewetted mode (figure 4-11). It has been shown that the film flow-based holdup model of Boyer & Fanget (2002) predict the holdup in the Kan-wetted mode very well (figure 5-7). Consider the volume of bed that is irrigated by the pore-rivulet and its surrounding film flow in the Levec-wetted mode. Because the rivulet can be thought of as a thick film, this volume of the bed can be thought of as similar in structure to the entire bed for the Kan-wetted mode. The Boyer and Fanget derivation (section 4.6.2) may be applied to this volume with the following changes:

- Only a fraction of the volume of the bed ( $\chi$ ) is under irrigation. The predicted holdup should therefore be adjusted:

$$h = h_{Kan-wetted} \times \chi \quad (5-7)$$

- The effective interstitial velocity of the liquid is higher:

$$\langle v_L \rangle = \frac{v_L}{\chi \varepsilon_L} \quad (5-8)$$

- There exist RLH in the non-irrigated fraction of the bed. Assuming the RLH to be constant over the volume of the bed, we have:

$$RLH^* = RLH(1 - \chi) \quad (5-9)$$

The RLH is taken at 3.1 % (from chapter 2).

In short, the predicted holdup for the Levec-wetted mode is obtained by substituting  $\chi \varepsilon_L$  for  $\varepsilon_L$  in equation 4-8, solving for the holdup and adding the RLH of the non-irrigated part of the bed. There are three underlying assumptions here:

- Those parts of the bed that are irrigated are constantly irrigated (no temporally wandering rivulets)
- The porosity of the volumes that are under irrigation are constant and equal to the porosity of the non-irrigated zones
- The RLH in the non-irrigated zones are equal to the bed averaged value

The resultant holdup model for the Levec-wetted regime has no fitted parameters, since the volumetric utilization coefficient is determined independently. Its predictive capability may be gauged by the AARE. The AARE of the original Boyer & Fanget (2002) model for the Levec-wetted mode is 37.1 %. The modified model has an AARE of only 8.8 %. However, it still slightly overpredicts the experimental data. The reason for this becomes apparent when the results of both the present chapter and that of chapter 3 are considered together.

Recall that:

- The RLH totals 3.1 %, of which 52 % is in the form of pendular rings at particle-particle contact points (i.e. 1.6 %) and the remainder in the form of globules at locations of low local porosity.
- Many investigators (including Lutran *et. al.*, 1991) state that pore-rivulets and filaments can be thought of as a continuous string of liquid pockets/globules.

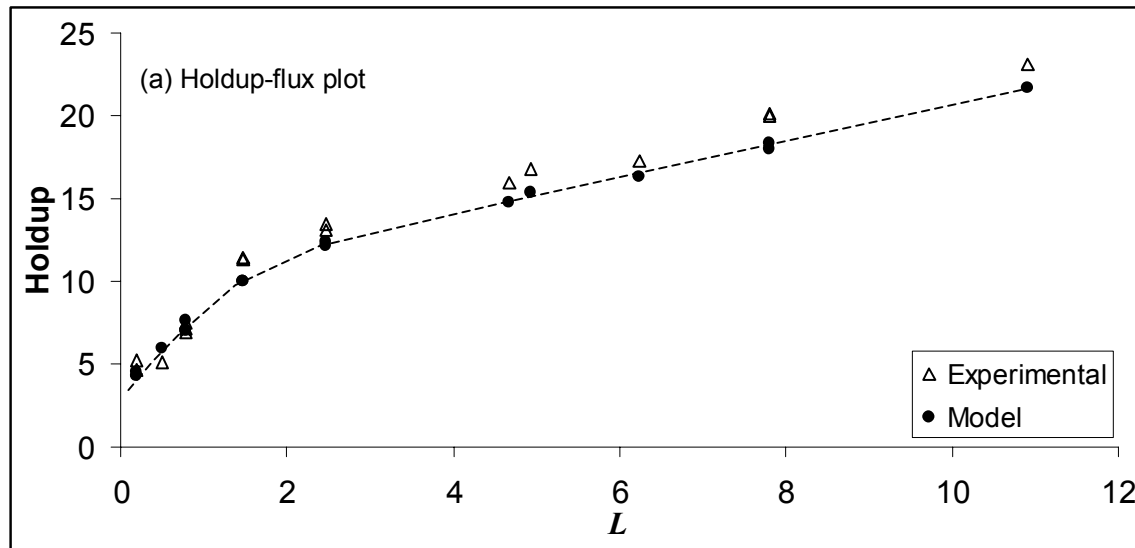
It is proposed that the irrigated parts of the bed in the Levec-wetted mode consist of those parts of the bed that form liquid globules upon drainage. This would imply that the RLH held in the non-irrigated parts consists mainly of pendular rings and has a volume of liquid 1.6 % that of the non-irrigated volume (and not 3.1 % as previously used). This is taken into account by using RLH = 1.6 % in equation 5-9. Also, the average porosity and tortuosity of the irrigated region are expected to be slightly higher than the bed averaged values. This too, should be compensated for in the model as it implies a higher liquid-solid stress term. It is unfortunately impossible to estimate the effects of these higher values given present data and they are neglected.

The final form of the Levec-wetted mode model is:

$$150\mu_L \frac{\chi^3(1-\varepsilon)^2}{(\varepsilon_L - 1.6\%)^3} \frac{v_L}{d^2} + 1.75\rho_L \frac{\chi^2(1-\varepsilon)}{\varepsilon(\varepsilon_L - 1.6\%)^2} \frac{v_L^2}{d} - \frac{\rho_L(\varepsilon_L - 1.6\%)g}{\varepsilon\chi} = 0 \quad (5-10)$$



The predictive capability of this model is highly satisfactory considering that there are no fitted parameters. It is shown in figure 5-11. The AARE is only 6.1 %, and it appears as though the model slightly underpredicts the data, probably because of a higher effective porosity.

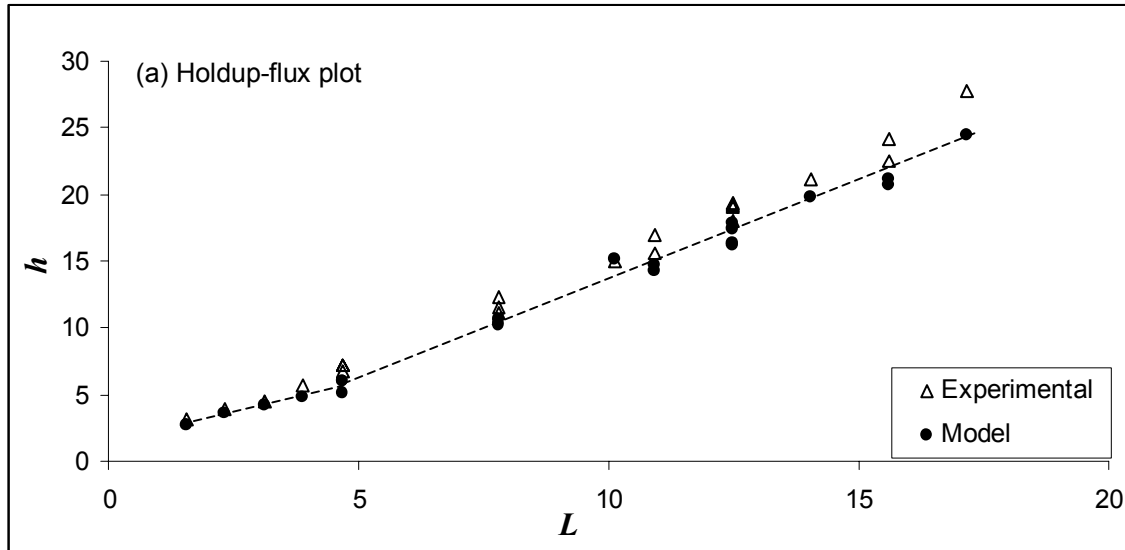


**Figure 5-11.** Final Boyer & Fanget-type model for the Levec-wetted mode

In a similar fashion, the holdup in the non-pretwetted mode can be predicted by assuming that only a fraction ( $\chi$ ) was under irrigation. In this case no RLH need be added for the non-irrigated zone. The prediction is shown in figure 5-12.

The model slightly under-predicts the holdup (AARE = 11.5 %), but is still satisfactory in light of there being no alternative models.

The Kan-wetted mode prediction can be improved to an AARE of 6.7 % (as opposed to 7.2 %) by employing the same procedure.



**Figure 5-12.** Holdup prediction for the non-pretreated mode

In summary, the holdup can be predicted by:

$$150\mu_L \frac{\chi^3(1-\varepsilon)^2}{(\varepsilon_L - RLH^*)^3} \frac{v_L}{d^2} + 1.75\rho_L \frac{\chi^2(1-\varepsilon)}{\varepsilon(\varepsilon_L - RLH^*)^2} \frac{v_L^2}{d} - \frac{\rho_L(\varepsilon_L - RLH^*)g}{\varepsilon\chi} = 0 \quad (5-11)$$

$$RLH^* = \begin{cases} 1.6\%, & \text{Levec- \& Kan-wetted} \\ 0, & \text{Non-wetted} \end{cases} \quad (5-12)$$

Again, all parameters were determined independently of the data. These equations show the applicability of the volumetric utilization coefficient.

## 5.5 Conclusions

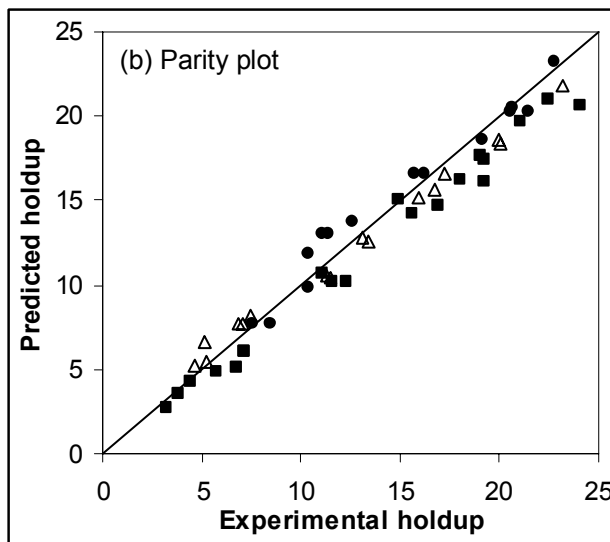
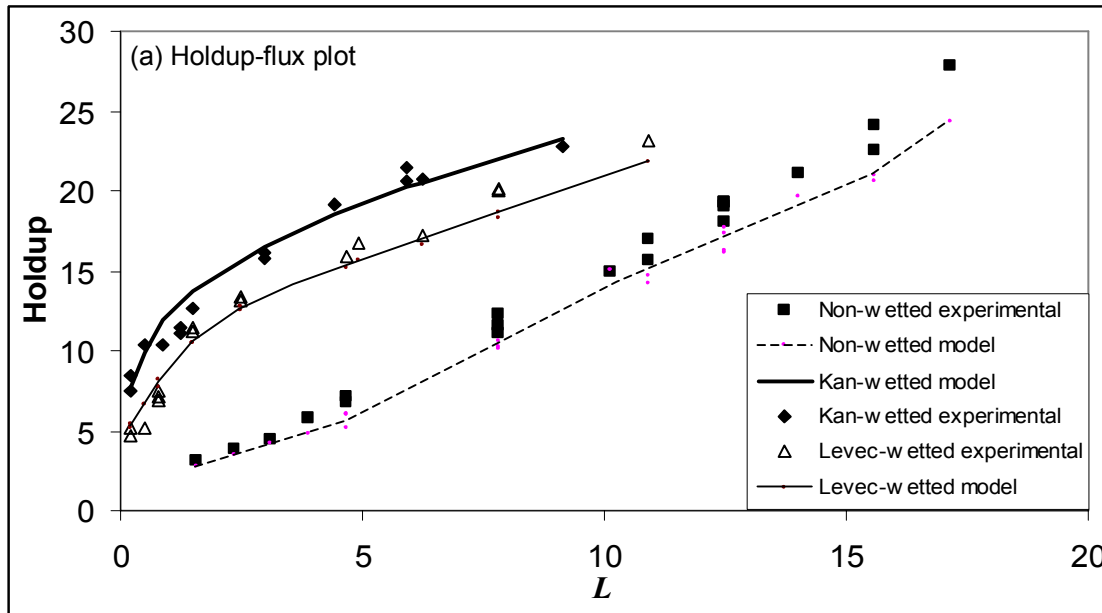
The following conclusions can be drawn from this chapter:

- There exist three limiting cases to the pretreating procedure: Kan-wetted, Levec-wetted and non-wetted.
- The operating holdup morphology depends on the pretreated mode

- The prewetted mode greatly influences the holdup, wetting efficiency and by implication all the transport parameters in the bed
- Different modes are characterized by different volumetric utilization coefficients, so much so that the incorporation of this coefficient in a holdup model is sufficient to greatly improve the prediction of holdup in every prewetted mode.
- The pressure drop hystereses trends observed in literature can be explained by the liquid morphology of the holdup and changes therein.
- In general, it is preferable to operate in the Kan-wetted mode as it is characterized by high solid-liquid and gas-liquid interactions, yielding high holdups (i.e. large residence times for the liquid) and high wetting efficiencies (which would be beneficial in mass transfer limited operations).

The ability of equations 5-11 to 5-12 to predict the holdup in the different prewetted modes using the bed average porosity is illustrated in figure 5-13.

The slight underpredictions in the Levec- and non-prewetted modes may be because of an overestimation of the volumetric utilization or because of the liquid's tendency to flow preferentially in the regions of low local porosity.



Total **AARE** = 9.2 %  
for 51 data points

Figure 5-13. Holdup prediction by the proposed model (all prewetted modes)



---

## Chapter 6. RTD analyses

---

### 6.1 Introduction and background

Residence time distribution (RTD) analysis is a recognized and widely used technique to study trickling flow hydrodynamics (Westerterp, Van Swaaij & Beenackers, 1984: 160). One example is the most commonly used wetting efficiency correlation, which is based on stimulus-response data on porous catalysts (Al-Dahhan & Dudukovic, 1995).

A great number of RTD models have been proposed and used with varying degrees of success in describing trickle flow mixing processes (Gianetto *et. al.*, 1978). Examples of commonly employed models are the piston-dispersion and piston-dispersion-exchange models. The model parameters (like the Peclet number) are solved for by minimizing the difference between the experimental and predicted responses or may be obtained from the moments of the stimulus-response data. However, the values of such parameters often depend on the chosen model as well as the chosen boundary conditions. Moreover, there is no fundamental connotation to the values of such parameters.

In general, the appropriate moments of the stimulus-response data serves as indications of various aspects of the flow in the bed. The zero-th moment is related to the amount of tracer injected, the first to the holdup and the second to the deviation from plug flow. Third and higher moments also contain information on the flow pattern in the bed but are difficult to evaluate because they depend critically on the accuracy to which the tail portion of the response can be measured.

The  $n$ -th moment for data obtained from a non-ideal stimulus is given by (Mills & Dudukovic, 1989):

$$\mu_n = \mu_{n,out} - \mu_{n,in} = \int_0^{\infty} t^n E(t) dt - \int_0^{\infty} t^n I(t) dt \quad (6-1)$$

The holdup obtained from the RTD is equal to:

$$h_{RTD} = \mu_1 \frac{Q}{V} \quad (6-2)$$

An indication of the spread in residence time is given by the variance (Westerterp *et. al.*, 1984):

$$\sigma_v^2 = \int_0^{\infty} (t - t_E)^2 E(t) dt = \mu_2 - \mu_1^2 \quad (6-3)$$

Here  $t_E$  is the apparent residence time of the outlet concentration profile.

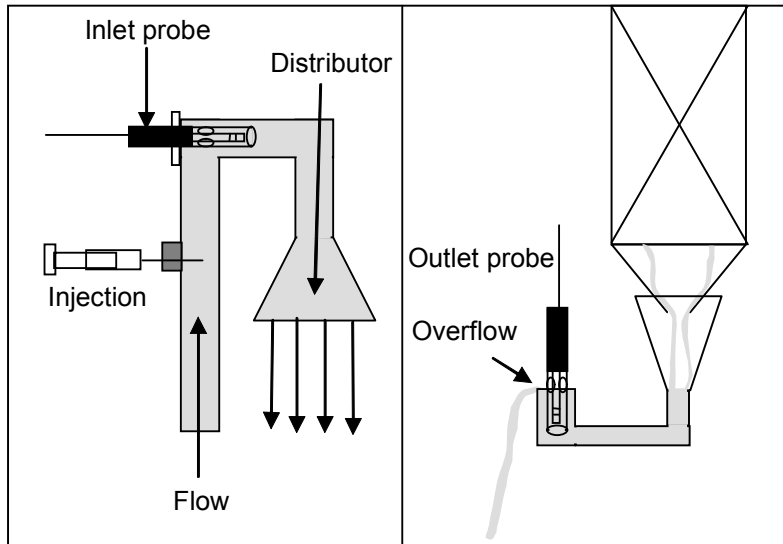
In terms of the present investigation, the existence of multiple hydrodynamic states as evidenced by the volumetric utilization coefficient developed in chapter 5, should be equally visible in the response data of beds operated in the different prewetted modes. The purpose of these analyses is firstly to gain an additional perspective on the three limiting cases of prewetted modes. Secondly, the effect of using porous catalyst particles instead of non-porous glass spheres is investigated in a preliminary fashion.

## 6.2 Experimental

### Setup

The experimental setup described in chapter 5 and depicted in figure 5-1 was used in the RTD analyses experiments. A NaCl tracer is used and detected with a dual channel Eutech PC 5500 conductivity instrument. Some details on the

locations and geometries of the conductivity probes and their cells are given in figure 6-1.



**Figure 6-1.** Conductivity cell geometries

Distilled water was used as liquid, with no air flow. The conductivity could be measured to an accuracy of 0.5 % across approximately 4.5 orders of magnitude. Only the 70 mm diameter column was used for the RTD experiments conducted in this chapter.

In the first series of experiments, the bed was packed with 3 mm glass beads. In order to confirm the existence of the three prewetted modes when porous particles are used, the bed was later packed with porous  $\alpha$ -alumina spheres (approximately 3 mm in diameter).

### **End effects**

The liquid volumes contained in the conductivity cells represent non-negligible end effects. The volume of liquid in the feed line (after the inlet conductivity probe) and the distributor was measured at 23 ml. Another 9 ml of water was present in the outlet conductivity cell. By virtue of the comparatively small diameter of these lines (1/2" compared to the 70 mm column) it is assumed that

the water is in plug flow here. In this case, subtracting a dead time equal to  $3Z/Q$  from the response curve can compensate for the end effects. This is supported by the near plug flow response obtained when a bed of small height is packed.

### **Stimulus**

The stimulus is obtained by syringe injecting 5 ml of concentrated salt solution into the feed line. As will be shown, the stimulus profile could be reproduced satisfactorily. The momentary increase in flow rate due to the injection was deemed negligible, especially in light of a very small but measurable increase in the holdup during this time.

### **Procedure**

The bed was packed and irrigation started at the desired flow rate. Once steady state had been achieved, the concentrated salt solution was injected and the conductivity monitored at the inlet and outlet locations. The conductivities were converted to concentrations and the resulting profile was normalized to its own area (tracer mass balances were satisfied in each run, as confirmed by the zero-th moments). The following liquid fluxes were investigated: 1.0, 2.0, 3.0 and 3.7 kg/m<sup>2</sup>s. All three prewetted modes were investigated.

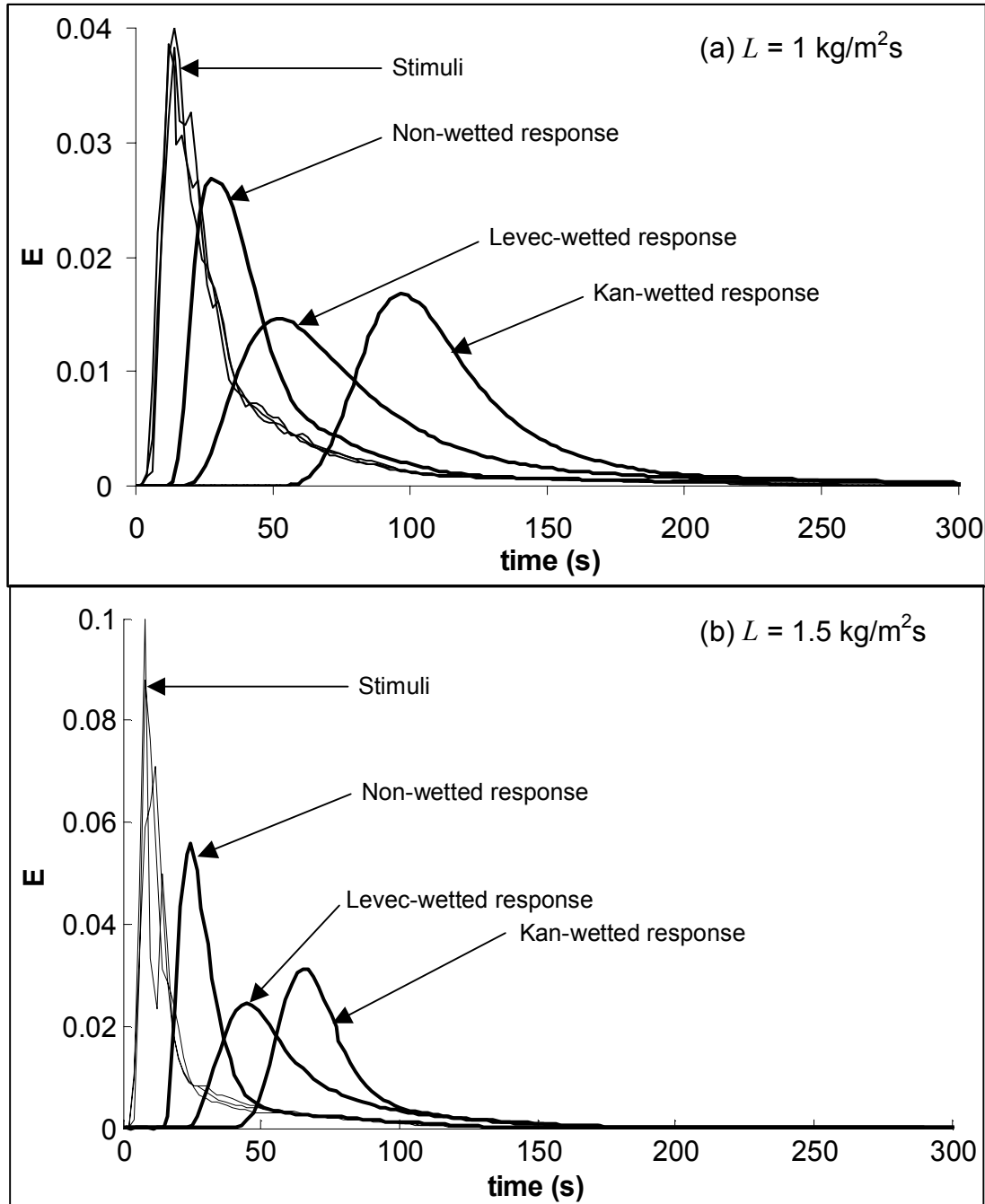
## **6.3 Results and discussion**

### **6.3.1 Non-porous**

#### **Stimulus-response data**

Typical profiles for each prewetted mode is shown in figure 6-2. As shown, the three injection pulses were equivalent for all practical purposes. This makes direct comparison of the response curves possible. Clearly, the difference between the three modes of operation is considerable.





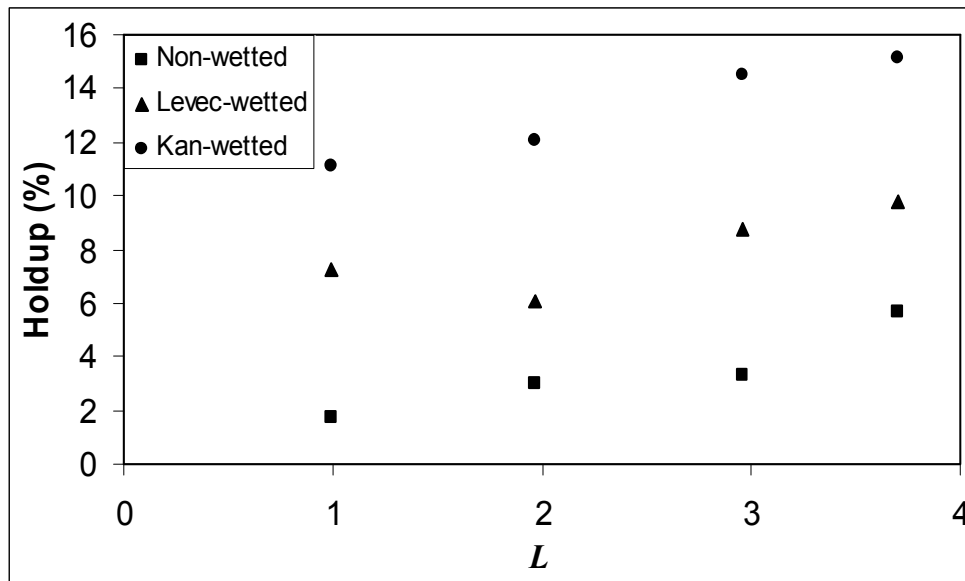
**Figure 6-2.** Stimulus-response data in each prewetted mode

### Moments

The evaluation of the first moments by equation 6-1 was done numerically by applying the Simpson rule. The upper boundary condition of the integral (which should theoretically be infinity) is taken as the time at which the first moment

changes less than 0.1 % per additional 10 seconds. Since the decline is sometimes assumed to be exponential at large times (Mills & Dudukovic, 1989), the integral beyond this point is deemed negligible. The holdup is then calculated from equation 6-2. Figure 6-3 illustrates the holdups thus calculated for different liquid flow rates.

As expected, the holdups show similar trends to those previously reported. The Kan-wetted holdup is the largest, followed by the Levec-wetted mode and then the non-wetted mode. The three modes are therefore evident by this technique as well.



**Figure 6-3.** Holdups determined from the RTD of each prewetted mode

Inspection of figure 6-2 clearly indicates that the mixing in the Kan-wetted mode is less severe than in the Levec-wetted mode despite the fact that the residence time was larger. Evaluation of the variance by equation 6-3 confirms this conclusion (Table 6-1). For the variance/deviation calculations the upper time limit is taken as 15 residence times, as the experimental scatter becomes significant at larger times. The  $L = 3 \text{ kg/m}^2\text{s}$  deviations are also omitted because

the experimental scatter became significant at lower times due to unknown reasons (the first moment was not affected as much as the second moment).

**Table 6-1.** Deviation of the outlet RTD's around their apparent means

$L$ (kg/m <sup>2</sup> s)	$\sigma_v$ (non-wetted)	$\sigma_v$ (Levec-wetted)	$\sigma_v$ (Kan-wetted)
1.0	29.5	55.4	46.8
2.0	13.6	19.7	16.8
3.7	7.0	14.1	10.3

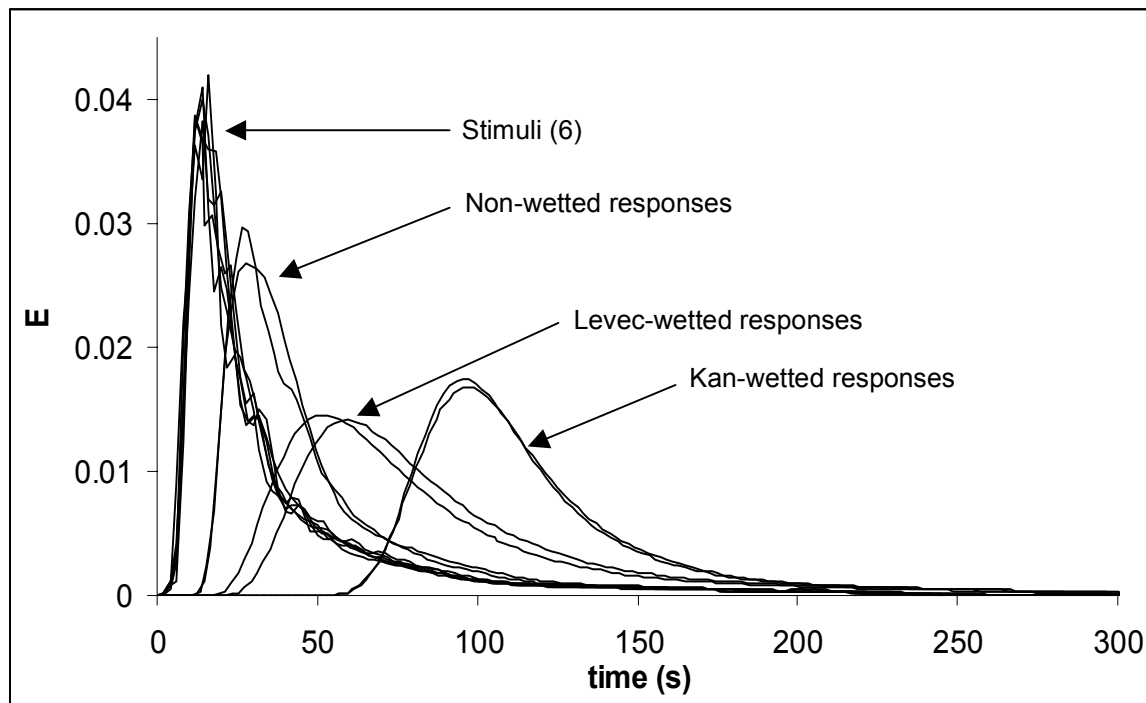
The fact that the residence times were different in the three modes is not fully compensated for in equation 6-3. The deviation simply indicates that the injection distribution had spread a certain amount around the average residence time. It is common practice to normalize the time axis to the residence time (or alternatively to the space time) in order to compare the mixedness in reactors with differing holdups. In the present case (of comparing different flow regimes) it is inadvisable to do so, since the mechanism of mixing is not understood. Considering Table 5-2 it is interesting to note that the holdup – velocity formulations for the three modes differ appreciably. A doubling of the linear liquid superficial velocity would result in a near doubling of the holdup in the non-wetted mode, resulting in an almost unchanged interstitial velocity (and an unchanged space velocity). In the Levec-wetted mode a doubling of the liquid velocity would result in a higher interstitial velocity and a space time 66 % of what it was. In the Kan-wetted mode the space time will be 60 % of its original value. The mixing mechanism may well depend on the flow morphology and the different flow regimes cannot be adequately characterized and compared by a simple linear normalization.

The only conclusion to be drawn from Table 6-1 is that the flow in the Kan-wetted regime is far closer to plug flow than the flow in the Levec-wetted regime. This is evident from figure 6-2 in that the pulse had spread less even though it had been in the bed for longer. This is an important conclusion as it indicates that the

mixing mechanisms (and by implication the holdup morphologies) in these modes are different.

### Reproducibility

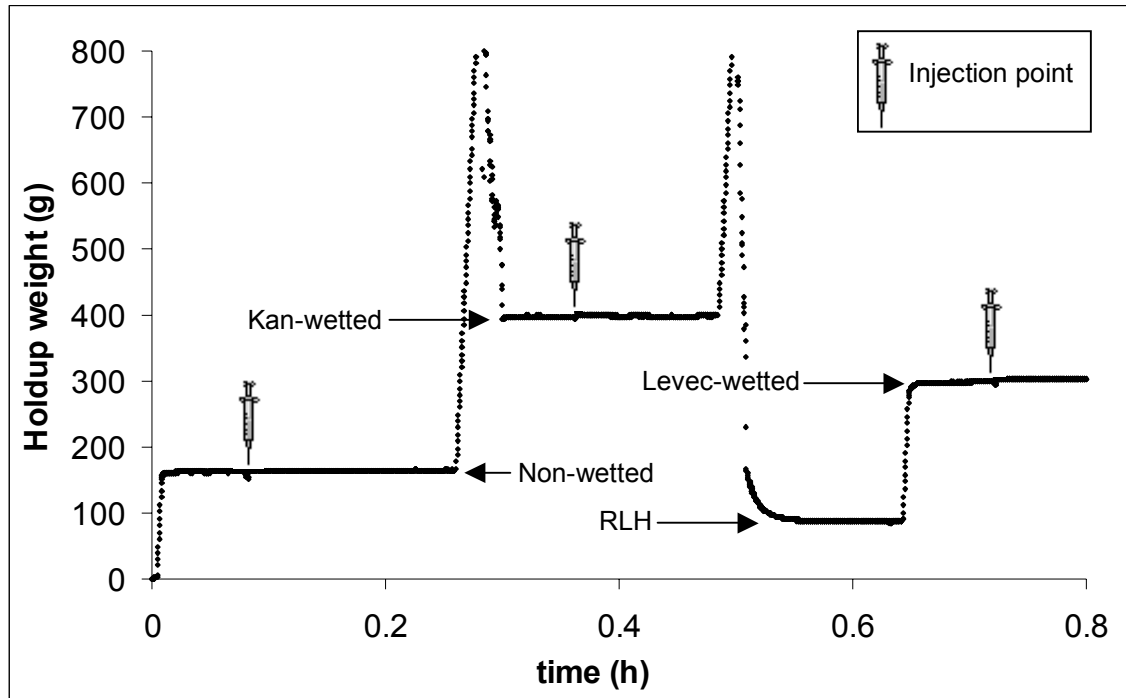
The reproducibility of these runs is illustrated by figure 6-5. Three RTD plots for  $L = 1 \text{ kg/m}^2\text{s}$  are shown. The bed was repacked for each run. Although there is some variance from run to run, each prewetted mode's response can clearly be distinguished from the other prewetted modes' responses. The reproducibility is deemed satisfactory in light of the facts that the beds may have differed slightly and the injection stimuli were not exactly equal.



**Figure 6-5.** Reproducibility of the RTD responses ( $L = 1 \text{ kg/m}^2\text{s}$ )

### Comparison of holdups by weighing and moments methods

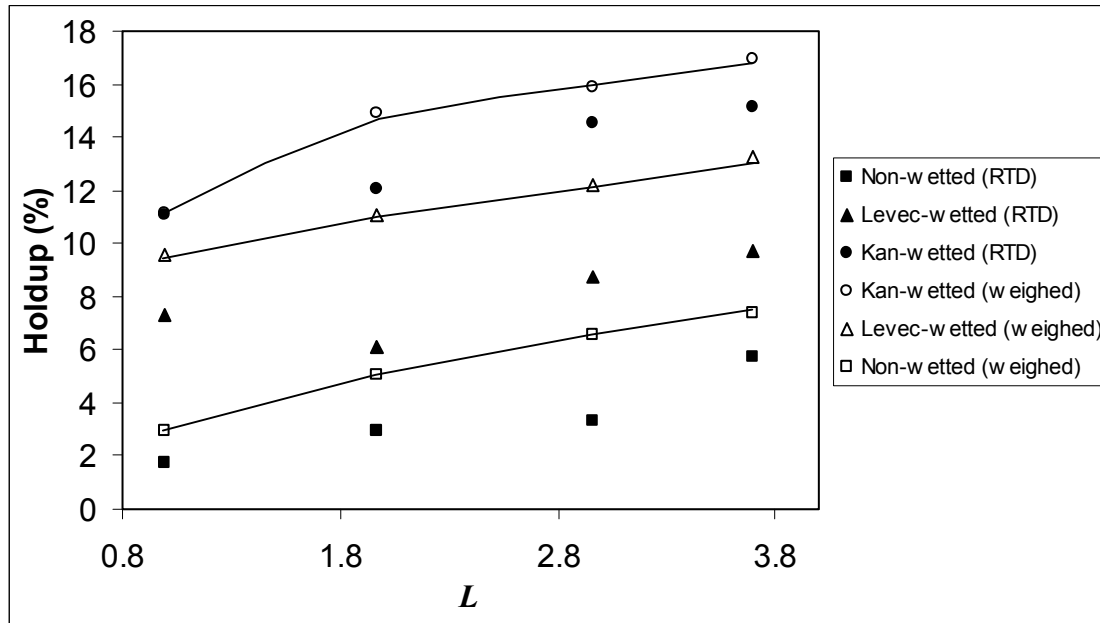
During each run, the weight of the column was continuously measured in order to confirm that the flow was at steady state. A typical plot is shown in figure 6-6.



**Figure 6-6.** Typical weight measurements during a RTD run ( $L = 3 \text{ kg/m}^2\text{s}$ )

The holdup calculated in this manner is exactly equal to the volume of liquid in the column divided by the bed volume. If all of the holdup is accessible to the tracer, this will correspond to the holdup obtained from the tracer residence time (first moment). Comparisons of the weighed holdup with the RTD holdup are given in figure 6-7.

Surprisingly, not all of the holdup was accessible to the tracer in any of the modes. In the Kan-wetted mode, almost all of the holdup was reached by the tracer (roughly 90 %). However, indication is that the tracer only sees around 70 % of the Levec-wetted mode holdup, and 60 % of the non-wetted mode holdup. Certainly, in the Levec-wetted mode one would expect that the tracer not to reach the RLH located in the non-irrigated volumes. However, it is apparent that the tracer does not access large volumes of the holdup.

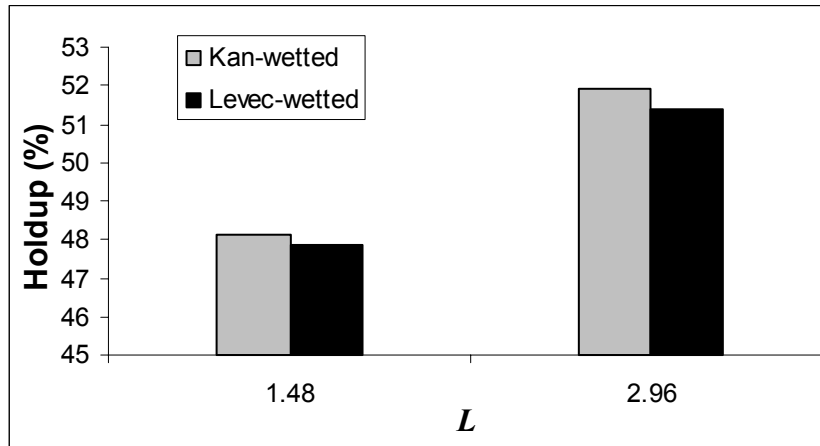


**Figure 6-7.** Weighed holdup compared to holdup obtained from the RTD

Although quantification of these effects is difficult based on only these few runs, it is evident that the RTD analyses clearly indicate differences in the holdup and mixedness in the different prewetted modes. This can only be attributed to differences in liquid holdup morphology.

### **6.3.2 Porous**

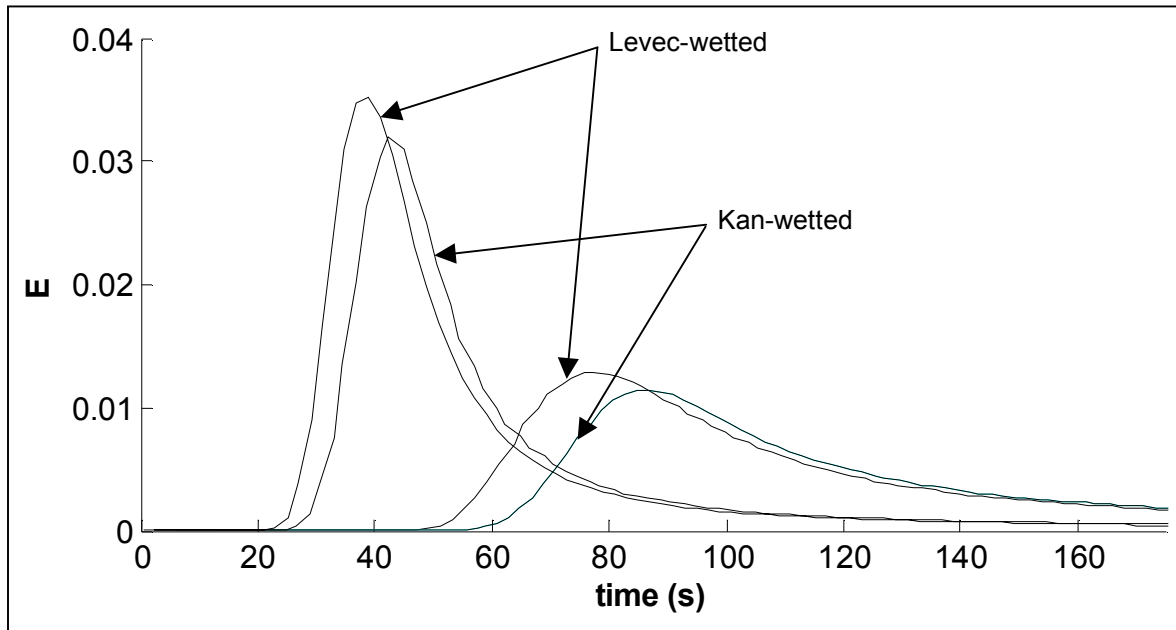
The results thus far presented in this study are applicable to non-porous systems (with a contact angle greater than zero) without gas flow. Because of the enhanced liquid spreading due to porosity (Maiti *et al.*, 2004) that effectively lowers the contact angle to zero, it may well be argued that the different prewetted modes (especially the Levec- and Kan-wetted modes) coincide for porous particles. In fact, an evaluation of the holdups (by weight) in the Kan- and Levec-wetted modes shows that there is no discernible difference (figure 6-8).



**Figure 6-8.** Comparison of holdups in Kan- and Levec-modes – porous particles

The applicability of the results presented thus far to trickle bed reactors (that use porous catalyst particles) may therefore be questioned. However, RTD analysis of these modes of operation indicates a clear difference. Figures 6-9 shows RTDs of such a system for the Kan- and Levec-modes. The injection pulses were equivalent and are omitted for the sake of clarity. Although the holdups are approximately equal, the average residence times differ, indicating that far less of the holdup was accessible to the tracer in the Levec-wetted mode. The inaccessible holdup in the non-irrigated zones is now much larger (compared to the non-porous data) because of the contribution of internal liquid holdup inside the catalyst pores.

The existence of the all three prewetted modes even when porous particles are used is therefore confirmed.



**Figure 6-9.** RTD – porous  $\alpha$ -alumina particles ( $L = 1.5$  and  $3.0 \text{ kg/m}^2\text{s}$ )

## 6.4 Conclusions

The existence of the three limiting cases of prewetted operational modes is confirmed by the technique of stimulus-response analysis. Moreover, preliminary tests show that the three modes of operation exist both in porous and non-porous systems when there is no gas flow.

Comparisons of the holdup determined by the weighing method and by the first moment of the RTD indicate that there are large volumes of liquid in the bed that are not connected to the main (tracer carrying) flow. This effect is more severe in the Levec-wetted and non-wetted modes.

In conclusion, there are some volumes of the bed that are not irrigated by the liquid for long periods of time ( $\chi$ ), some volumes that are irrigated by liquid that is detached from the “main” flow (as evidenced by the smaller holdups obtained from the first moments of the RTD experiments) and the remaining volume that is irrigated by the “main” flow.





---

## Chapter 7. Conclusions

---

The morphology of the liquid holdup in a packed bed of spheres is an important hydrodynamic parameter. This study investigated aspects of the morphology both under trickle flow irrigation and under static conditions.

The RLH was found to be made up of pendular ring structures and liquid globules at locations of low local porosity. For the air-water-glass system, 52 % of the holdup was present as pendular rings at particle-particle contact points and the remainder as irregularly shaped globules. The theoretical prediction of RLH cannot be based on the geometry of pendular rings alone.

The morphology of the operating holdup was investigated by using the RLH in a novel way. Using this technique, this study quantified how the prewetting procedure impacts the operating holdup value and morphology (and by implication the wetting efficiency) in trickle flow. The hysteresis behaviour observed in literature was rationalized by identifying that varying liquid and gas flow rates places varying parts of the bed in the different prewetted modes.

Subsequently, a volumetric utilization coefficient was defined and correlated independently in terms of the liquid flow rate. This coefficient is a quantitative measure of bed scale partial wetting. Importantly, the results show that bed scale partial wetting occurs in all modes, and large parts of the bed remain non-irrigated in the Levec-wetted and non-wetted modes. The volumetric utilization coefficient's incorporation into a holdup model was sufficient to accurately predict the holdup in all three limiting cases of prewetting for the quiescent air-distilled water-3 mm glass spheres system. The importance the prewetting procedure is reaffirmed.

A brief study of the stimulus-response behaviour of non-porous systems confirms the existence of the three prewetted modes. Interestingly, it was shown that the mixedness in these modes differ drastically. It is apparent that the Kan-wetted mode is clearly closer to plug flow behaviour than the Levec-wetted mode. Also, comparison of the weighed holdup to the holdup determined from the first moment of the RTD indicates that there are volumes of liquid in the bed that contribute to the holdup but are never reached by the tracer. The fraction of the holdup not reached by the tracer is higher in the non-wetted mode, followed by the Levec-wetted mode and then the Kan-wetted mode. Preliminary investigations into the responses of beds packed with porous particles confirm the existence of the various prewetted modes.

The implications of operating in the correct prewetted mode may well be drastically increased bed utilization and overall unit performance. Direct visualization of each prewetted mode by tomographic or colorimetric methods will enable the investigator to quantify important hydrodynamic characteristics like wetting efficiency, interfacial areas and bed-scale flow phenomena.

The present study is limited in scope; only one particle shape and diameter was used with one liquid and one gas phase at atmospheric conditions. No gas flow was employed. Despite the lack of generality, the results are significant in that they enable a visualization of trickle flow to be made. This visualization is all-important, not only because it increases our understanding of trickle flow on a fundamental level, but also because it provides an intellectual platform from which future experimental investigation may be pursued.



## References

---

Al-Dahhan, M. H. and Dudukovic, M. P. (1994) "Pressure drop and liquid hold-up in high pressure trickle-bed reactors" *Chem. Eng. Sci.*, 49, 5681-5698.

Al-Dahhan, M. H. and Dudukovic, M. P. (1995) "Catalyst wetting efficiency in trickle-bed reactors at high pressure" *Chem. Eng. Sci.*, 50, (15), 2377-2389.

Al-Dahhan, M. H., Larachi, F., Dudukovic, M. P. and Laurent, A. (1997) "High-Pressure Trickle-Bed Reactors: A Review" *Ind. Eng. Chem. Res.*, 36, 3292-3314.

Beimesh, W. E. (1972) *Pulsing, pulse characteristics, liquid distribution, pressure drop, and holdup in downward, two-phase, liquid-gas concurrent flow in packed beds*, Ph.D. Thesis, Purdue University, Purdue, USA.

Bennett, A. and Goodridge, F. (1970) "Hydrodynamics and mass transfer studies in packed absorption columns" *Trans. Instn. Chem. Engrs*, 48, T232.

Boyer, C. and Fanget, B. (2002) "Measurement of liquid flow distribution in trickle bed reactor of large diameter with a new gamma-ray tomographic system" *Chem. Eng. Sci.*, 57, 1079-1089.

Burdett, I. D., Webb, D. R. and Davies, G. A. (1981) "A new technique for studying dispersion flow, holdup and axial mixing in packed extraction columns" *Chem. Eng. Sci.*, 36, (12), 1915-1919.

Carbonell, R. G. (2000) "Multiphase flow models in packed beds" *Oil & Gas Sci. Tech. – Rev.*, 55, (4), 417-425.

Charpentier, J. C. and Favier, M. (1975) "Some liquid hold-up experimental data in trickle bed reactors for foaming and non-foaming hydrocarbons" *A.I.Ch.E. J.*, *21*, 1213-1218.

Charpentier, J. C., Prost, C., Van Swaaij, V. and LeGroff, P. (1968) "Etude de la Retention de Liquide dans une Colonne a Garnissage a Co-Courant et a Contre-Courant de Gaz-Liquide" *Chim. Ind. Genie Chim.*, *99*, 803-808.

Christensen, G., McGovern, S. J. and Sundaresan, S. (1986) "Cocurrent downflow of air and water in a two-dimensional packed column" *A.I.Ch.E. J.*, *32*, (10), 1677-1689.

Colombo, A. J., Baldi, G. and Sicardi, S. (1976) "Solid-liquid contacting effectiveness in trickle bed reactors" *Chem. Eng. Sci.*, *31*, 1101-1108.

De Klerk, A. (2003) "Liquid holdup in packed beds at low mass flux" *A.I.Ch.E. J.*, *49*, (6), 1597-1600.

Dombrowski, H. S. and Brownell, L. E. (1954) "Residual equilibrium saturation of porous media" *Ind. and Eng. Chemistry*, *46*, 1207-1219.

Dudukovic, M. P. (1977) "Catalyst effectiveness factor and contacting efficiency in trickle-bed reactors" *A.I.Ch.E. J.*, *230*, 940.

Dudukovic, M. P., Larachi, F. and Mills, P. L. (1999) "Multiphase reactors – revisited" *Chem. Eng. Sci.*, *54*, 1975-1995.

Dudukovic, M. P., Larachi, F. and Mills, P. L. (1999) "Multiphase reactors – revisited" *Chem. Eng. Sci.*, *54*, 1975-1995.

Ellman, M. J., Midoux, N., Laurent, A. and Charpentier, J. C. (1988) "A New, improved pressure drop correlation for trickle-bed reactors" *Chem. Eng. Sci.*, **43**, 2201-2210.

Ergun, S. (1952) "Fluid flow through packed columns" *Chem. Eng. Progress*, **48**, (2), 89-94.

Fukutake, T. and Rajakumar, V. (1982) "Liquid holdup and abnormal flow phenomena in packed beds under conditions simulating the flow in the dropping zone of a blast furnace" *Trans. Inst. Steel and Iron Japan*, **22**, 355-364.

Gelbe, H. (1968) "A new correlation for liquid holdup in packed beds" *Chem. Eng. Sci.*, **23**, (11), 1401-1403.

German, R. W. (1989) *Particle packing characteristics*. Princeton, USA.

Gianetto, A., Baldi, G., Specchia, V. and Sicardi, S. (1978) "Hydrodynamics and the solid-liquid contacting effectiveness in trickle-bed reactors" *A.I.Ch.E. J.*, **24**, (6), 1087-1104.

Gianetto, A. and Silveston, P. L. (1986) *Multiphase Chemical Reactors*, Hemisphere, Berlin.

Gladden, L. F., Lim, M. H. M., Mantle, M. D., Sederman, A. J. and Stitt, E. H. (2003) "MRI visualization of two-phase flow in structured supports and trickle bed reactors" *Catalysis Today*, **79-80**, 203-210.

Gonzalez-Mendizabal, D., Aguilera, M. E. and Pironti, F. (1998) "Solid-liquid mass transfer and wetting factors in trickle bed reactors: Effect of the type of solid phase and the presence of chemical reaction" *Chem. Engng. Commun.*, **169**, 37.

Hasokowati, W., Hudgins, R. R. and Silveston, P. L. (1994) "Loading, draining and hold-up in periodically operated trickle-bed reactors" *Can. J. Chem. Eng.*, 72, (3), 405-410.

Haughey, D. P. and Beveridge, G. S. G. (1969) "Structural properties of packed beds – Review" *Can. J. Chem. Engng.*, 47, 130-140.

Holup, R. A., Dudukovic, M. P. and Ramachandran, P. A. (1992) "A phenomenological model for pressure drop, liquid hold-up and flow regime transition in gas-liquid trickle flow" *Chem. Eng. Sci.*, 47, 2343-2348.

Iliuta, I. and Larachi, F. (2001) "Wet air oxidation solid catalysis of fixed and sparged three-phase reactors" *Chem. Eng. and Processing*, 40, 175-185.

Iliuta, I., Larachi, F. and Al-Dahhan, M. H. (2000) "Double-slit model for partially wetted trickle flow hydrodynamics" *A.I.Ch.E. J.*, 46, (3), 597-609.

Iliuta, I., Larachi, F. and Grandjean, B. P. A. (1999) "Residence time, mass transfer and back-mixing of the liquid in trickle flow reactors containing porous particles" *Chem. Eng. Sci.*, 54, 4099-4109.

Jiang, Y., Al-Dahhan, M. H. and Dudukovic, M. P. (2001) "Statistical characterization of macroscale multiphase flow textures in trickle beds" *Chem. Eng. Sci.*, 56, 1647-1656.

Kan, K. M. and Greenfield, P. F. (1978) "Multiple hydrodynamic states in cocurrent two-phase down-flow through packed beds" *Ind. Eng. Chem. Process Des. Dev.*, 17, 482-485.

Kan, K. M. and Greenfield, P. F. (1979) "Pressure drop and holdup in two-phase

cocurrent trickle flows through packed beds” *Ind. Eng. Chem. Process Des. Dev.*, 18, 740-745.

Kantzas, A. (1994) Computation of holdups in fluidized and trickle beds by computer-assisted tomography” *A.I.Ch.E. J.*, 40, (7), 1254-1261.

Kumar, S. B., Moslemiam, D. and Dudukovic, M. P. (1995) “A gamma-ray tomographic scanner for imaging voidage distribution in two-phase flow systems” *Flow Meas. Instrum.*, 6, (1), 61-73.

Kushalkar, K. B. and Pangarkar, V. G. (1990) “Liquid holdup and dispersion in packed columns” *Chem. Eng. Sci.* 45, (3), 759-763.

Lakota, A. and Levec, J. (1990) “Solid-liquid mass transfer in packed beds with cocurrent downward two-phase flow” *A.I.Ch.E. J.*, 36, 1444.

Larachi, F., Belfares, L., Iliuta, I. and Grandjean, B. P. A. (2004) “Liquid hold-up correlations for trickle beds without gas flow” *Chem. Eng. Processng.*, 43, (1) 85-90.

Lazzaroni, C. L., Keselman, H. R. and Figoli, N. S. (1988) “Colorimetric evaluation of the efficiency of liquid-solid contacting in trickle flow” *Ind. Eng. Chem. Res.*, 27, 1132-1135.

Lazzaroni, C. L., Keselman, H. R. and Figoli, N. S. (1989) “Trickle bed reactors. Multiplicity of hydrodynamic states. Relation between the pressure drop and the liquid holdup” *Ind. Eng. Chem. Res.*, 28, 119-121.

Levec, J., Grosser, K. and Carbonell, R. G. (1988) “The hysteretic behaviour of pressure drop and liquid holdup in trickle beds” *A.I.Ch.E. J.*, 34, 1027-1030.

Levec, J., Saez, A. E. and Carbonell, R. G. (1986) "The hydrodynamics of trickling flow in packed beds, part I: Conduit models" *A.I.Ch.E. J.*, 32, 515-523.

Li, M., Bando, Y., Tsuge, T., Yasuda, K. and Nakamura, M. (2001) "Analysis of liquid distribution in non-uniformly packed trickle bed with single phase flow" *Chem. Eng. Sci.*, 56, 5969-5976.

Llano, J. J., Rosal, R., Sastre, H. and Fernando V. D. (1997) "Determination of wetting efficiency in trickle-bed reactors by a reaction method" *Ind. Eng. Chem. Res.*, 36, 2616-2625.

Lutran, P. G., Ng, K. M. and Delikat, E. P. (1991) "Liquid distribution in trickle beds. An experimental study using computer-assisted tomography" *Ind. Eng. Chem. Res.*, 30, 1270-1280.

Maiti, R. N., Khanna, R., Sen, P. K. and Nigam, K. D. P. (2004) "Enhanced liquid spreading due to porosity" *Chem. Eng. Sci.*, 59, 2817-2820.

Mao, Z. S., Xiong, T. Y. and Chen, J. Y. (1993) "Theoretical prediction of static liquid holdup in trickle bed reactors and comparison with experimental results" *Chem. Eng. Sci.*, 48, 2697-2703.

Mao, Z. S., Xiong, T. Y., Wang, R. and Chen, J. Y. (1994) "Note on the thermodynamic stability of pendular rings between solid particles" *Chem. Eng. Sci.*, 49, (20), 3519-3521.

Marcandelli, C., Lamine, A. S., Bernard, J. R. and Wild, G. (2000) "Liquid distribution in trickle-bed reactor" *Oil & Gas Sci. and Tech.*, 55, 407-415.

Matsuura, A., Akehata, T. and Shirai, T. (1979) "Correlation for dynamic holdup in packed beds with cocurrent gas-liquid downflow" *J. Chem. Eng. Japan*, 12, (4),



263-268.

Matsuura, A., Akehata, T. and Shirai, T. (1979) "Correlation for dynamic holdup in packed beds with cocurrent gas-liquid downflow" *J. Chem. Eng. Japan*, 12, (4), 263-268.

Mills, P. L. and Dudukovic, M. P. (1981) "Evaluation of liquid-solid contacting in trickle beds by tracer methods" *A.I.Ch.E. J.*, 27, 893.

Mills, P. L. and Dudukovic, M. P. (1989) "Convolution and deconvolution of nonideal tracer response data with application to three-phase packed-beds" *Computers Che. Engng.*, 13, (8), 881-898.

Morita, S. and Smith, J. M. (1978) "Mass transfer and contacting efficiency in a trickle bed reactor" *Ind. Eng. Chem. Fundam.*, 17, 113.

Moseley, W. A., Dhir, V. K. (1996) "Capillary pressure-saturation relations in porous media including the effect of wettability" *J. of Hydrology*, 178, 33-53.

Nigam, K. D. P., Iliuta, I. and Larachi, F. (2002) "Liquid back-mixing and mass transfer effects in trickle-bed reactors filled with porous catalyst particles" *Chem. Eng. and Processing*, 41, 365-371.

Nijhuis, T. A., Dautzenberg, F. M. and Moulijn, J. A. (2003) "Modeling of monolithic and trickle-bed reactors for the hydrogenation of styrene" *Chem. Eng. Sci.*, 58, 1113-1124.

Ortiz-Arroyo, A., Larachi, F. and Iliuta, I. (2003) "Method for inferring contact angle and for correlating static liquid hold-up in packed beds" *Chem. Eng. Sci.*, 58, 2835-2855.

Patwardhan, V. S. (1978) "Effective interfacial area in packed beds for absorption with chemical reaction" *Can. J. Chem. Eng.*, 56, (1), 56-64.

Pietsch, W. and Rumpf, H. (1967) "Haftkraft, Kapillardruck, Flüssigkeitsvolumen und Grenzwinkel einer Flüssigkeitsbrücke zwischen zwei Kugeln" *Chemie-Ing.-Techn.* 39,15, 885-893.

Pironti, F., Mizrahi, D., Acosta, A. and Gonzalez-Mendizabal, D. (1999) "Liquid-solid wetting factor in trickle-bed reactors: its determination by a physical method" *Chem. Eng. Sci.*, 54, 3793-3800.

Puranik, S. S. and Vogenpohl, A. (1974) "Effective interfacial area in irrigated packed columns" *Chem. Eng. Sci.*, 29, 501-507.

Rajashekharam, M. V., Jaganathan, R. and Chaudhari, V. (1998) "A trickle-bed reactor model for hydrogenation of 2,4-dinitrotoluene: experimental verification" *Chem. Eng. Sci.*, 53, 787-805.

Ravindra, P. V., Rao, D. P. and Rao, M. S. (1997) "Liquid flow texture in trickle-bed reactors: an experimental study" *Ind. Eng. Chem. Res.*, 36, 5133-5145.

Reddy, P. N., Rao, D. P. and Rao, M. S. (1990) "The texture of liquid flow in trickle-bed reactors" *Chem. Eng. Sci.*, 45, (10), 3193-3197.

Reinecke, N. and Mewes, D. (1997) "Investigation of the two-phase flow in trickle-bed reactors using capacitance tomography" *Chem. Eng. Sci.*, 52, (13), 2111-2127.

Saez, A. E. and Carbonell, R. G. (1985) "Hydrodynamic parameters for gas-liquid cocurrent flow in packed beds" *AIChE Journal*, 31, 52-62.

Saez, A. E., Yepes, M. M., Cabrera, C. and Soria, E. M. (1991) "Static liquid holdup in packed beds of spherical particles" *A.I.Ch.E. J.*, 37, 1733-1736.

Saez, A. E.; Carbonell, R. G. (1990) "The Equilibrium and Stability of Menisci between Touching Spheres under the Effect of Gravity" *J. Colloid Interface Sci.*, 140, 408-416.

Satterfield, C. N. (1975) "Trickle-bed reactors" *A.I.Ch.E. J.*, 21, (2), 209-228.

Schubert, C. N., Lindner, J. R. and Kelly, R. M. (1986) "Experimental methods for measuring static liquid holdup in packed columns" *A.I.Ch.E. J.*, 32, (11), 1920-1923.

Schwartz, T. G., Wegwe, E. and Dudukovic, M. P. (1976) "A new tracer method for determination of the liquid-solid contacting effectiveness in trickle bed reactors" *A.I.Ch.E. J.*, 22, 894.

Sederman, A. J. and Gladden, L. F. (2001) "Magnetic resonance imaging as a quantitative probe of gas-liquid distribution and wetting efficiency in trickle-bed reactors" *Chem. Eng. Sci.*, 56, 2615-2628.

Sedriks, W. and Kenney, C. N. (1973) "Partial wetting in trickle bed reactors – the reduction of crotonaldehyde over a palladium catalyst" *Chem. Eng. Sci.*, 28, 559.

Shulman, H. L., Ullrich, C. F. and Wells, N. (1955) "Performance of packed columns. 1: Total, static and operating holdups" *A.I.Ch.E. J.*, 1, 247-252.

Sicardi, S., Baldi, G. and Specchia, V. (1980a) "Hydrodynamic models for the interpretation of the liquid flow in trickle-bed reactors" *Chem. Eng. Sci.*, 35, 1775-1782.

Sicardi, S., Baldi, G., Specchia, V., Mazzarino, I. and Gianetto, A. (1980b) "Catalyst areas wetted by flowing and semistagnant liquid in trickle bed reactors" *Chem. Eng. Sci.*, 35, 67-73.

Sicardi, S., Baldi, G., Specchia, V., Mazzarino, I. and Gianetto, A. (1980c) "Packing wetting in trickle bed reactors: influence of the gas flow rate" *Chem. Eng. Sci.*, 36, 226-228.

Škrbić, B. and Cvejanov, J. (1994) "Liquid holdup determination in packed columns for sulfur dioxide absorption" *Gas Separation and Purification*, 8, (1), 13-16.

Specchia, V. and Baldi, G. (1977) "Pressure drop and liquid holdup for two phase concurrent flow in packed beds" *Chem. Eng. Sci.*, 32, 515–523.

Stanek, V. and Kolar, V. (1973) "A model of the effect of the distribution of liquid on liquid hold-up in a packed bed and a new concept of static hold-up" *Chem. Eng. J.*, 5, 51-60.

Stanek, V. and Kolar, V. (1973) "A model of the effect of the distribution of liquid on liquid hold-up in a packed bed and a new concept of static hold-up" *Chem. Eng. J.*, 5, 51-60.

Stegeman, D., Van Rooijen, F. E., Kamperman, A. A., Weijer, S. and Westerterp, K. R. (1996) "Residence time distribution in the liquid phase in cocurrent gas-liquid trickle bed reactor" *Ind. Eng. Chem. Res.*, 35, 378-385.

Stein, W. A. (2000) "Der statische Flüssigkeitsanteil in Packungskolonnen" *Forschung im Ingenieurwesen*, 66, 129-137.

Toye, D., Marchot, P., Crine, M., Pelsser, A. M. and L'Homme, G. (1998) "Local

measurements of void fraction and liquid holdup in packed columns using X-ray computed tomography” *Chem. Eng. Proc.*, 37, 511-520.

Tsamatsoulis, D. and Papayannakos, N. (1995) “Simulation of non-ideal flow in a trickle bed hydrotreater by the cross-flow model” *Chem. Eng. Sci.*, 50, (23), 3685-3691.

Tsochatzidis, N. A., Karabelas, A. J., Giakoumakis, D. and Huff, G. A. (2002) “An investigation of liquid maldistribution in trickle beds” *Chem. Eng. Sci.*, 57, 3543-3555.

Turner, G. A. and Hewitt, G. F. (1959) “The amount of liquid held at the point of contact of spheres and the static liquid holdup in packed beds” *Trans. Instn. Chem. Engrs.* 37, 329-334.

Van Swaaij, W. P. M., Charpentier, J. C. and Villermaux, J. (1969) “Residence time distribution in the liquid phase of trickle flow in packed columns I” *Chem. Eng. Sci.*, 24, 1083.

Wammes, W. J. A., Mechielsen, S. J. and Westerterp, K. R. (1991) “The influence of pressure on the liquid hold-up in a cocurrent gas-liquid trickle-bed reactor operating at low gas velocities” *Chem. Eng. Sci.*, 46, (2), 409-417.

Wang, R., Mao, Z. and Chen, J. (1995) “Experimental and theoretical studies of pressure drop hysteresis in trickle bed reactors” *Chem. Eng. Sci.*, 50, (14), 2321-2328.

Westerterp, K. R., Van Swaaij, W. P. M. and Beenackers, A. A. C. M. (1984) *Chemical Reactor Design and Operation*, John Wiley & Sons, Norwich.

Yin, F., Afacan, A., Nandakumar, K. and Chuang K. T. (2002) “Liquid holdup

distribution in packed columns: gamma ray tomography and CFD simulation”  
*Chem. Engng. Processng.*, 41, 473-483.

Zimmerman, S. P. and Ng, K. M. (1986) “Liquid distribution in trickling flow  
trickle-bed reactors” *Chem. Eng. Sci.*, 41, 861.



---

## Appendix A: RLH supporting information

---

### A.1 Influential parameters and trends

Parameters that have been found to influence the overall value of residual liquid holdup are listed in Table A-1. Because RLH and static liquid holdup (SLH) are often assumed to be equal, parameters that influence static holdup have also been listed. Table A-1 also lists the changes in RLH due to changes in each parameter, as well as substantiating references.

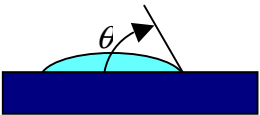
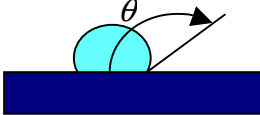

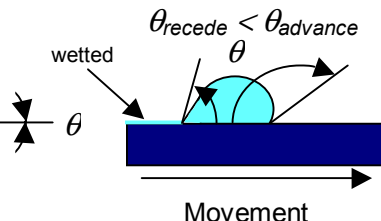
Note that the packing material is not listed in Table A-1, because it is only important insofar as it affects the wettability and liquid-solid surface tension. Another important parameter that influences RLH but is not listed is the particle or packing material shape. Most RLH studies have dealt with either spheres or Raschig rings, although other shapes have been considered (Ortiz-Arroyo *et. al.*, 2003). One way of dealing with non-spherical shapes is by defining a characteristic length (which is then included in the Bond number in place of diameter). The following characteristic lengths have been used:

- The equivalent particle diameter, defined as the diameter of a sphere having the same volume as the particle under consideration. From experimental data, this diameter has proven unable to fully characterize particle shape. For example, Charpentier & Favier (1975) found a difference of 38 % in RLH for spheres and cylinders with the same equivalent diameter.
- Nominal particle diameter (Charpentier *et. al.*, 1968, reported by Saez *et. al.*, 1991)
- Characteristic length proportional to the hydraulic diameter (Saez & Carbonell, 1985) which represents the ratio of void volume to particle surface area

**Table A-1.** The influence of certain parameters on RLH

Parameter	Influence	Reference(s)
Particle or packing size	Constant values of approximately 5% for the RLH have been measured by a number of early researchers. This is attributed to the fact that small particles featured in the investigations. RLH is relatively independent of particle size for Eötvös numbers smaller than approximately 5. Above this value, the static liquid holdup decreases with increasing packing material size. At very small particle diameters the RLH can be much larger due to liquid retention.	Specchia & Baldi (1977) Beimesch (1972) Mao <i>et. al.</i> (1993) Saez & Carbonell (1985) Saez <i>et. al.</i> (1991) Ortiz-Arroyo <i>et. al.</i> (2003)
Packing method and porosity	Various packing geometries for spherical packings are known, and each of these has associated properties like porosity and number of contact points per particle. A great number of correlations exist to relate these two properties. The denser the packing (small voidage) the greater number of contact points and the stronger the capillary force, resulting in larger RLH. For non-spherical packings the situation is more complex although the general trend remains the same. For porosities in the range 30-50 %, the effect is nearly negligible and the RLH is hardly affected by it. The structure of the packing also impacts the RLH orientation toward the desaturation	Stein (2000) Pietsch & Rumpf (1967) Haughey & Beveridge (1969) German (1989) Saez <i>et. al.</i> (1991) Dombrowski & Brownell (1954) Turner & Hewitt (1959)



	force (usually gravity) which may impact the RLH value.	
Liquid density	Liquid density appears in the gravity desaturation force expression and it is therefore expected that liquids of high density will have less RLH. However, dimensional analysis has indicated that this effect can be fully compensated for by including the liquid density in the Eötvos number. Experiments with three liquids of differing density suggest that its effect is practically negligible except at high Eötvos numbers where the RLH is small in any case.	Dombrowski & Brownell (1954) Saez <i>et. al.</i> (1991)
Surface tension	The surface tension features in both the surface force (which is proportional to $\sigma d$ ) and the solid-liquid interfacial force (which is proportional to $\sigma d(1+\cos\theta)$ ). The surface force is regarded as a resistance against desaturation. Accordingly, large surface tensions are associated with large RLH values. The surface tension is included in the Eötvos number.	Fukutake & Rajakumar (1982)
Solid wettability (contact angle)	<div style="display: flex; justify-content: space-around; align-items: flex-end;"> <div style="text-align: center;"> <p><math>0^\circ &lt; \theta &lt; 90^\circ</math></p>  <p>Wetting liquid</p> </div> <div style="text-align: center;"> <p><math>90^\circ &lt; \theta &lt; 180^\circ</math></p>  <p>Non-wetting liquid</p> </div> <div style="text-align: center;"> <p><math>\theta = 180^\circ</math> or <math>0^\circ</math></p>  <p>Perfect wetting</p> </div> <div style="text-align: center;"> <p><math>\theta_{recede} &lt; \theta_{advance}</math></p>  <p>Movement</p> </div> </div>	

Solid wetability (cont.)	<p>The solid wetability is expressed in terms of the solid-liquid contact angle that is measured in the manner depicted above. Contact angles measured on previously wetted surfaces are smaller than those measured on dry surfaces for <math>\theta &lt; 90^\circ</math>. Contact angles used for the glass-water-air system range from zero to values exceeding <math>30^\circ</math>. Researchers disagree on its effects on the RLH, with increases in RLH being associated with both increases and decreases in contact angle. Some data suggest that the RLH is invariant to contact angle, while other authors state that the contact angle is one of the primary parameters in RLH formation.</p>	<p>Ortiz-Arroyo <i>et. al.</i> (2003)  Moseley &amp; Dhir (1996)  Kramer (1998)  Saez <i>et. al.</i> (1991)  Mao <i>et. al.</i> (1993)  Dombrowski &amp; Brownell, 1954</p>
Liquid flow rate	<p>Empirical correlations in terms of the Eötvös or Bond numbers do not take the liquid flow rate prior to flow interruption into account. Indeed, some authors define the RLH or SLH as that part of the total holdup that is independent of the liquid rate. In contrast, SLH determined through the use of RTD models show a liquid velocity dependency. However, conflicting results have been reported, with both increases and decreases of SLH having been found with increasing liquid velocity.</p>	<p>Saez &amp; Carbonell (1985)  Mao <i>et. al.</i> (1993)  Dombrowski &amp; Brownell (1954)  Stein (2000)  Ortiz-Arroyo <i>et. al.</i> (2003)  Fukutake &amp; Rajakumar (1982)  Stanek &amp; Kolar (1973)  Matsuura, Akehata &amp; Shirai (1979)  Sicardi, Baldi &amp; Specchia (1980)  Kushalkar &amp; Pangarkar (1990)</p>

Liquid flow rate (cont.)		Tsamatsoulis & Papayannakos (1995) Burdett, Webb & Davies (1981) Hasokowati, Hudgins & Silveston (1994)
Gas flow rate	The gas-liquid drag force acts as a desaturation driving force. It increases with gas flow rate. If the bed is drained with gas flow present, the RLH may decrease with gas flow rate, although this effect is expected to be small.	Specchia & Baldi (1977)
State variables (and gas density)	High pressure operation results in higher gas density. Although it has been reported that high pressure operation does not affect the RLH, it is also known that the gas-liquid drag force increases with increased gas density. This force is an additional desaturation force, and RLH may be significantly lower if the bed is drained with an appreciable gas flow at high pressure. Temperature may become a telling factor when volatile liquids are used since the rate of RLH evaporation into the gas will depend on the volatility of the liquid at that temperature.	Van Swaaij, Charpetier & Villermaux (1969) Al-Dahhan & Dudukovic (1994) Specchia & Baldi (1977) Patwardhan (1978)

- Characteristic length proportional to the square root of the absolute bed permeability (Dombrowski & Brownell, 1954)

Ortiz-Arroyo *et. al.* (2003) incorporates a sphericity factor into their comprehensive artificial neural network (ANN) correlation for RLH. The scatter in data such as that presented by Saez & Carbonell (1985) and Ortiz-Arroyo *et. al.* (2003) clearly indicates the inability of the characteristic length approach to accurately represent the particle shape.

An additional complicating factor is the possibility of concave particle shapes (i.e. particles that are hollow such as bowl-shaped saddles or hollow cylinders of small inner voidage) that may trap additional liquid. It is also very difficult to obtain reliable porosity-number of contact points relations for non-spherical particles.

The draining kinetics and its effect on RLH have received brief attention in literature (Turner & Hewitt, 1959, Dombrowski & Brownell, 1954, Wakeman & Vince, 1986). The draining kinetics has not been included in any empirical correlations. It has been speculated that different draining rates are accountable for some of the scatter in literature (Saez & Carbonell, 1985) but no experimental verification has been done. Draining times ranging between 10 and 60 minutes have been used (Škrbić & Cvejanov, 1994, Stanek & Kolar, 1973, Saez *et. al.*, 1991, Pironti *et. al.*, 1999, Iliuta *et. al.*, 1999, Van Swaaij *et. al.*, 1969).

## **A.2 Residual liquid holdup correlations**

Numerous residual and static liquid holdup correlations exist. Table A-2 lists them, along with a very brief description of each. It does not include studies based on residence time distributions as this is usually seen as an indication of the static liquid holdup and are therefore not directly relevant to the present

investigation into the morphology of the residual liquid holdup. Similarly, those based on reaction and mass transfer methods are also omitted.

**Table A-2.** RLH correlations

Study	Description
Dombrowski & Brownell (1954)	Graphical log-log plot of RLH vs. Capillary number (modified to include the contact angle)
Shulman, Ullrich & Wells (1955)	Two parameter model in terms of diameter
Turner & Hewitt (1959)	One parameter model in terms of the reciprocal of Bond number (large spheres only)
Kunugita, Otake & Yoshii (1962)	One parameter model in terms of the reciprocal of diameter
Gelbe (1968)	In terms of Bond number applicable to typical absorption conditions
Charpentier <i>et. al.</i> (1968)	$h_s = \frac{1}{20 + 0.9E\ddot{o}} \quad (\text{A-1})$
Stanek & Kolar (1973)	RLH taken as the operating holdup in the limit of zero liquid velocity
Mersman (1975)	Similar to equation A-1 but with a porosity term added
Fukutake & Rajakumar (1982)	Same form as equation A-1 but the functional parameter is the ratio of capillary number to dimensionless interfacial force
Saez & Carbonell (1985)	$h_s = \frac{1}{20 + 0.9E\ddot{o}^*} \quad (\text{A-2})$ Here a porosity term is included in $E\ddot{o}^*$
Saez <i>et. al.</i> (1991)	The same form as equation A-2 but different constants
Mao <i>et. al.</i> (1993)	Theoretical model based on pendular ring theory

Kramer (1998)	Theoretical model based on critical percolation theory
Stein (2000)	Empirical correlation in terms of Bond number, porosity and contact angle.
Ortiz-Arroyo <i>et. al.</i> (2003)	Inferred contact angles and an artificial neural network based correlation in terms of Bond number, the solid-to-void volume ratio, the packing sphericity and the bed-to-packing ratio

### A.3 Surface tension

The surface tension has been shown experimentally to influence the RLH and also impacts the theoretical procedure adopted in chapter 2. In the case of the top-view experiments, the surface tension was determined through capillary rise experiments. A 3.1 mm inner diameter glass capillary tube was placed in the water and the height of the capillary rise was measured at 8.0 mm with a Vernier calliper. The surface tension is given by ([www.me.rochester.edu](http://www.me.rochester.edu), 10/4/2004):

$$\sigma = \frac{9800hR}{2 \cos \theta} \quad (\text{A-3})$$

The side view experiments were conducted with the tap water of a few weeks later, but the surface tension was not determined in that case. If the mineral content of the water had varied in the time between experiments, that may account for the difference in the average wetting angles of the top and side view data. However, the difference needed to be very large to account for the variance and it is therefore concluded that it was a statistical anomaly.

## A.4 Porosity of the packed bed

The porosity of the packed bed was determined upon each repacking of the bed. The weight of glass beads needed to fill the column to the desired height of 900 mm was measured. The porosity is given by:

$$\varepsilon = 1 - \frac{\text{Mass of beads}}{\text{Density of glass} \times \text{Bed volume}} \quad (\text{A-4})$$

The porosity was equal to approximately 36.5 % for every repacking.

## A.5 Contact angles

35 contact angles were measured. These are shown in figure A-1 below along with the average value (solid line) of 32.4°. An RSD of 6 % indicates that the contact angle remained approximately constant.

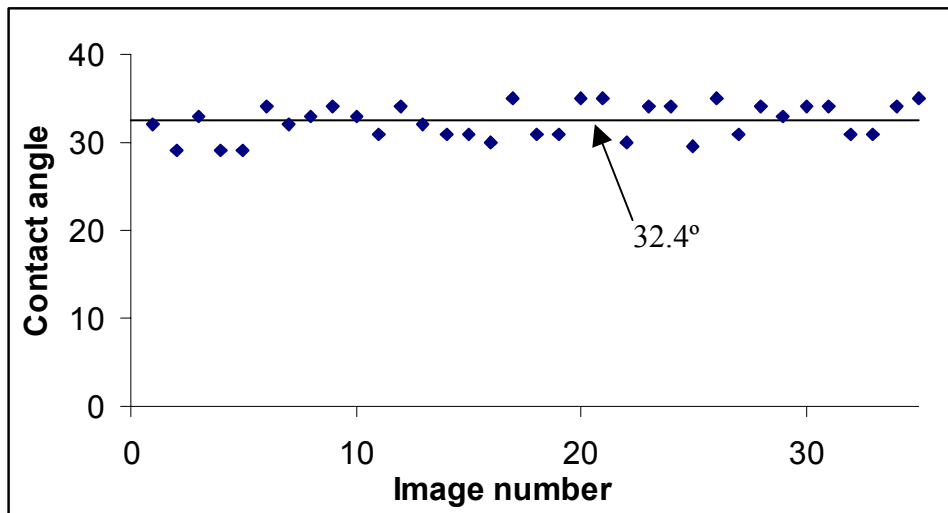


Figure A-1. Contact angle measurements

---

## Appendix B: Operating holdup: additional information

---

### Calibration curve (concentration – conductivity)

The concentration-conductivity calibration curve was obtained by measuring the conductivities of standard solutions and then fitting equations of the form given in equation B-1 to the data in the Matlab environment. The calibration functions for the two probes differed because of differing cell constants.

$$F(C) = \exp\{a(\ln C)^3 + b(\ln C)^2 + c \ln C + d\} \quad (\text{B-1})$$

**Table B-1.** Constants for use in equation B-1

Constant	Probe 1	Probe 2
<i>a</i>	0.003503	0.00419
<i>b</i>	-0.0669	-0.08053
<i>c</i>	1.429	1.507
<i>d</i>	-8.67	-9.016

The AARE's of these functions are less than 1 % for probes 1 and 2.

### Adsorption testing

Adsorption of the salt on the glass or alumina surface was tested for by making up a dilute well-mixed salt solution, adding a handful of particles and monitoring the conductivity. In both cases the conductivity remained approximately constant indicating that no adsorption was taking place.